FACULTY
OF MATHEMATICS
AND PHYSICS
Charles University

DOCTORAL THESIS

Petra Šimáková

Surface-enhanced Raman microspectroscopy of biomolecules and biological systems

Institute of Physics of Charles University

Supervisor: Doc. RNDr. Marek Procházka, PhD.

Study programme: Physics
Specialization: Biophysics, Chemical and Macromolecular Physics

Prague 2017

I declare that I carried out this doctoral thesis independently, and only with the cited sources, literature and other professional sources.

I understand that my work relates to the rights and obligations under the Act No. 121/2000 Coll., the Copyright Act, as amended, in particular the fact that the Charles University has the right to conclude a license agreement on the use of this work as a school work pursuant to Section 60 paragraph 1 of the Copyright Act.

In Prague, 30th of July 2017 Petra Šimáková

Acknowledgements

I would like to thank my supervisor Marek Procházka for his help and advice. I thank Jiří Bok as the author of several software utilities for calibration and data conversion, Jan Palacký as the author of CellViewer software used for processing and visualisation of spectral mapping data and Natália Hajduková-Šmídová for preparation of Au surfaces. Then I have to thank our colleagues from the Faculty of Nuclear Sciences and Physical Engineering - Jan Proška for many scientific insights and Lucie Štolcová for preparation of film-over-nanospheres SERS substrates, as well as our French colleagues - Igor Chourpa for kind welcome to his department and help with experiments and Juliette Gautier for preparation of PEGylated Ag nanoparticles and help with all the joint experiments.

Of course a huge thank you goes to my family and friends for their support. Last but not least, I would like to thank my colleagues at the Czech Academy of Sciences for helping me to finish this thesis. Special thanks belong to a collegue and friend Michal Šindler for his unceasing moral support.

The financial support by the Czech Science Foundation (Project P205/13/20110S) is gratefully acknowledged.

Title: Surface-enhanced Raman microspectroscopy of biomolecules and biological systems

Author: Petra Šimáková

Department: Institute of Physics of Charles University

Supervisor of the doctoral thesis: Doc. RNDr. Marek Procházka, Dr., Institute of Physics of Charles University

Abstract: The aim of this thesis was using surface-enhanced Raman scattering (SERS) microspectroscopy for the study of biomolecules and biological systems. The main probe molecule was cationic porphyrin H_2TMPyP, however, other porphyrins, tryptophan and two lipids were also used. The sensitivity and reproducibility of several solid SERS substrates: (i) Au and Ag nanoparticles (NPs) immobilized via a bifunctional linker, (ii) AgNPs immobilized by drying, (iii) highly ordered Au and Ag film-over-nanosphere (FON) and (iv) Ag-coated insect wings were compared. On most of the solid substrates, the lowest detected H_2TMPyP concentration was ~10^{-8} M. The highest sensitivity was provided by the dried drops of AgNPs/analyte mixture, where concentrations 1×10^{-10} M TMPyP, 1×10^{-5} M tryptophan, 2×10^{-7} M DSPC and 3×10^{-7} M DMTAP were detected. Nevertheless, the spectral reproducibility was decreased due to porphyrin metallation and perturbation of the lipid spectra in comparison to their Raman spectra from solution. The highest reproducibility was achieved by AuFON and Ag-coated insect wings. Finally, the AgNPs modified by PEG polymers were tested for intracellular application using HeLa cancer cells. Metallation of H_2TMPyP served to probe the accessibility of PEG-AgNPs surface. The results proved that the accessibility was dependent on the chemical properties of both polymer and porphyrin.

Keywords: SERS, Raman microspectroscopy, colloidal nanoparticles, porphyrins, FON, biotemplating

Contents

1 Introduction

1.1 Raman spectroscopy

1.1.1 Theory of Raman scattering

Raman scattering (RS) is an inelastic scattering with frequency shift between the incident and the scattered light corresponding to energy of molecular vibrations. RS therefore provides information about the molecular structure. The effect was discovered by C. V. Raman [1,2] in solutions in 1928 and simoultaneously by L. I. Landsberg and G. S. Mandelstam for crystals [3]. The effect had been theoretically predicted by Austrian physicist A. Smekal in 1923 [4], however, his work was not generally known at that time. The first systematic theory of the Raman effect was developed by a physicist of Czech origin G. Plazcek in the 1930s [5].

The scattering is produced by oscillating electric and magnetic multipoles induced in the molecule by an incident electromagnetic field. The most significant is the electric dipole. A molecule interacts with an electric field $\vec{E}$ via its electron cloud, flexibility of which is characterized by the molecular polarizability $\vec{\vec{\alpha}}$. The molecular polarizability is a function of nuclear coordinates as the electron density depends on the motion of the nuclei. The oscillating induced electric dipole moment is given by the expression

$$\vec{p} = \vec{\vec{\alpha}} \cdot \vec{E} . \tag{1}$$

The induced electric dipole emits scattering with the frequency at which it oscillates. There will be three types of components. One with the same frequency υ_0 as the incident electric field corresponding to the Rayleigh scattering. For the rest of the components the frequency υ_0 is modulated by frequencies of the vibrational modes υ_k. The scattering with lower frequency than the incident radiation $\upsilon_0 - \upsilon_k$ is called Stokes RS. Here, the molecule takes part of the energy of light and is excited to a vibrational state with higher energy. Anti-Stokes scattering with frequency $\upsilon_0 + \upsilon_k$ corresponds to a situation when the molecule gives energy to the light and transitions to a lower vibrational level. The Stokes part of the spectra is usually measured because populations of the excited states decrease rapidly with energy at room temperature according to the Boltzmann distribution causing that the Stokes RS is more intense than anti-Stokes RS.

A molecular vibration is active in Raman spectrum if the polarizability changes during the vibration, i.e. $(\partial\vec{\vec{\alpha}}/\partial Q_k)_0 \neq 0$, where Q_k is the k-th normal vibrational coordinate. The vibrational bands of a molecule are independent of the technique used for their detection, but their intensity is different for Raman and IR spectroscopy. While polar groups (e.g. –OH, –C=O, $–NO_2$) are intense in IR spectra, symmetrical and in phase vibrations, especially multiple symmetrical bonds –C≡C–, –C=C–, –N=N–, are intense in Raman spectra.

RS is a very weak process; only approximately 1 out of 10^7 scattered photons are scattered by the Raman process. Raman cross sections are 10^{-31}–10^{-29} cm^2/molecule [6]. In comparison an average fluorescence cross section is about 10^{-19} cm^2/molecule [7, p. 31]. There are two types of RS based on the frequency of excitation (see Fig. 1.1). When the frequency of the incident radiation is much higher than the vibrational levels energy difference, but much lower than the energy of the electronic transition, non-resonance RS occurs. When the incident radiation frequency is close to the energy of the electronic transition, resonance Raman scattering (RRS) takes place. RRS can be used for selective excitation of a chromophore. On the other hand, in the case of resonance excitation, fluorescence or photoinduced changes of molecular structure can occur complicating the RRS measurement. RRS intensity is 10^4-10^6-times higher than the intensity of non-resonance RS [7, p. 112]. For non-resonance and RRS apply different selection rules. In harmonic approximation only fundamental vibrational transitions are allowed for non-resonance RS, whereas overtones and combination vibrational transitions are active for RRS.

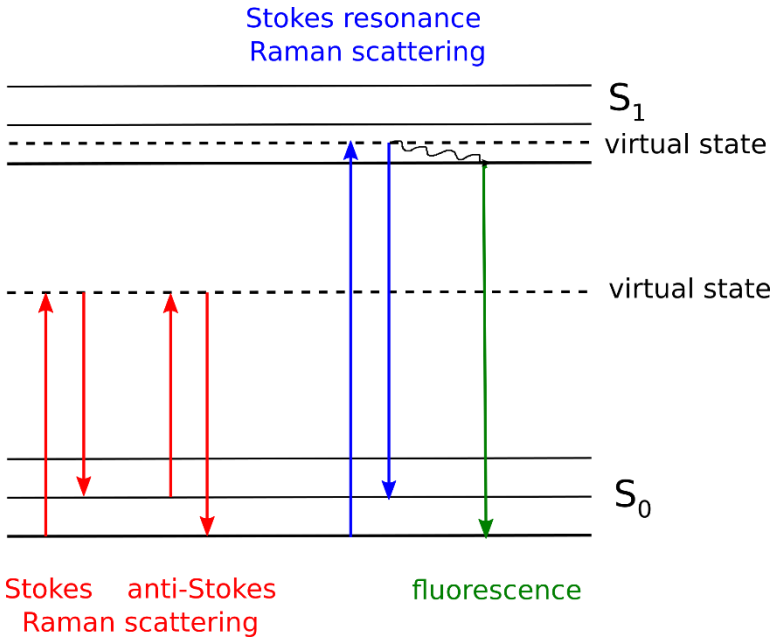

Fig. 1.1: Molecular energy levels diagram illustrating Stokes and anti-Stokes Raman scattering, resonance Raman scattering and fluorescence.

1.1.2 Application of Raman Spectroscopy

The development and present-day significant position of Raman spectroscopy was made possible by the introduction of lasers in the 1960s and sensitive CCD detectors in the 1990s.

NIR, VIS and UV radiation are employed for excitation. The advantage of high energy excitation (UV-VIS region) is a higher intensity of the RS which increases with the fourth power of frequency, however, it brings along possible excitation of fluorescence or activation of photochemical processes [8]. Many organic molecules

fluoresce when excited by high energy photons, in such case an excitation in the red end of the visible range or NIR is usually advantageous.

Acquisition of Raman spectra is rapid, non-destructive (with the exception of possible photoinduced changes of the sample when using high laser power) and usually without need of any special preparation of the sample. Raman spectroscopy is used for identification of compounds, study of molecular structure and molecular interactions. Raman cross section of water is low, which is a great advantage for analysis of water-based solutions and therefore biomolecules.

Raman spectrometers are either dispersion based or Fourier transform based. We will focus on the dispersion based spectrometers which are more common. They are composed of a laser as a light source, sample part, monochromator and CCD detection. Laser is used for the excitation because the light source has to be monochromatic in order to determine the freququency shift. In the case of ion gas lasers (such as argon and krypton), interference filters are employed to eliminate the lines of spontaneous emission of gas. There are two standard geometries of the instruments: 90° and 180° (backscattering geometry). The 90° geometry is advantageous because of minimalization of the Rayleigh scattering. In the backscattering geometry the light is delivered and collected by the same way. It is the case of Raman microspectrometers (Raman spectrometers equipped with an optical microscope). The light can be also conducted through optical fibers. An important part of the spectrometer is an edge or notch filter to remove the Rayleigh line from the scattered light. The RS is then dispersed by monochromator composed of grating(s) and detected by air or nitrogen-cooled CCD chip. Portable Raman spectrometers are available for Raman analysis in situ.

1.1.3 Raman microspectrometer

Raman microspectrometer is a Raman spectrometer equipped with an optical microscope. Nowadays, the microscope usually possess a confocal arrangement. It is the case also of the Raman microspectrometer LabRAM HR800 used for our measurements. The principle of confocality is demonstrated in Fig. 1.2. A pinhole is added in front of the detector in the confocal plane where the image of input pinhole is created. Its function is to eliminate the rays coming from spots out of the focal plane and in that way provide better resolution than classical optical microscope. Confocal microscope enables the reconstruction of three-dimensional structures from a set of optical sections obtained at different depths within a thick object. Combination of Raman spectrometer with a (confocal) microscope brings possibility of spectral mapping of the sample as well as higher signal to noise ratio and elimination of unwanted signal (e.g. of a support of the sample). Raman microspectrometer can be used for measurement of solid surfaces and small amounts of solutions. A general scheme of a Raman microspectrometer is shown in Fig. 1.3.

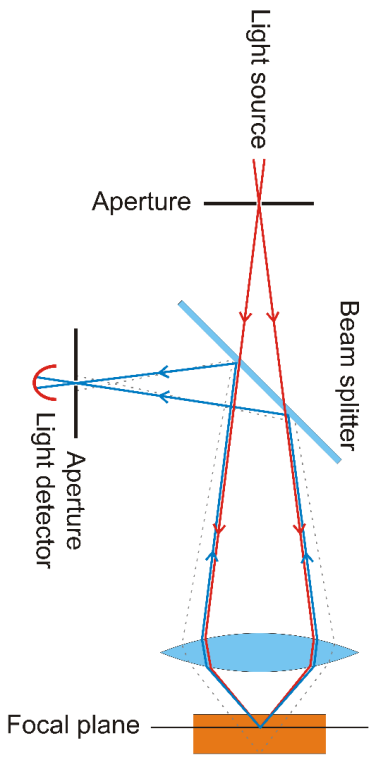

Fig. 1.2: Principal of confocal microscope. Reproduced from [**9**].

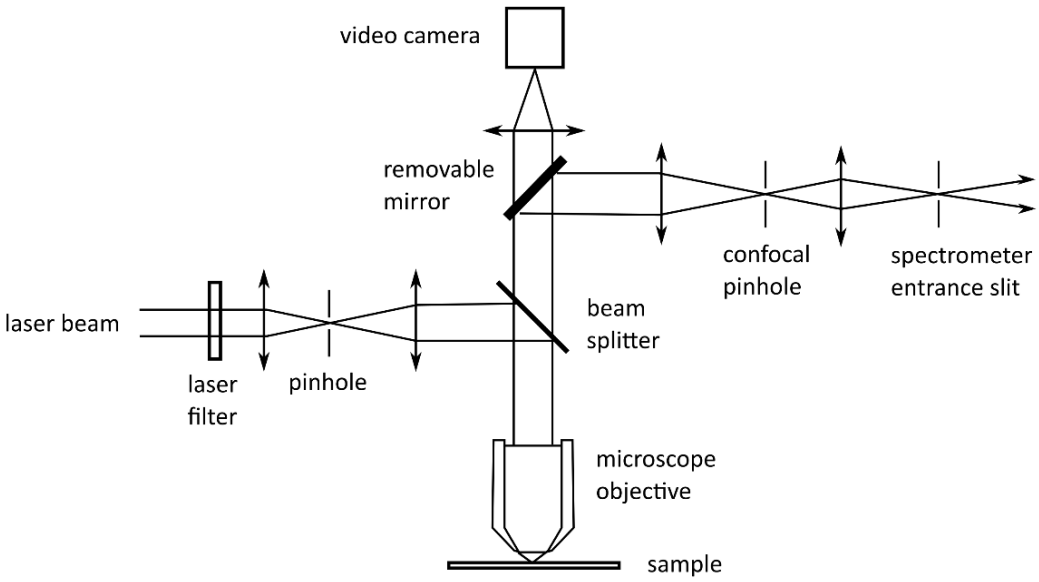

Fig. 1.3: Basic optical scheme of Raman microspectrometer.

1.2 Surface-Enhanced Raman Spectroscopy

Surface-enhanced Raman scattering (SERS) is the effect of enhancement of RS on rough metal nanostructures. It was discovered by M. Fleischmann in 1973 [10]. Fleischmann used an electrochemically roughened electrode with the intention to obtain observable Raman spectra of pyridine due to higher adsorbed amount of pyridine on the enlarged surface. In 1977 two groups noted independently that it is not possible to explain the unusually intense Raman signal just by a higher number of molecules [11, 12]. Jeanmaire and Van Duyne measured the dependence of the Raman signal of pyridine on the applied potential [11]. Their explanation of the behaviour of the bands´ intensities was "an electric field modulation of the RS tensor of the adsorbed molecule" dubbed electric field enhanced RS – an effect analogous to previously observed electric-field-induced enhancement of RS at semiconductors caused supposedly by excitons [13].

Albrecht and Creighton explored the change in the intensity of Raman signal of pyridine during one oxidation-reduction cycle. After the roughening part of the cycle, Raman signal of pyridine was higher, just as in Fleischmann´s experiment [12]. They compared the signal with the spectrum of liquid pyridine and calculated that after taking into account the increase in the electrode´s surface, there was a net enhancement of approximately 10^5. As a possible explanation they proposed RRS of the pyridine-metal system induced by the surface plasmons which had been suggested by Phillpot [14].

Later in 1977, after hearing a conference speech by Van Duyne about the effect of SERS, Mostkovits realized its connection to localized surfaced plasmon resonance (LSPR) he was dealing with in his own research [15] as he reminisces in [16]. Now we know that LSPR is the main cause of SERS enhancement. It is called the electromagnetic mechanism of SERS. Nevertheless, the presence of the metal influences the selection rules of the scattering as well as can contribute to further smaller enhancement. This is called the chemical (molecular) mechanism of SERS. In the following chapter we shall describe both mechanisms in more detail.

The scattered light intensity is proportional to the power of the induced electric dipole moment of the molecule

$$\mathrm{I} \sim |\vec{\mathrm{p}}|^2, \tag{2}$$

where according to (1) the relation for the dipole moment is

$$\vec{\mathrm{p}} = \vec{\alpha} \cdot \vec{\mathrm{E}}\,.$$

The light scattered by the molecule can be therefore principially enhanced by two mechanisms:

- by increasing the intensity of the local electromagnetic field $\vec{\mathrm{E}}$, which is the basis of the electromagnetic mechanism,

– by change of the polarizability $\vec{\alpha}$, which is the basis of the chemical mechanism.

The most important aspects of electromagnetic mechanism can be found in the SERS retrospective by Moskovits [17], for a summary of the theory of SERS and its application in biophysics are recommended the articles by Kneipp et al. [6] and Stiles et al. [18]. The theory of SERS is also explained in several books on SERS, e.g. Surface-Enhanced Vibrational Spectroscopy by Aroca [7], Principles of Surface-Enhanced Raman Spectroscopy by Le Ru and Etchegoin [20], Surface-Enhanced Raman Scattering edited by K. Kneipp, H. Kneipp and Moskovits [19] and the recent monography Surface-Enhanced Raman Spectroscopy by Procházka [21].

1.2.1 Theory of SERS

We will start with the explanation of the **electromagnetic mechanism**, the main source of the SERS enhancement.

The electromagnetic mechanism of SERS is based on the increase in the local electric field intensity near metal nanostructures caused by resonance excitation of localized surface plasmons (LSP) [26, 17]. Surface plasmons (SPs) are quasi-particles describing collective oscillations of free-electron plasma on a metal-dielectric interface induced by the incident electromagnetic radiation [22]. If the SP is coupled to a photon, the quasi-particle is called surface plasmon-polariton (SPP) [23]. When the SPs are confined to a space of a size comparable to the wavelength of the incident radiation, the collective oscillations do not propagate, but become localized [24]. We obtain LSP and localized surface plasmon-polaritons (LSPP). For specific frequencies LSPR occurs giving rise to areas with enhanced electromagnetic field. If a molecule is present in such a place, its RS will be enhanced compared to a situation without the metal structure.

We will now derive the plasmon resonance conditions in terms of classical physics. A comprehensive theory of light interacting with spherical particles was created by Mie [25]. However, in the case of spheres that are small compared to the wavelength of the incident radiation, the problem can be treated quasi-electrostatically.

Let us assume a metal sphere of radius a and complex relative permittivity $\varepsilon_m(\lambda)$ which is small compared to wavelength λ of the incident radiation, i.e. the Rayleigh approximation $a < \lambda/20$ is fulfilled. The sphere is surrounded by a dielectric environment with a constant relative permittivity ε_s. Under Rayleigh approximation we can treat the sphere as though it lies in a time-dependent electrostatic field $\vec{E}_0$ (in the z direction). The field produced by the sphere is a field $\vec{E}_d$ of an electric dipole positioned in the centre of the sphere and oriented in the z direction. Induced dipoles oscillate and irradiate at the same frequency as the incident field.

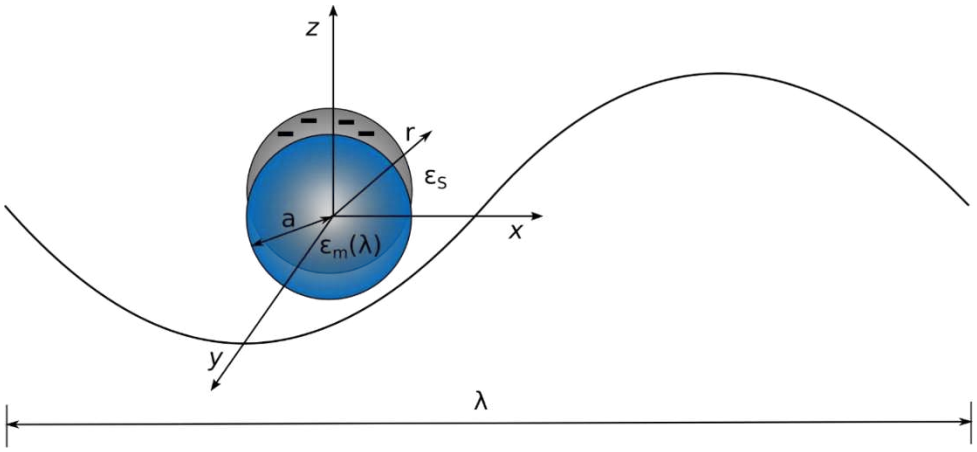

Fig. 1.4: Schematic representation of LSP in a metal sphere induced by an electromagnetic wave.

The resulting field $\vec{E}$ is a vector sum of the incident field $\vec{E}_0$ and a field of an electric dipole $\vec{E}_d$

$$\vec{E} = \vec{E}_0 + \vec{E}_d. \tag{7}$$

The enhancement $A(\lambda_L)$ in distance r from the metal sphere centre for the incident radiation with the wavelength λ_L equals [6]

$$A(\lambda_L) = \frac{E}{E_0} \propto g(\lambda_L)\left(\frac{a}{r}\right)^3, \tag{8}$$

$$\text{where } g(\lambda_L) = \frac{\varepsilon_m(\lambda_L) - \varepsilon_S}{\varepsilon_m(\lambda_L) + 2\varepsilon_S}. \tag{9}$$

The surface plasmon resonance takes place when the factor $g(\lambda)$ is maximal. It happens when the real part of the metal sphere relative permittivity equals

$$\mathrm{Re}\varepsilon_m(\lambda) = -2\varepsilon_s \tag{10}$$

and the imaginary part nears zero

$$\mathrm{Im}\varepsilon_m(\lambda) \approx 0\,. \tag{11}$$

The excitation of LSP can be pictured as all electrons in the sphere moving in response to the incident electromagnetic plane wave and as a result a time-varying build-up of polarisation charges on the surface of the NP is created (see Fig. 1.4). As a result an electric field with opposite direction appears that acts as a restoring force. At specific excitation frequencies this process leads to resonant oscillation.

Besides the incident field, the RS with the wavelength λ_S can be enhanced as well. The total enhancement factor EF is then

$$EF = |A(\lambda_L)|^2 |A(\lambda_S)|^2 \propto \left|\frac{\varepsilon_m(\lambda_L)-\varepsilon_s}{\varepsilon_m(\lambda_L)+2\varepsilon_s}\right|^2 \left|\frac{\varepsilon_m(\lambda_S)-\varepsilon_s}{\varepsilon_m(\lambda_S)+2\varepsilon_s}\right|^2 \left(\frac{a}{r}\right)^{12}. \quad (12)$$

For every metal and surrounding medium the resonance occurs at a different wavelength. The surrounding environment is usually air or water. The plasmon resonance conditions (10) and (11) are fulfilled by gold, silver, copper and some alcali metals for the visible light in these environments. For these metals $g \gg 1$ [17]. UV SERS is possible on aluminium or transition metals [27]. When $\lambda_L \approx \lambda_S$ the plasmon resonance is attainable for both the incident and the scattered radiation. In that case the SERS enhancement is the largest possible. It means that, assuming that the incident radiation is in resonance with the LSP, the spectral bands with the shortest Raman shift are enhanced the most.

The sizes of nanostructures in which LSPR can be excited are approximately in the range 5-100 nm [17]. Smaller structures are not able to support the surface plasmons. The upper limit depends on the wavelength of the excitation and is approximately given by the Rayleigh approximation a < λ/ 20, because for larger sizes the non-radiating higher multipoles cannot be neglected. The molecules of interest do not have to be adsorbed at the metal surface for the enhancement of RS to take place but the enhancement decreases very rapidly with distance as r^{12} as can be seen from the expression (12).

Apart from the material and size, the LSPR also depends on the shape of the nanostructures. The enhancement of the field near the metal sphere is 10^6-10^7 [26]. Shapes with high curvature produce higher enhancement. In SERS spectroscopy interacting and interconnected particles play a more important role than single NPs. Images of the enhanced field intensity based on computations for single particle and a dimer were published by Käll [28,29]. For two interacting particles devided by less then 1 nm and the incident field polarized along the axis of the dimer, the enhancement in between them can be even 10^{11} [17]. It illustrates that the enhancement also depends on the orientation of the polarization of the field. A space of such a high enhancement is called a "hot spot". The metal particles can create fractal-like structures, for example by the aggregtion of metal colloidal NPs or in the case of metal island films. The enhancement can equal that for dimers and the lack of translational symmetry in the NP aggregate causes resonance over a very broad range of wavelengths [17].

The **chemical mechanism** accounts for properties of SERS that cannot be explained by the electromagnetic mechanism as a result of changes the molecular polarizability $\vec{\alpha}$ due to interaction between the adsorbates and the metal surface [34, 20]. Roughness of the metal in the nanoscale is not important here. The interaction is so called chemisorption (interaction with energy less than -40kJ/mol [7]). The change in the molecule´s electronic structure causes changes in its spectrum compared to a free molecule. Depending on the nature of the molecule-metal interaction, several principles have been proposed [20]. Aroca states that the chemical mechanism can be in fact considered just as a special case of RRS [7]. The most significant theory for the changes in the polarizability is the charge transfer (CT) model [30, 7]. The CT can

occur when the Fermi level of the metal lies between the highest occupied molecular orbital (HOMO) and the lowest unoccupied molecular orbital (LUMO) (see Fig. 1.5). Upon the laser irradiation an electron from the metal can be excited to the LUMO energy level. If the excited state exists long enough, the molecular vibrations will adopt a new equilibrium state. Upon the transition of the electron back to the metal, a photon with the energy of the vibration is irradiated. Apart from the enhancement of the Raman signal, which is estimated as $10\text{-}10^2$ [31], shift of the spectral bands´ maxima or their width appear. The enhancenemts by the electromagnetic and the chemical mechanisms are multiplicative. A band belonging to the metal-molecule chemical bond may also appear in the spectrum. Unlike the plasmon resonance, the chemical mechanism is a first-layer effect due to the necessity of direct adsorbate-metal interaction.

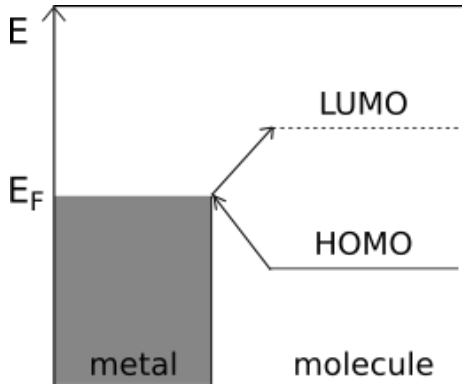

Fig. 1.5: Energy diagram illustrating the band structure of the metal and the HOMO and LUMO levels of the adsorbed molecule.

Surface-enhanced resonance Raman scattering (SERRS) occurs when the energy of the incident light is in resonance with both the LSP of the metal nanostructure and the adsorbed molecule. The difference between SERRS and the chemical mechanism is that in SERRS the electronic absorption transition corresponds to that of the free molecule whereas in the case of chemical mechanism new absorption transitions of the metal-molecule surface complex is created.

1.2.2 SERS-Active Substrates

SERS-active substrates must meet two principal requirements: (i) surface roughness on the nanometric scale which can support localized surface plasmons, and (ii) adsorption of the molecules of interest at the surface. Usually gold and silver are employed for preparation of the SERS substrates, less frequently also the transition metals and aluminium. Historically, the first SERS surfaces were roughened electrodes, vapour-deposited island films and colloidal suspensions. However, these substrates were not very reproducible. Then the achievement of the single-molecule detection by Kneipp in 1997 [32] and development in nanofabrication renewed the interest in SERS spectroscopy which resulted in design of many new types of SERS-active substrates with controlled size, shape and arrangement of the structure.

Nevertheless, roughened electrodes are still used for SERS because of the possibility to regulate the electrical potential. Aqueous metal colloidal suspensions are also still popular, mainly because of their easy preparation and high SERS enhancement when aggregated.

It is necessary to choose the SERS substrate according to the planned experiment, for example, whether high reproducibility or high enhancement is needed. Quantitative chemical analysis is one of the applications where reproducibility is essential. It is also important to take into account the molecule of interest, above all its charge, so that it would adsorb. To achieve better adsorption the chemical properties of the SERS substrate can be modified by functionalization of the substrate or by application of potential in the case of metal electrodes.

Several spectroscopic and imaging techniques can be used for characterization of SERS substrates, e.g. atomic force microscopy (AFM), scanning electron microscopy (SEM), UV-VIS absorption spectroscopy and X-ray photoelectron spectroscopy.

SERS-active substrates can be divided into colloidal suspensions and solid substrates. We shall now introduce the most important substrates with regard to substrates used in this thesis. Several reviews can be recommended as a source of the information about SERS substrates: Tian et al. (2002) [33], Lin et al. (2009) [34], Fan et al. (2011) [35] or Jahn et al. (2016) [36].

1.2.2.1 Metal colloidal suspensions

Suspensions of metal NPs are still very popular SERS substrates because they are easy and cheap to prepare, applicable in situ and very versatile. The most commonly used method of preparation is the chemical reduction although several other methods have been developed [34].

In the chemical reduction method the metal NPs are created by reduction of metal salt by a reducing agent, such as sodium borohydride (Creighton 1979) [37], trisodium citrate (Lee, Meisel 1982) [38] or hydroxylamine hydrochloride (Leopold, Lendl 2003) [39]. Ag colloids prepared using different reduction agents are compared in [40]. NPs of different size and shape can be created depending on the preparation procedure. Sizes of NPs for SERS spectroscopy usually lie between 10–80 nm [7]. Shapes of the NPs range from spheres to cubes, rods with various aspect ratios, triangles and many other [41]. Capping agents can be added to the reaction mixture to influence the growth of the NPs or to protect them from aggregation or oxidation [34]. Metals used for the colloidal solutions are usually Ag and Au. Metals can also be combined to prepare bi-metal NPs [42,43]. NPs with dielectric core and metal shell are also prepared [44].

The SPR properties of NPs are characterized by surface plasmon extinction (SPE) measured by the UV-VIS absorption spectrometer. The resonance is dependent on the metal, shape, size and aggregation state of the NPs. The trend is to prepare colloidal suspensions with narrow size distribution which makes them well-defined. FWHM of the SPE band corresponds to the size distribution of the NPs. When the particles agrregate, the band broadens and its maximum moves to longer wavelengths. This change of colour is often observable with naked eye. The stability of a colloidal

solution is characterized by zeta potential. Suspensions with zeta potential with absolute value higher than 30 mV are considered stable [45]. The NPs can aggregate spontaneuously during time or the aggregation can be induced by addition of the analyte. Colloids can be also aggregated intentionally by addition of aggregation agents, usually inorganic salts (NaCl, KI), in order to obtain higher SERS enhancement. On the other hand, the changing aggregation state, which is difficult to control, decreases reproducibility of the measurements. Stabilization agents can be added to obtain well-dispersed stable colloidal suspensions. The stabilizers are charged molecules or large molecules with the steric hindrance effect [34].

An example of a molecule used as a stabilization agent is polyethylene glycol (PEG). Stabilized isolated NPs are fundamental in the intracellular SERS experiments because bare Ag- and AuNPs aggregate in the cell culture medium and the intracellular environment. Maintaining the NPs well dispersed during their incubation to cells is important for their transportation through the cell membrane and their fate inside the cell. Isolated NPs should be less perturbing and should have a more homogeneous intracellular distribution which is crucial for SERS spectral mapping of cells [46]. Coating the Ag- and AuNP surfaces with a polymer layer such as polyethylene glycol (PEG) can also protect them from being captured by the immune system in vivo [47-49]. The NPs coated with longer PEG (molecular weight 2000−5000 g/mol [48,50,51] seem to be better suited for biological applications. There are more protocols to prepare PEGylated NPs as reviewed in [47]. PEG can even serve as a reducer of the metal salt in some of them, though to employ a more efficient reducer seems advisable. Procedure when PEG is added during the reduction, but sodium borohydride was employed as the reduction agent described in [51] was applied in this thesis. Thiol-terminated PEG 5000 (SH-PEG, MW 5000 g/mol) was used. The thiol terminal groups of the polymeric chains provide nucleation seeds during the early stages of the particle formation, resulting in a small NP size. Furthermore, the strong affinity of the thiol group for Ag ensures high stability of the resulting PEG-AgNPs against aggregation. This was seen even in the high ionic strength of biologically relevant media as was proven by dynamic light scattering (DLS) and UV−VIS spectroscopy [51].

The colloidal NPs can be also employed for indirect detection. For example, Raman marker (usually a molecule with a resonance Raman effect at the excitation wavelength) is adsorbed on the NP surface. Then the surface is further modified with an inert layer (e.g. SiO2, thiol-modified PEG) with a very weak Raman signal on which molecules that can specifically interact with the target molecules (antibody–antigen, biotin–avidin, aptamer–protein specific interaction) are linked [34]. It is used for indirect chemical analysis of the target molecules by detection of the SERRS signal of the Raman marker.

The problem of the chemical preparation as well as the use of stabilization agents is that they decrease the number of adsorption sites and their SERS signal may interfere with the signal of analyte.

1.2.2.2 NPs immobilized by drying

Another possibility is to use colloidal NPs immobilized directly on glass by drying of a colloid or colloid/analyte droplet on a glass substrate [20,52]. During evaporation the "coffee ring effect" [53] causes formation of a ring at the contact line of the drop containing most of the NPs [54]. Aggregation of the NPs upon drying leads to creation of fractal-like structures with "hot spots" with high SERS enhancement [20]. For example, SERS spectra of proteins were measured from the ring [55].

1.2.2.3 NPs immobilized by a self-assembled monolayer

Colloidal NPs can be immobilized on a solid substrate via a self-assembled monolayer of bifunctional molecules. This type of SERS substrate was first prepared in the 1990s [61]. The preparation procedure which was in detail described in a tutorial [63] is presented in Fig. 1.6. A glass slide is immersed into a solution of organosilane which creates on it a self-assembled monolayer. Then the functionalized slide is immersed into a metal colloidal solution. The NPs are attached by the end functional groups of the silane (–NH_2, –SH, –CN). Au- or AgNPs are mostly used. If a colloidal solution with narrow distribution of NP sizes is used, a well-defined SERS substrate is created. The result is a homogeneous and reproducibly prepared SERS substrate that is unlike the colloidal solution stable against aggregation and therefore can generate more reproducible measurements. Reported SERS enhancements range between 10^5-10^7 [21].

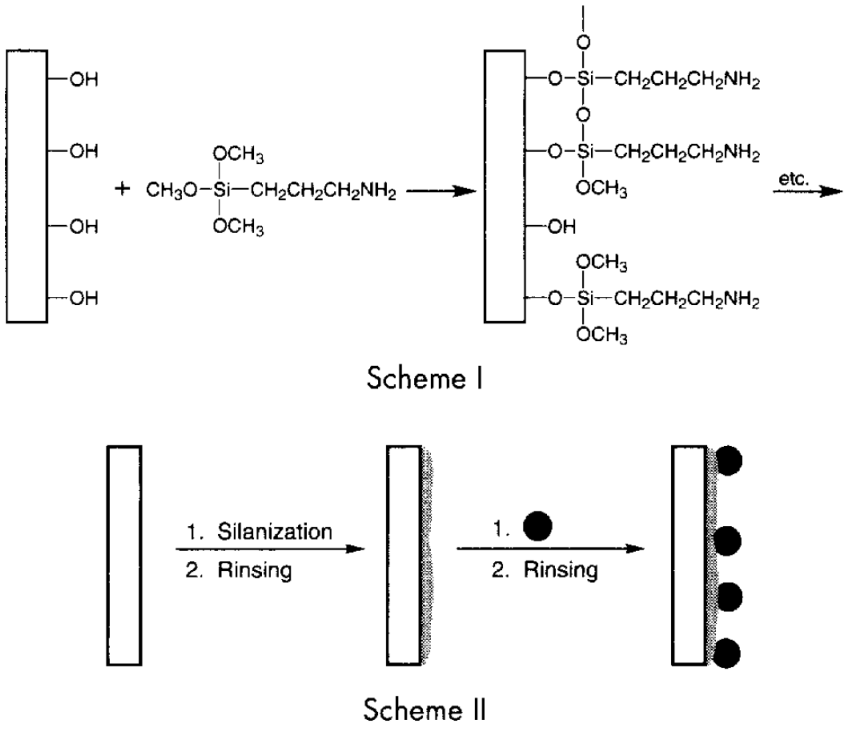

Fig. 1.6: Preparation of immobilized colloidal NPs on a solid substrate via organosilane. Scheme I: silanization of the solid substrate, scheme II: particular steps of the preparation. Reproduced from [63].

If the support slide is transparent, the SERS surfaces can be characterized by SPE spectra measured with UV-VIS absorption spectrometer.

Optimization of preparation parametres for gold and silver colloidal NPs immobilized via organosilane on a glass plate (further denoted as ImAuNP and ImAgNP) was conducted in our department by N. Hajduková [56,57] and P. Molnár [57], respectively, as a task of their master theses.

There are other SERS substrates using this approach. Mixture of Ag and Au NPs was used to prepare the SERS substrate [60] which brought the advantage that SERS of analytes that are able to adsorb at least at one of the metals could be detected. The Fan and Brolo prepared substrates with more linker and NP layers [58]. It was reported that reduction of the interparticle spacings by chemical or electrochemical methods can improve SERS enhancement [59].

1.2.2.4 Highly ordered SERS substrates

Nanofabrication methods have been developing rapidly in the last 20 years. This made possible preparation of a variety of well-defined highly ordered nanostructures on a solid support applicable as SERS substrates. The methods of preparation can be divided into two groups: maskless nanolithography (NL) methods and templating methods where a mask shelters certain portions of the substrate against metal deposition. This methods were reviewed in [21,35].

Nanolithographic techniques are based on a combination of shaping a resist layer by a beam of electrons (electron beam lithography – EBL) or ions (focused ion beam - FIB), etching and metal deposition [68]. The huge advantage of nanolithography is the precise control of the size of the metal features and distances between them.

Templating techniques use a mask. This mask is made by electrochemical etching that creates nanopores in an aluminium [69] or polycarbon membrane [70]. These pores are then basis for electrochemical growth of metal nanowires or nanotubes. Another way to prepare a mask is based on self-assembly of small colloidal spheres. This method is the principle of so-called nanosphere lithography (NSL) [71,72]. Several different types of nanostructures can be prepared by NSL – periodic triangle array (see Fig. 1.7), nanobowls, film-over-nanospheres (FON) [73-75]. NSL is a simple, inexpensive and reproducible nanofabrication technique.

The FON substrates are one of the SERS substrates used in this thesis. They were first introduced by Van Duyne´s group [75]. The preparation is shown in the left part of Fig. 1.7. A self-assembled monolayer (SAM) of polystyrene nanospheres is created on a solid support (glass, silica) either by spin-coating deposition or by the deposition on a liquid surface [76]. The nanospheres are then covered by metal (usually 100 nm and more). To prevent oxidation or to improve molecule adsorption FON substrates can be functionalized by SAM of thiols, aluminium oxide or other molecules [18]. FON substrates were, for example, applied as sensors of glucose in blood [77] and azorubine dye in drinks [78].

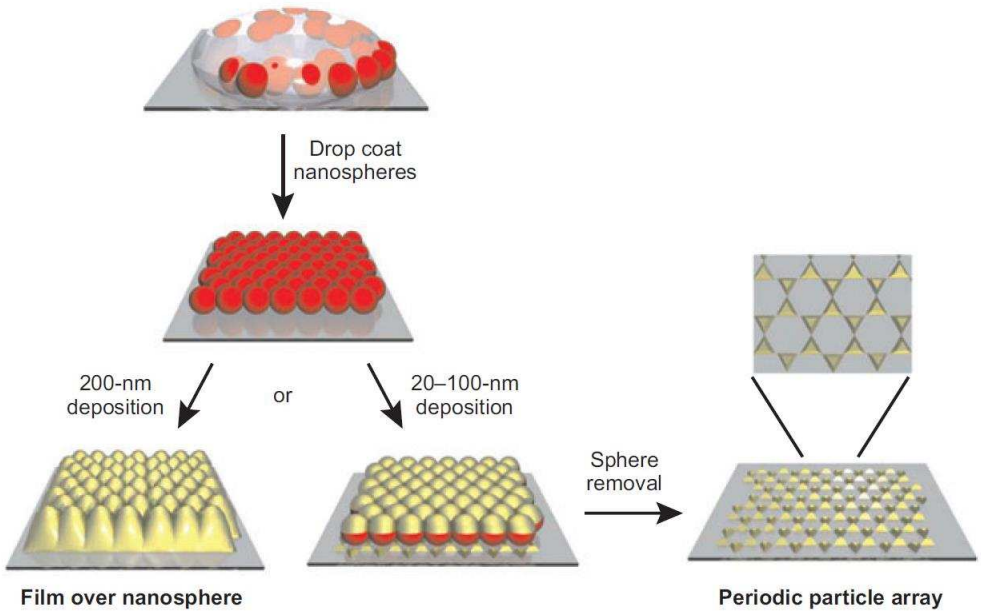

Fig. 1.7: Schematic representation of the nanosphere lithography process for fabricating metal FON and periodic particle arrays of metal nanotriangles. Reproduced from [18].

However, there are also other approaches than nanolithography and methods using masks to obtain highly ordered SERS substrates. One of them is biotemplating that uses a natural nanostrustructure as a template to prepare the SERS substrate. Complicated chemical processes present in the living nature create many fascinating structures that are difficult to imitate artificially. These are, for example, photonic structures giving various species of insects their iridescent colours or anti-reflective surfaces. Although these natural nanostructures on the bodies of insects are usually made of chitin, they show significant structural diversity. The SERS substrates can be fabricated simply by covering the biological object with a metal whithout removing the template or imprinting the object forming replicas [79].

Silver- or gold-plated wing areas of a butterfly species Graphium weiskei exhibiting conical nanostructures were used as SERS substrates for protein assaying [80]. Thermal evaporation was used for the metal deposition in this case. Cu-plated and Ag-plated replicas of rib structure of the butterfly wing scales were tested as SERS substrates using rhodamin-6-G [81,82].

The transparent wings of some cicada species present arrays of hexagonally ordered pillars with spacings of approximately 200 nm [83]. They were assessed as a SERS substrate in [83] or proposed as a possible stamp for nanoimprint lithography [79].

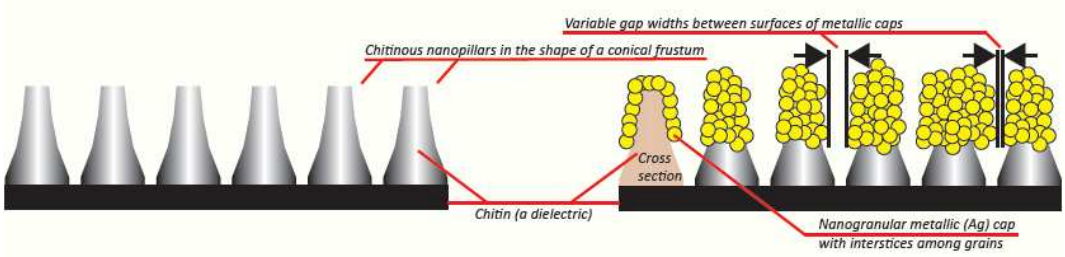

Fig. 1.8: Scheme of cicada nanopillars covered by electroless chemical plating. Reproduced from poster of the author for ICAVS 2013. The sheme was drawn by J. Proška.

In this thesis butterfly wings with rib structure and cicada wings were employed as SERS substrates. They were prepared by electroless silver plating. The basic electroless silver plating bath consists of silver nitrate, ammonium hydroxide, hydrazine hydrate and water. The problem of high hydrophobicity of micro-structured surfaces was surmounted by pretreatment of substrates with aliphatic alcohols. The technological process consists in mixing of solutions of silver salt with reducer in thin layer on the surface of processed material. A common method in holographic industry is spraying solutions by dual nozzle spray guns. The method creates grains of silver on the plated surface as is sketched in Fig. 1.8.

1.2.3 SERS of biomolecules

A number of studies published during the last few decades indicate that SERS is a feasible analytical technique for detection and indentification of biomolecules and biological systems including cells, viruses and microorganisms [21]. On the other hand, each application requires an appropriate combination of the studied molecule and SERS-active substrate. In this thesis, various derivatives of porphyrins, lipids and amino acid trypthophan were selected as probe biomolecules that can be detected directly without using chemical labels or derivatization chemistry.

Porphyrins are derivatives of porphin, an aromatic macrocycle composed of four pyrrole subunits interconnected at their α carbon atoms via methine (=CH−) bridges. In organisms they are present in metallated forms with a metal atom complexed to the nitrogens in the central part of the macrocycle, functioning as cofactors in proteins. One example is heme which is Fe-metallated protoporphyrin IX present in hemoglobin. Porphyrins without the complexed metal atom are called free-base porphyrins. Synthetic porphyrins have found application in molecular biology and medicine: in photodynamic therapy of cancer, antiviral treatment or selective detection of DNA sequences. All of these applications are based on porhyrins´ capability to bind to nucleic acids.

Porphyrins are very good SERS probes as they have strong Raman signal. A problem can present their metallation on Ag or Cu surfaces. SERS spectra are then mixtures of metallated and free-base porphyrin spectral bands and their ratio changes in time. Nevertheless, the effect of metallation can be also used for assessment of the SERS substrate.

Porphyrins were used as probes in the following studies containing Ag NPs: surface properties of ablated and chemically reduced Ag colloidal solutions [85], interaction of analytes with large biomolecules such as nucleic acids [86] and efficiency of different molecular spacers [87,88]. A quantitative analysis of two forms of H_2TMPyP, free-base (form I) and Ag^+-metallated (form II), was enabled using the intensity ratio of their characteristic metallation marker Raman bands [89]. Ag(0)-metallated TMPyP (form III) was observed after treatment of the NPs with chlorides (e.g. HCl, NaCl) or in a strongly reducing environment in the presence of an analyte capable to stabilize these sites [90].

The following porphyrins were used in this thesis:

- 5,10,15,20-tetrakis(1-methyl-4-pyridyl)-21H,23H-porphine (H_2TMPyP)
- 5,10,15,20-tetrakis(4-trimethylammoniophenyl)-21H,23H-porphine (H_2TMAP)
- 5,10,15,20-tetrakis(4-carboxypheny1)-21H,23H-porphine (H_2TCPP)
- 5,10,15,20-tetrakis(4-sulfonatophenyl)-21H,23H-porphine (H_2TSPP)
- 5,10,15,20-tetraphenyl-21H,23H-porphine (H_2TPP)
- protoporphyrin IX

Their chemical formulas are shown in Fig. 1.9.

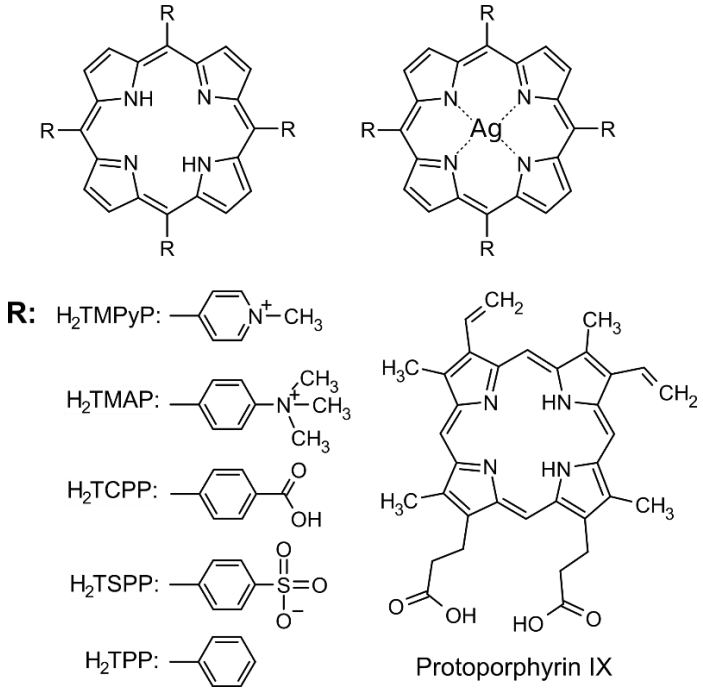

Fig. 1.9: Chemical formulas of studied porphyrins.

Tryptophan is an essential non-polar aromatic amino acid with indole side chain (see Fig. 1.10). Amino acids are the building blocks of proteins. Tryptophan is also a

precursor to the neurotransmitter serotonin and the hormone melatonin. Like other amino acids, tryptophan is a zwitterion at physiological pH where the amino group is protonated and the carboxylic acid is deprotonated [91]. Attribution of the SERS bands to molecular vibrations of tryptophan was done in [92]. A SERS detection in the concetration range of 10^{-8}–10^{-4} M was conducted in [93].

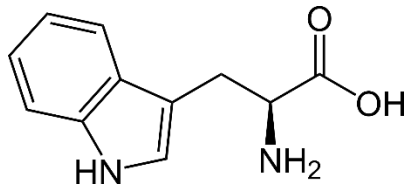

Fig. 1.10: Chemical formula of tryptophan.

Lipids have three main functions in the body: storing energy, signaling and acting as structural components of cell membranes. Major components of the membrane are phosholipids of amphiphilic character that is given by their composition of hydrophylic head and hydrophobic tail. They create a lipid bilayer with the hydrophylic heads inside the membrane and the hydrophobic tails aiming into the aqueous environment. In research synthetic membrane bilayer vesicles – liposomes and monolayers – micelles are often prepared. They can also be prepared from synthetic amphiphilic lipids not present in the natural structures.

Cationic lipids and liposomes are used as transfection vehicles to introduce a gene inside the cells, and in vivo cationic liposome-mediated transfection requires low detection limits of liposomes [94].

Raman spectroscopy can determine the order (gel)/disorder (liquid crystalline) properties of lipids according to the ratio of the C–H stretching vibrations in the 2800–3100 cm^{-1} region [95]. Lipids belong to poorly SERS-active species [96]. Although some SERS studies were already reported on model lipid membranes including Langmuir–Blodgett monolayers, hybrid bilayers, vesicles and micelles [96], SERS of lipids is a newly emerging area.

1,2-dimyristoyl-3-trimethylammonium-propane (DMTAP, see Fig. 1.11) was chosen as a model cationic lipid suitable for this study since it possesses a cationic head, which should benefit the adsorption onto the chemically prepared Ag NPs with a negative surface potential.

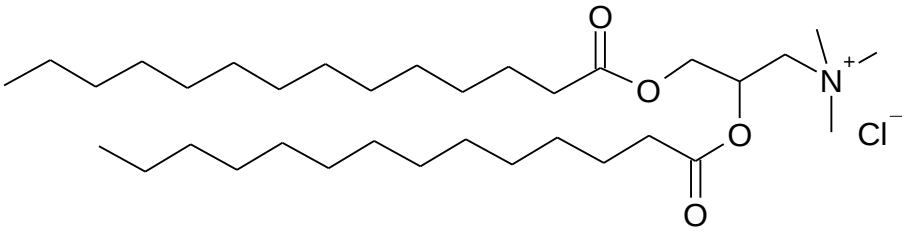

Fig. 1.11: Chemical formula of 2-dimyristoyl-3-trimethylammonium-propane (DMTAP).

Another lipid used in this thesis was 1,2-distearoyl-sn-glycero-3-phosphocholine (DSPC, see Fig. 1.12). This phospholipid should also adsorb well on the negatively charged Ag colloidal NPs Thanks to the positive head group.

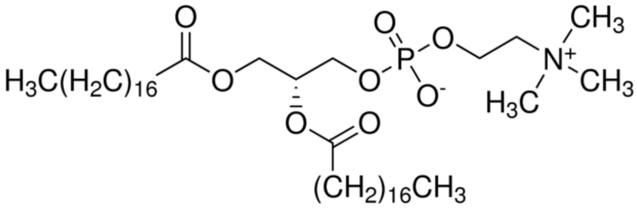

Fig. 1.12: Chemical formula of 1,2-distearoyl-sn-glycero-3-phosphocholine (DSPC).

2 Aims of the thesis

The goal of this thesis was the use of surface-enhanced Raman microspectroscopy for study of biomolecules and biological systems (including living cells).

Various derivatives of porphyrins, lipids and amino acid trypthophan were selected as probe biomolecules that can be detected directly without using chemical labels or derivatization chemistry. Several types of SERS substrates were tested for SERS microspectroscopy of biomolecules, namely Au and Ag colloidal NPs immobilized on solid substrate by a self-assembled monolayer of organosilane, Ag colloidal NPs immobilized by drying, PEGylated Ag colloidal NPs and ordered nanostructures – Au- and AgFONs and Ag-coated natural templates (insect wings).

In the topic of immobilized colloidal NPs the aim was to continue in experiments with hydroxylamine-reduced AgNPs immobilized by drying done in my master thesis and to find out whether the exquisite LOD is also achievable for other biomolecules.

Another aim was to test the efficiency of PEGylated Ag NPs to detect porphyrins of different size and charge. Beside that our aim was to try out the PEGylated-NPs with porphyrin for possible intracellular applications. This study was conducted in cooperation with J. Gautier and I. Chourpa from the University of Tours, France.

Our final goal was to assess the reproducibility and sensitivity of ordered substrates – FONs and metal-coated insect wings. This was done in cooperation with L. Štolcová and J. Proška from the Faculty of Nuclear Sciences and Physical Engineering, Czech Technical University in Prague, who prepared the SERS substrates.

3 Experimental

3.1 Instrumentation

3.1.1 Confocal Raman Microspectrometer

LabRAM HR800 with Olympus BX40 microscope by Horiba Jobin Yvon was used for SERS and Raman microspectroscopy experiments. It includes a Czerny-Turner monochromator (300, 600 or 1800 grooves/mm diffraction gratings) and liquid nitrogen cooled CCD. There are two excitation lasers – integrated He-Ne laser (632.8 nm, output power 20 mW) and Ar^+ laser by Melles Griot (514.5 nm laser line used, output power 40 mW). The scattering is collected in 180° (backscattering) geometry. The elastic Rayleigh scattering is eliminated by an edge filter. A video camera enables observing the sample and focusation. The sample stage is movable by piezoelectric motors along all three axes with a 1 μm step. The confocal slit can be adjusted between 0–1000 μm. The spectral resolution of the microspectrometer is 2-4 cm^{-1}.

The laser light was let through the optics for about an hour before the measurement to thermally stabilize the system. The calibration was verified by checking the position of the most intense Raman band of silicon at 520.7 cm^{-1}. The spectra were acquired at room temperature (20 ºC). Unless stated otherwise the confocal slit was set to 400 μm and the entrance slit to the monochromator to 100 μm, objective ×100, 600 grooves/mm diffraction grating was used. The spectra can be viewed in the Real Time Display (RTD) mode or accumulated.

The samples of ImAuNP and ImAgNP (1×2 cm metal colloid covered glass plates), FONs and insect wings were attached to a microscope slide by double-sided adhesive tape. The droplets were dried directly on a clean microscope slide.

The same confocal Raman microspectrometer LabRAM HR800 by Horiba Jobin-Yvon, although with air-coold CCD, was used for SERS experiments in France. Two dispersion gratings of 300 and 1800 grooves/mm were available. The 632.8 nm line of the built-in He-Ne laser and 488.0 nm line of Ar^+ laser were used for excitation.

3.1.2 Raman Spectrometer

The classical macro-Raman spectrometer was used for experiments with PEGylated AgNPs. It is a home-built instrument with a 1800 grooves/mm diffraction grating monochromator (Jobin Yvon Spex 270 M) and a liquid nitrogen cooled CCD (Princeton instruments). Laser lines 441.6 nm (He-Cd laser, Liconix, approx. 3 mW at the sample) and 532.0 nm (a diode-pumped frequency-doubled Nd:YVO_4 laser Verdi, Coherent, approx. 100 mW at the sample) were used for excitation. The lasing power can be reduced by density filters. The light scattered by a sample in the 1×1 cm cuvette is collected in 90º configuration, which minimizes the elastic scattering contribution. The elastic scattering is supressed by an edge filter. The spectra were acquired at room temperature (20 ºC). Calibration spectra of neon lamp were measured before each acquisition of the sample spectrum.

3.1.3 Other Instrumentation

Surface plasmon extinction (SPE) spectra of the colloids used for preparation of ImAuNP and ImAgNP and of these substrates were recorded by UV-VIS absorption spectrometer Lambda 12 by Perkin Elmer. In the case of the PEGylated Ag colloid, SPE spectra were measured using a UV−VIS absorption spectrometer Specord 250, Analytik Jena.

The hydrodynamic diameter was measured by dynamic light scattering (DLS) using an Autosizer 2c (Malvern Instruments, Orsay, France) equipped with a He−Ne laser operating at 632.8 nm (output laser power 4 mW), with a scatter angle of 173°. A Malvern NanoZ (Malvern Instruments, Orsay, France) with a He−Ne laser operating at 632.8 nm (output laser power 4 mW), with a scatter angle of 17°, was used on the same samples to determine the zeta potential of the NPs. In both cases, the samples were diluted in deionized water or in NaCl solutions (0.1 M). Each measurement was performed at 25 °C at least three times.

SEM images were acquired by scanning electron microscope JEOL JSM-7500.

3.2 Preparation of SERS Substrates and Samples

3.2.1 Au Colloidal Suspension

The ImAuNP were prepared by Natália Hajduková-Šmídová using citrate-reduced Au prepared according to Keating et al. [63]. 250 ml of 1mM chloroauric acid $HAuCl_4$ solution is brought to the boiling point and then 25 ml of 38.8mM trisodium citrate $C_6H_5O_7Na_3 \cdot 2H_2O$ solution is added. The initial yellow colour of the solution turns into dark blue, which gradually changes into dark reddish violet. The mixture is boiled for 15 min and then left to cool. The extinction maximum of the colloid is approximately 525 nm.

Although ImAuNP substrates were prepared during her PhD, they could be used because they show long-term stability.

3.2.2 Ag Colloidal Suspensions

The borohydride-reduced colloid was prepared according to [98] which uses slightly modified procedure optimized by Garrell et al. [97] going out from the original recipe by Creighton [37]. 3.5 mg of sodium borodydride ($NaBH_4$) was diluted in 75 ml of deionized water (1.2×10^{-3} M solution), then cooled in an ice cooling bath to 2 °C, placed on a magnetic stirrer where 9 ml of refridgerated 2.2×10^{-3} M $AgNO_3$ solution was added dropwise. The colloidal solution is then stirred for approximately 45 min to reach the room temperature. The final colour is yellow-brown. The extinction maximum lies around 390 nm.

Hydroxylamine-reduced Ag colloid was prepared according to one of the procedures by Leopold et al. [39]. 4.5 ml of 0.1 M NaOH is added to 5 ml of 6×10^{-2} M hydroxylamine hydrochloride $NH_2OH \cdot HCl$ solution to provide alcaline pH. It is then

added to 90 ml of 1.11×10^{-3} M $AgNO_3$ solution. The mixture is shaken until it obtains a milky gray colour. The extinction maximum is approximately 410 nm.

3.2.3 ImAuNP and ImAgNP

The preparation procedure of these substrates was generally described in the part 1.2.2 of the Introduction. Clean glass plates of approximately 1 × 2 cm were immersed into 10% solution of (3-aminopropyl)trimethoxysilane in methanol for 30 min. After silanization, the substrates were rinsed several times with methanol and deionized water to remove unbound silane which could cause aggregation of the colloidal NPs. After that, the substrates were soaked separately (to prevent destroying of the whole set) in vials with 1 ml of the citrate-reduced Au colloidal solution for 3–4 h in the case of ImAuNP or in a borohydride-reduced Ag colloidal solution for 6 h in the case of ImAgNP. Most of the successful ImAgNP were prepared using borohydride-colloid heated during its preparation to 80–90 ºC. Finally, they were rinsed with deionized water. The ImAuNP were subsequently heated at 100 ºC for 10 min which led to appearance of a long-wavelength extinction band. As a result the SERS spectrum is composed of two overlapping bands at 520-530 nm and 600-650 nm. This structure was stable in time [56]. The SERS substrates were stored at a dark place.

SERS systems were prepared by dipping of the Ag substrate into H_2TMPyP solution for 15–20 min and then measured.

3.2.4 AgNPs immobilized by drying

The other SERS system of immobilized colloidal NPs were drops of hydroxylamine-reduced Ag colloidal suspension mixed with the adsorbate solution. Several microliters (usually ~2 μl) were pipetted carefully on a clean microscope slide and left to dry at a room temperature.

3.2.5 PEGylated Ag Colloidal Suspension

The PEG-AgNPs were prepared according to [51], which is a modification of the method described in [99]. The reaction was carried out under nitrogen atmosphere to prevent oxidation of the reducer $NaBH_4$ and polyethylene glycol during formation of the metal NPs. 4 ml of 7.5 mM $AgNO_3$ ethanol solution was mixed with 75 mg of PEG-SH powder and sonicated for 5 min. Ag reduction was achieved by a dropwise addition of 1.3 ml of 90 mM $NaBH_4$ ethanol solution to the $AgNO_3$ solution with PEG-SH under vigorous stirring. After 2 h reaction time in the dark, the obtained brown suspension was diluted four times with deionized water and dialyzed against deionized water to remove the excess of PEG molecules. Both batches (PEG1-Ag and PEG2-Ag) were reconcentrated by evaporation to 1 g of Ag per liter, to use them at the same concentration.

PEG-AgNPs/porphyrin and borohydride-reduced Ag NPs/porphyrin systems were prepared by the addition of an appropriate amount of a porphyrin solution to the NP suspension. H_2TCPP, H_2TPP, and protoporphyrin IX had to be dissolved in DMSO

first, and then they were diluted with water. The concentration of the water-insoluble porphyrins was achieved only approximately. NaCl was added after porphyrins, its final concentration in the Ag NP/porphyrin system being 0.01 M in all SERS experiments.

3.2.6 HeLa cells

Human cervix epitheloid carcinoma HeLa cells were cultured according to protocol used in Prof. Chourpa´s laboratory which is described for example in [100]. The culturing medium was aspirated taking with it dead cells. The living cells were detached from the wall of the flask by a short incubation with trypsin, then moved to a Falcon tube and centrifuged. The obtained cell pellet was resuspended in fresh culture medium and the cells were seeded in well plates with clean microscope cover slips previously covered with poly-D-lysine improving attachment of cells to glass at the bottom. Manipulation with the cell culture was done in a laminar flow cabinet to avoid contamination. PEGylated AgNPs mixed with solution of H_2TMPyP were added to the cells. For the SERS measurement the circular cover slip with cells was placed on a microscope slide and covered with another slip.

3.2.7 Film over nanosphere substrates

The FON substrates were prepared by Lucie Štolcová at The Department of Physical Electronics, Faculty of Nuclear Sciences and Physical Engineering, Czech Technical University in Prague, by a method of deposition on a still water surface [101,76]. Cleaned glass substrates (approx. 1×1 cm) were placed closely next to each other on the bottom of a cleaned Petri dish with water. Aqueous dispersions (10 wt %) polystyrene (PS) nanospheres of (253±8 nm sphere diameter) purchased from MicroParticles GmbH (Berlin, Germany) were mixed with ethanol (1:1 v/v), stirred by ultrasound and carefully deposited on the water surface in the Petri dish using a glass pipette. Although polystyren has a higher density than water, the PS spheres keep on the surface due to the surface tension of water. The microspheres tend to form a monolayer with hexagonal order. After several days most of the remaining water was sucked away, thus transfering the monolayer of the nanoparticles on the glass substrate. They were left to dry for several days at ambient conditions. Thin layers of Au or Ag (20 or 40 nm in thickness) were applied by magnetron sputtering deposition on the PS templates in Cressington 208HR sputter coater.

FONs were dipped into solution of H_2TMPyP for several hours and then dried by nitrogen flow.

3.2.8 Metal-coated insect wings

These substrates were prepared by RNDr. Jan Proška at The Department of Physical Electronics, Faculty of Nuclear Sciences and Physical Engineering, Czech Technical University in Prague. Wings of a cicada Cryptotympana aquila and a butterfly Papilio palinurus were covered with Ag by electroless plating. The basic electroless silver

plating bath consists of $AgNO_3$, NH_4OH, hydrazine hydrate $N_2H_4 \cdot H_2O$ and water. The problem of high hydrophobicity of micro-structured surfaces was overcome by pretreatment of the substrates with aliphatic alcohols. On some samples a <2 nm layer of Au was deposited on the Ag surface by magnetron sputtering.

Another batch of cicada wings samples was covered with Ag by magnetron sputtering.

For the SERS experiments, 8µl drop of aqueous solution of the adsorbate was pipetted on the Ag-coated wing and left to dry at ambient conditions.

4 Results and Discussion

This chapter presents results of my doctoral research. The chapter 4.1 contains results obtained from metal colloidal NPs immobilized on a solid substrate. As my Ph.D. thesis followed my master thesis [102], the chapter contains also some data obtained during the master thesis.

A study of SERS of porphyrins on PEGylated silver colloid is summarized in the chapter 4.2. At the end of the chapter, a SERS experiment on human cancer cells is described. Finally, the chapter 4.3 addresses experiments carried out on ordered SERS substrates prepared by Lucie Štolcová and Jan Proška, namely film over nanospheres (FON) and silver-coated insect wings.

Most of the results have been published in peer-reviewed articles in international journals. The articles are attached at the end of the thesis. The first article [I] contains data on the performance of ImAgNP and dried drops of AgNPs and the article [II] describes sensitivity and reproducibility of SERS microspectroscopy from ImAuNP substrates. Both papers contain some data obtained during my master thesis. Since the experiments and both papres were completed during my Ph.D. thesis, they have been included. The articles [III], [IV], [V] are based on data obtained during my doctoral study.

4.1 Metal Colloidal NPs Immobilized on a Solid Substrate

4.1.1 ImAuNP

ImAuNP substrates prepared by the method optimized by Natália Hajduková during her doctoral study (see Experimental, part 3.2.3) were used for the SERS experiments. Free-base porphyrin 5,10,15,20-tetrakis(1-methyl-4-pyridyl)porphyrin (H_2TMPyP) was employed as the probe molecule to determine SERS sensitivity and spectral reproducibility of ImAuNP.

The ImAuNP were characterized by SEM and SPE. The SEM image (see Fig. 4.1) shows that the glass plate is totally covered by AuNPs and small aggregates. SPE spectra of the citrate-reduced Au colloidal suspension used for the preparation and of an ImAuNP substrate are shown in Fig. 4.2. The used excitations 514.5 nm and 632.8 nm both fall into the plasmon resonance of the ImAuNP, thus fulfilling the prerequisite for SERS (see Fig. 4.2, spectrum b). Broadening of the plasmon resonance compared to the SPE spectrum of the initial colloidal suspension (Fig. 4.2, spectrum a) is probably caused by aggregated NPs which have plasmon resonance red-shifted compared to isolated NPs. This is in agreement with the observation of aggregates in SEM images. In the case of 514.5 nm excitation, the excitation line coincides with the electronic absorption Q-band of H_2TMPyP with maximum at ~518 nm (Fig. 4.2, spectrum c), therefore SERRS spectra of H_2TMPyP are observed.

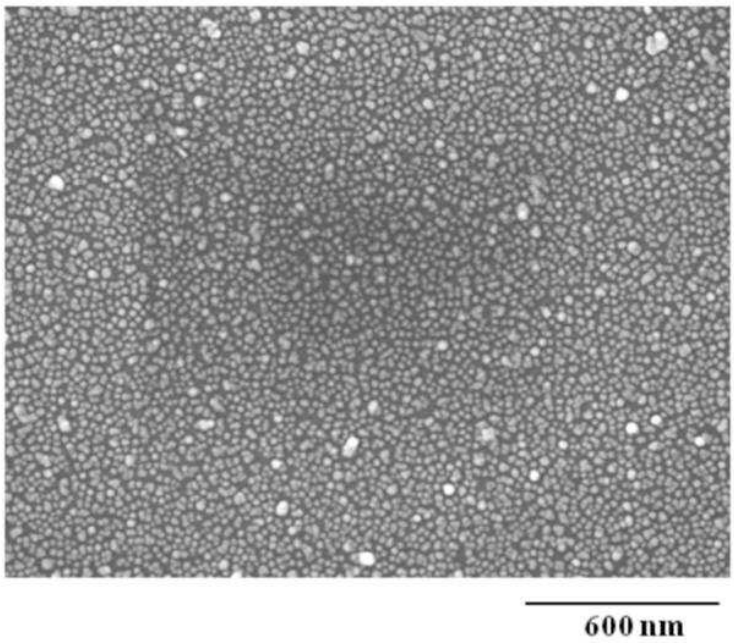

Fig. 4.1: SEM image of ImAuNP (performed by B. Šmíd, National Institute for Materials Science, Tsukuba, Japan).

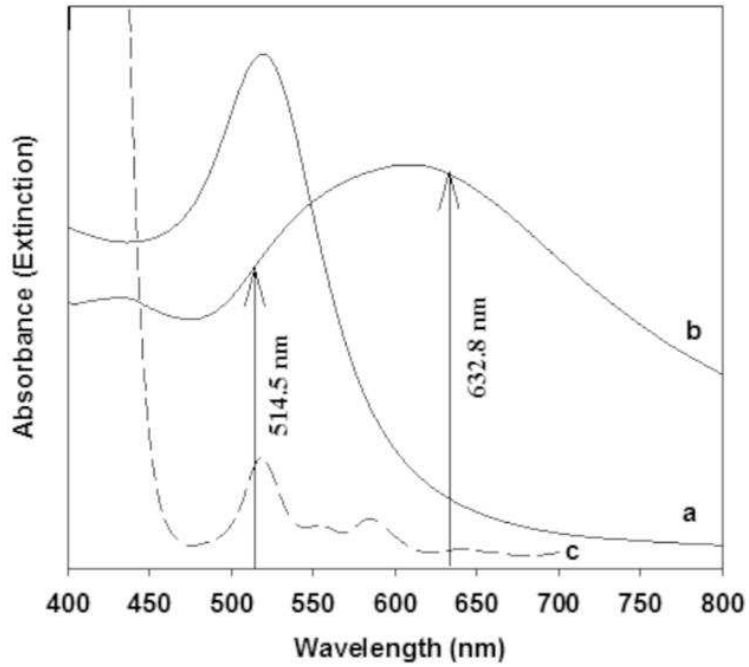

Fig. 4.2: SPE spectra of the parent Au colloidal suspension (a), ImAuNP (b) and the electronic absorption spectrum of H_2TMPyP solution (c). The excitation wavelengths are represented by arrows.

The thermal decomposition of the sample can sometimes occur using Raman microspectrometer due to the high energy density in the focused laser beam. In our case, no adsorbate decomposition was observed for laser powers below 0.2 mW that

were sufficient to acquire good H_2TMPyP spectra. In the case of higher laser powers, strong bands appeared in the spectral region 1300–1600 cm^{-1}. They were either fluctuating narrow bands or two broad bands with maximum at ~1350 cm^{-1} and ~1580 cm^{-1}, which are probably the narrow bands accumulated to the broad ones. The broad bands were assigned to amorphous carbon [103].

One way to determine the enhancement of Raman signal by a SERS substrate is the analytical enhancement factor (AEF) defined as the ratio of SE(R)RS intensity I_{SERS} and (resonance) Raman intensity I_{RS} divided by their corresponding molar concentrations [104]:

$$AEF = \frac{I_{SERS}/c_{SERS}}{I_{RS}/c_{RS}} \tag{13}$$

The stumbling block of this simple definition of SERS enhancement is the fact that only molecules adsorbed at the substrate contribute significantly to the signal. To get an AEF that is reliably related to the SERS substrate it is therefore necessary to calculate it using I_{SERS} obtained for submonolayer coverage by the analyte [104]. We calculated the enhancement factor with an estimation of molar concentration that corresponds to the amount of H_2TMPyP adsorbed to the substrate. The substrate was dipped into 1×10^{-6} M H_2TMPyP solution. In my bachelor thesis it was determined by absorption measurements that for the soaking concentration 1×10^{-6} M the adsorbed amount corresponds to molecular concentration $c_{SERS} = 1\times10^{-7}$ M [105]. Converted to the surface density using the volume of the solution and SERS substrate area, it makes approximately 10^{14} molecules/cm^2, which corresponds to submonolayer coverage of metal colloidal NPs [85]. The integral intensity of the strongest band (here 1555 cm^{-1} for 514.5 nm and 976 cm^{-1} for 632.8 nm excitation) of SE(R)RS and (R)RS was used as I_{SERS} and I_{RS}, respectively. Raman spectra of H_2TMPyP were measured from a drop of H_2TMPyP solution of the concentration $c_{RS} = 1\times10^{-3}$ M. Thus, AEF was determined as ~10^5 and ~10^6 at 514.5 nm and 632.8 nm, respectively.

ImAuNP substrate sensitivity can be expressed by the limit of detection (LOD). A way to determine LOD was described in [106] as extrapolation to the concentration for which the intensity (height) of the strongest porphyrin band exceeds a triple of the standard deviation of the blank sample signal[1]. SE(R)RS spectra were measured in the concentration range of 6×10^{-8} M–1×10^{-5} M. The best spectrum for each concentration was chosen for the extrapolation which gave the LOD 6.5×10^{-8} M and 4.0×10^{-8} M soaking concentrations for 514.5 nm and 632.8 nm excitation, respectively. It is

[1] Details of the LOD calculation: First, the standard deviation of a blank sample was determined: each spectrum was smoothed by a Savitzky-Golay filter and subtracted from the original spectrum. Thus, a spectrum of noise was obtained. Then the standard deviation of the noise σ was calculated. Dependence of 3σ on molar concentration of the analyte was plotted. By the extrapolation to zero the value of 3σ for a blank sample was obtained. Finally, from the concentration dependence fitted with a suitable curve, we determine the LOD – the concentration for which the SERS signal is equal to 3σ.

comparable to the value 5×10^{-8} M achieved by the classical Raman spectrometer at 514.5 nm in the same type of SERS substrate [57].

To assess the macroscopic spectral reproducibility, spectra were taken from 8 spots of an ImAuNP substrate. Relative standard deviation of the SERS signal was 15.3%.

Spectral mapping of the surfaces provided information about reproducibility on µm-scale with mapping steps 2 or 20 µm (Fig. 4.3). The measured spectral maps were treated by factor analysis (FA) in a CellViewer sotfware created in MATLAB by our collegue Dr. Jan Palacký. FA is a statistical method based on singular value decomposition algorithm and it is used to reduce the size of a dataset without loss of information [107]. The intensity maps are constructed from the normalized coefficients of the first subspectrum of the factor analysis (the intensity is the most significant factor here). The map for the excitation wavelength 514.5 nm showed uniform intensities, while for the wavelength 632.8 nm a few spots provided several times higher intensities, which we ascribed to excitation of "hot spots" formed by Au aggregates (see Fig. 4.3).

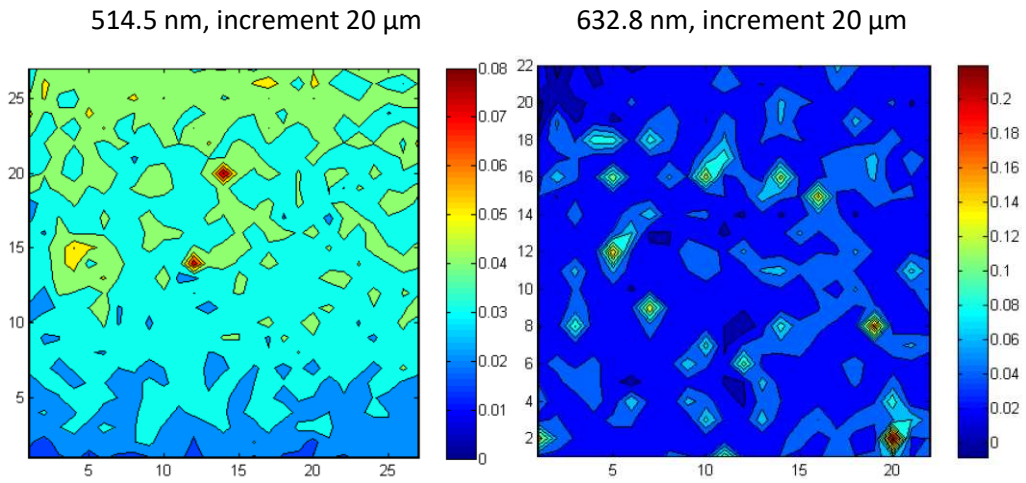

Fig. 4.3: Spectral maps of H_2TMPyP (1×10^{-6} M soaking concentration) on Au substrate: excitation 514.5 nm and 632.8 nm, 20 µm between mapping points. The scale represents a relative intensity.

4.1.2 ImAgNP

ImAgNP substrates were prepared using the borohydride-reduced colloidal AgNPs according to the procedure optimized by Peter Molnár (see the Experimental, part 3.2.3). The aim was (similarly to the ImAuNP) to determine their applicability for SERS microspectroscopy using H_2TMPyP as a probe molecule.

Characterization by SEM (see Fig. 4.4) showed that unlike the ImAuNP a complete monolayer of metal NPs was not formed. ImAgNP have SPE bands at ~390 nm and ~465 nm (see Fig. 4.5). Only the excitation 514.5 nm was used because the excitation 632.8 nm is out of the plasmon resonance.

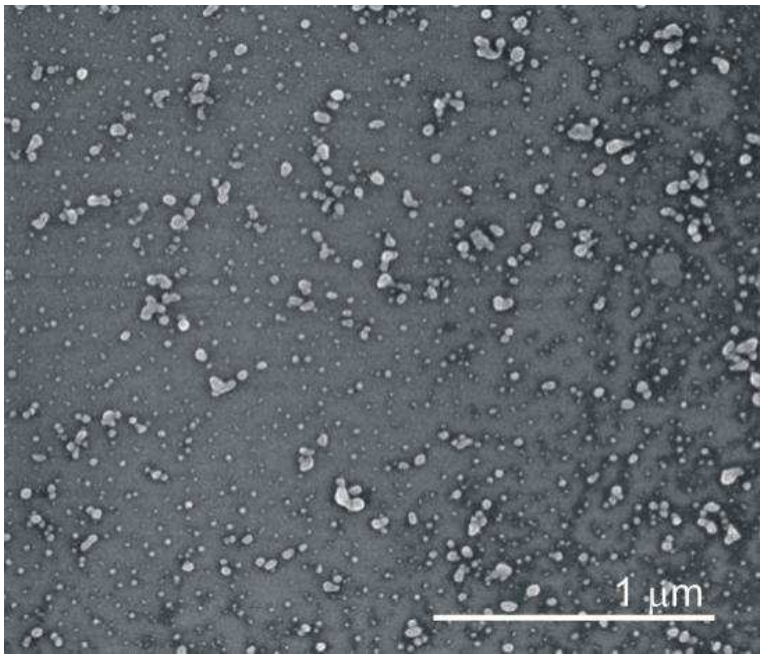

Fig. 4.4: SEM image of ImAgNP substrate.

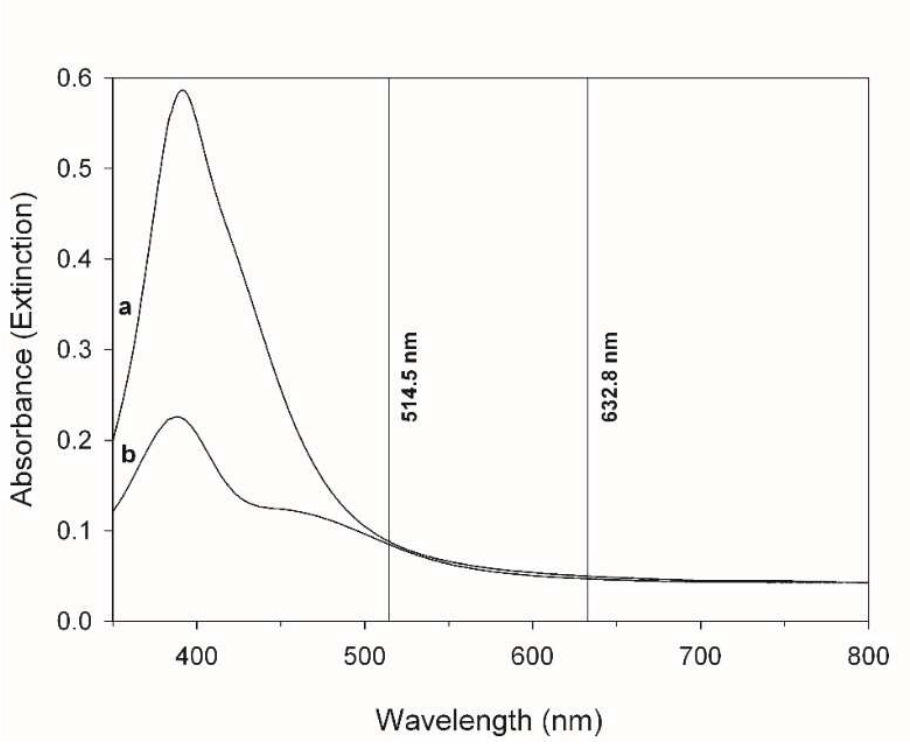

Fig. 4.5: SPE spectra of parent borohydride-reduced Ag colloidal suspension (a) and a ImAgNP substrate (b).

Typical SERRS spectra of H_2TMPyP for concentrations 1×10^{-7}, 3×10^{-7} and 1×10^{-6} M are shown in Fig. 4.6. LOD 1×10^{-8} M was determined from SERRS spectra in the concentration range 1×10^{-8}–1×10^{-6} M by the same method as in the case of

ImAuNP. The detection is slightly more sensitive than for ImAuNP where it was 6.5×10^{-8} M, which agrees with the fact that silver provides higher electromagnetic enhancement than gold. On the other hand, it is almost an order of magnitude worse than the value obtained for ImAgNP using macro-Raman (3×10^{-9} M) [57]. The reason why a better sensitivity could not be achieved was a decrease of the H_2TMPyP with the accumulation time and the presence of spurious bands of amorphous carbon in the 1200-1700 cm^{-1} region [103]. Their main source is probably thermal decomposition of the organosilane linker as they were as often present in the spectra from a bare ImAgNP surface, less on ImAuNP with better coverage by the NPs and lower SERS enhancement, and rarely present in SERS spectra of TMPyP from the dried Ag NPs droplets where no organosilane is present.

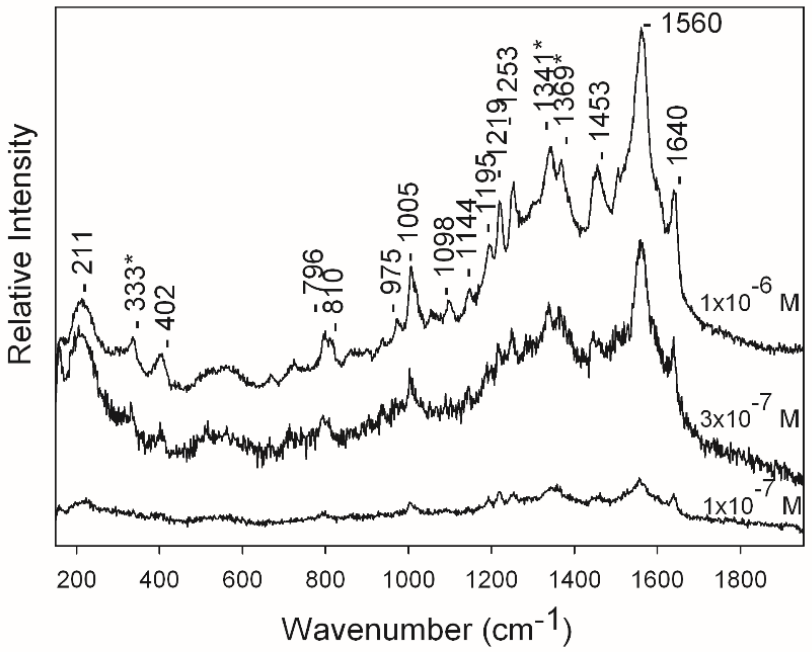

Fig. 4.6: SERRS spectra of various H_2TMPyP concentrations measured from AgNPs immobilized on a glass plate by organosilane: 1×10^{-7} M (~0.02mW at the sample, 5×12 s), 3×10^{-7} M (~0.02 mW at the sample, 5×12 s) 1×10^{-6} M (~0.2mW at the sample, 2×60 s), free-base spectral markers of H_2TMPyP are labeled with an asterisk.

Owing to the problem with signal loss and burning, we did not determine the relative standard deviation of the signal over the substrate or acquire spectral maps.

Despite the problems with spurious bands, Raman microspectroscopy from immobilized Ag colloidal NPs improves SERS sensitivity and reproducibility in comparison to macro-Raman measurements from Ag colloidal suspensions, which provide "average" enhancement up to 10^6 [7, p 152].

4.1.3 Immobilization of NPs by Drying

Another possibility of immobilization of NPs is to drop a NPs suspension on a glass slide and let it dry. In my master thesis SERS spectra of H_2TMPyP from hydroxylamine-reduced and borohydride-reduced Ag colloidal drops were measured.

Since the hydroxylamine-reduced Ag colloidal NPs achieved a better LOD we used it in the following experiments with other biomolecules.

In the drying process, a ring of concentrated NPs is formed at the perimeter of a pinned colloidal drop by a so-called “coffee ring effect” [53]. It seems to promote creation of “hot spots” with molecules of the analyte trapped inside. Although a dried drop cannot be considered a uniform and reproducible SERS substrate, it gives more reproducible spectra than a colloidal suspension, since the aggregation state of the particles is fixed in time. Details of a dried drop of hydroxylamine-reduced AgNPs captured by the video camera of the Horiba Jobin Yvon microspectrometer are shown in

Fig. 4.7. The crystals visible in the right image are probably crystals NaCl created during the preparation of the colloidal suspension (reaction of HCl from the hydroxylamine hydrochloride salt with added NaOH). SEM images (see Fig. 4.8) of the drops were acquired by the colleagues from the Faculty of Nuclear Sciences and Physical Engineering of the Czech Technical University in Prague.

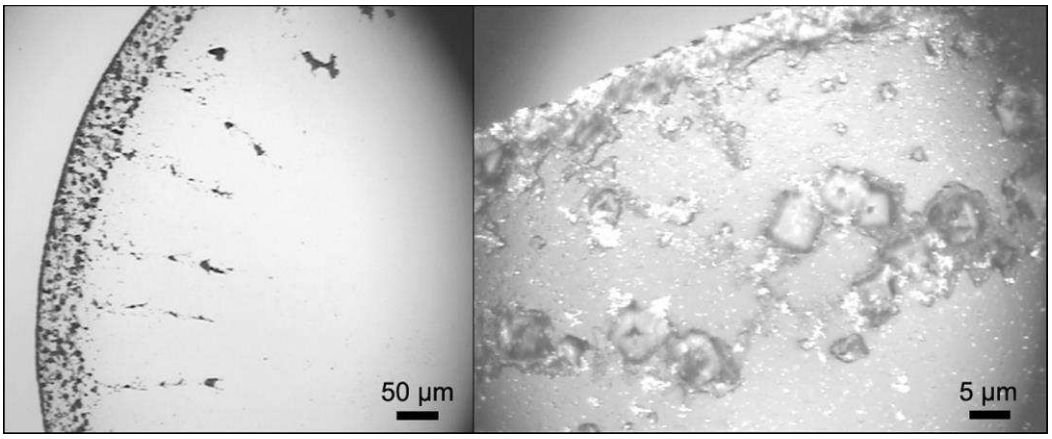

Fig. 4.7: Optical microscope images of a dried hydroxylamine-reduced Ag colloid/H_2TMPyP drop (1×10^{-7} M H_2TMPyP): edge part of the drop (left) and detail of the ring (right).

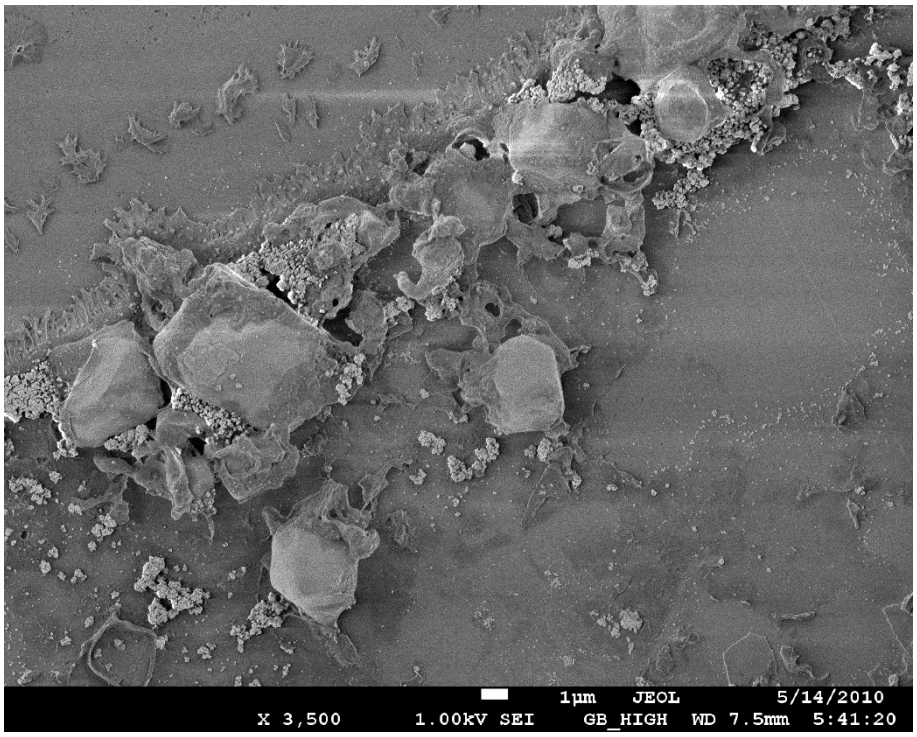

Fig. 4.8: SEM images of a ring of a dried drop of hydroxylamine-reduced Ag colloidal NPs mixed with 1×10^{-9} M H_2TMPyP.

An example of the SERRS spectrum of 1×10^{-8} M H_2TMPyP is shown in Fig. 4.9 spectrum (a). The bands at 1364 cm^{-1} and 1562 cm^{-1} indicate H_2TMPyP metallation with Ag(0) atoms (probably induced by chlorides coming from the reducing agent) [108]. The problems with spurious bands were negligible compared to AgNPs immobilized by silane.

As other probe molecules, tryptophan and a phospholipide 1,2-distearoyl-sn-glycero-3-phosphocholine (DSPC) and 1,2-dimyristoyl-3-trimethylammonium-propane (DMTAP) were chosen. Since these molecules are more sensitive to photodecomposition, we tested both 514.5 nm and 632.8 nm excitations and found that the latter one was better. An example of the SERS spectrum of tryptophan is shown in Fig. 4.9 b. 1×10^{-5} M tryptophan was measured with the excitation 632.8 nm. It was not possible to obtain spectra of lower concentration. Only a spectrum of water was observed when measuring SERS of the same tryptophan concentration in Ag colloidal suspension, demonstrating that the conglomeration of the NPs in the ring brings the advantage of higher SERS sensitivity.

SERS study of lipids using Ag colloidal NPs is difficult due to the presence of both a positive and a negative charge on the head of DSPC which hamper adsorption of lipids on chemically prepared colloidal NPs covered with anions (i.e. with a negative surface potential). Moreover, long lipid chains can hinder aggregation of NPs. We were able to obtain SERS spectra of DSPC in 2×10^{-6} M and 2×10^{-7} M (Fig. 4.9 c) concentrations from dried Ag colloidal drops using the excitation 632.8 nm. No SERS

spectra of DSPC were obtained directly from Ag colloidal suspension of the same concentration.

SERS spectra of DMTAP of concentrations 0.3 and 3 μM are shown in Fig. 4.10. The latter concentration was about two orders of magnitude lower than the lowest concentration observable for drop-coating Raman scattering (DCDR) spectroscopy.

The SERS spectra indicate perturbation of the carbon backbone structure (1050-1150 cm^{-1} region) as well as the order/disorder properties of the hydrocarbon chains (2850-2960 cm^{-1} region). Thus, we conclude that the structural properties of DMTAP were significantly perturbed by adsorption on the AgNPs.

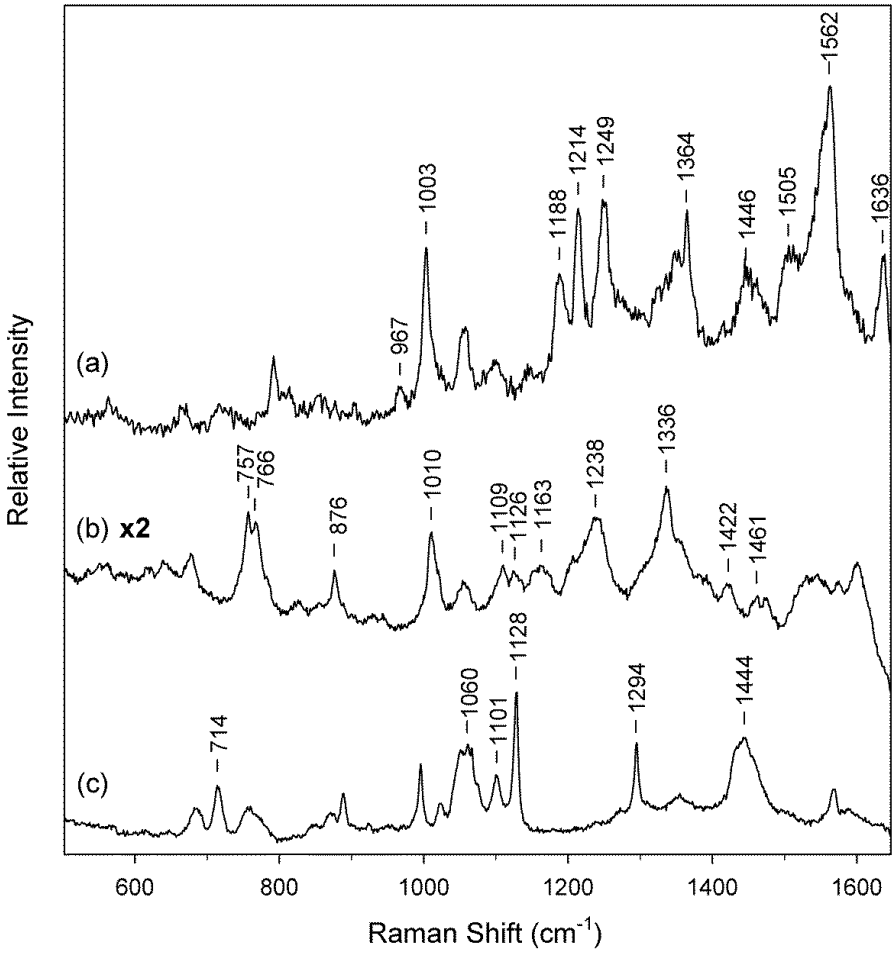

Fig. 4.9: Examples of SE(R)RS spectra obtained from the dried Ag colloid/biomolecule drops with (a) 1×10^{-8} M H_2TMPyP (514.5 nm excitation, 0.19 mW, 1 s), (b) 1×10^{-5} M tryptophan (632.8 nm excitation, 0.07 mW, 1 s × 60) and (c) 2×10^{-6} M (1.7×10^{-3} mg/mL) DSPC (632.8 nm excitation, 0.07 mW, 5 s × 40).

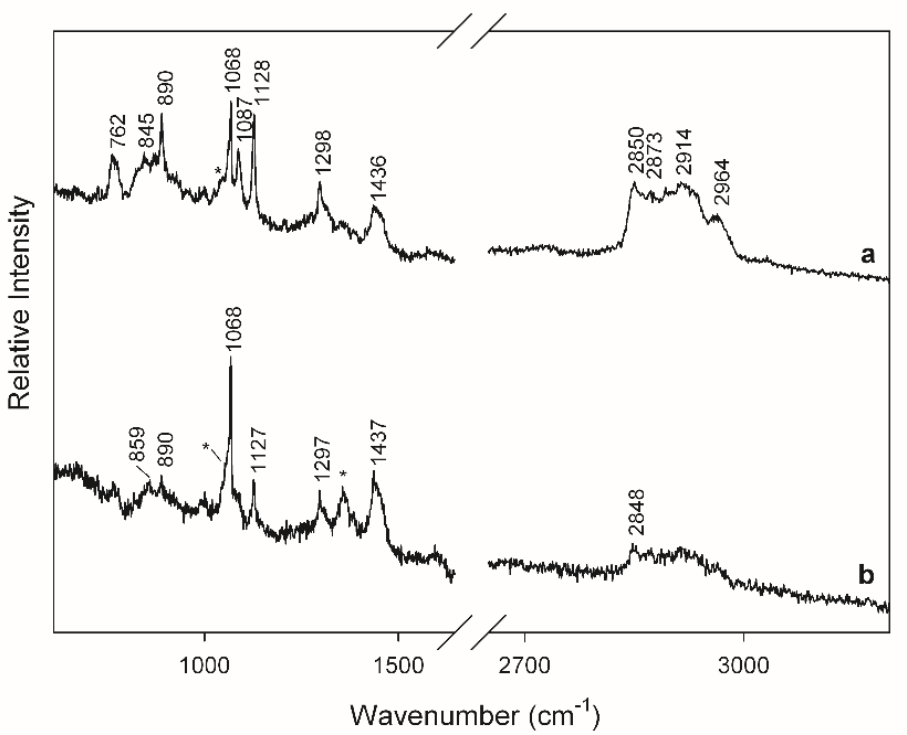

Fig. 4.10: SERS spectra of DMTAP measured from the ring of Ag hydrosol/DMTAP mixture drop dried on a clean glass slide: (a) 3 μM and (b) 0.3 μM DMTAP concentration (632.8 nm excitation, 0.07 mW, 1s×60). Spectral features of Ag hydrosol are marked by an asterisk.

4.2 SERS of porphyrins on PEGylated Ag NPs

The work was done in cooperation with Juliette Gautier and Igor Chourpa from the University of Tours, France during the 2-year exchange project MOBILITY of the Czech Ministry of Education, Youth and Sports. In one part of the project we focused on the efficiency of Ag NPs functionalized with PEG in SERS spectroscopy of biomolecules. The results were published in [V]. Two different thiol-terminated PEG with average molecular weight 5000 g/mol were employed in the study: O-[2-(3-mercaptopropionylamino)ethyl]-*O′*-methylpolyethylene glycol and α-methoxy-ω-mercaptopolyethylene glycol shortened here as PEG1 and PEG2, respectively (see Fig. 4.11). PEG1 contains the amino group next to the end thiol group in contrast to PEG2. The thiol group attahes PEG covalently to the Ag NPs.

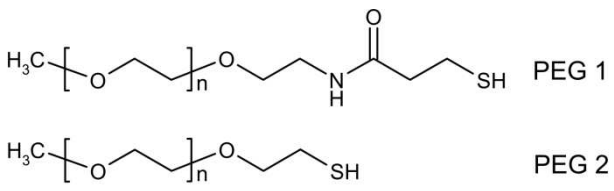

Fig. 4.11: Structural formulas of the used polyethylene glycol polymers.

To test the permeability of the stabilizing PEG layer six porphyrins differing in size and charge were chosen. We were interested in the ease of their adsorption and in their orientation at the Ag surface. Metallation (incorporation of Ag atom from Ag surface to the porphyrin macrocycle) can be used as a probe of this. Free-base specimen were employed so that we could tell when they are in contact with the Ag surface and compare the speed of adsorption according to the metallation markers in SERS spectra. Influence of the ionic strength of the medium on the adsorption on the Ag surface was studied by addition of NaCl. The SERS measurements were conducted on a home-built Raman spectrometer described in section 3.1.2 in 90° geometry. The excitation wavelength 441.6 nm is in resonance with both the SPE band of isolated PEG-AgNPs (ca. 400 nm) and the Soret electronic absorption band of the porphyrins (ca. 420 nm) which means that SERRS spectra were obtained. Spectra were accumulated 1s×60 or 5s×60.

The results on PEGylated borohydride-reduced Ag NPs were compared with results on uncoated borohydride-reduced Ag NPs. For the preparation procedures of these colloidal solutions see sections 3.2.5 and 3.2.2, respectively. For each experiment the appropriate amount of a porphyrin aqueous solution was added. NaCl was added after the porphyrin, its final concentration being 0.01 M in all experiments.

The six used porphyrins differed in the charge and sizes of their side groups (see Fig. 1.9 in the chapter 1.2.3). H_2TMAP and H_2TMPyP are both cationic porphyrins possessing four positive charges on nitrogen atoms, but side groups of H_2TMAP are larger than by H_2TMPyP. H_2TSPP contains four negatively charged sulfonyl groups and H_2TCPP four carboxyl groups that are negatively charged when dissociated. H_2TPP is neutral and it is the smallest porphyrin used. Protoporphyrin IX possesses six nonpolar and two carboxyl functional groups that are negatively charged when dissociated.

The PEGylated AgNPs were stable in higher ionic strength – the addition of NaCl (0.1 M) did not increase their hydrodynamic diameter. It remained about 150 nm for both types of PEG. SPE spectra of both types of PEGylated Ag NPs colloidal suspension were measured both before and after additon of cationic porphyrin H_2TMPyP and NaCl (0.01 M). Fig. 4.12 shows the SPE spectra for PEG2-Ag colloidal suspension, for PEG1-Ag suspension they were similar. SPE band with a maximum lies at ca. 400 nm corresponding to well-dispersed isolated Ag NPs. Neither addition of porphyrin, nor the salt caused aggregation of the NPs, the spectrum remained unchanged after six days. The excitation 441.6 nm was used for the experiments. Another available excitation – 532.0 nm is out of plasmon resonance of the NPs.

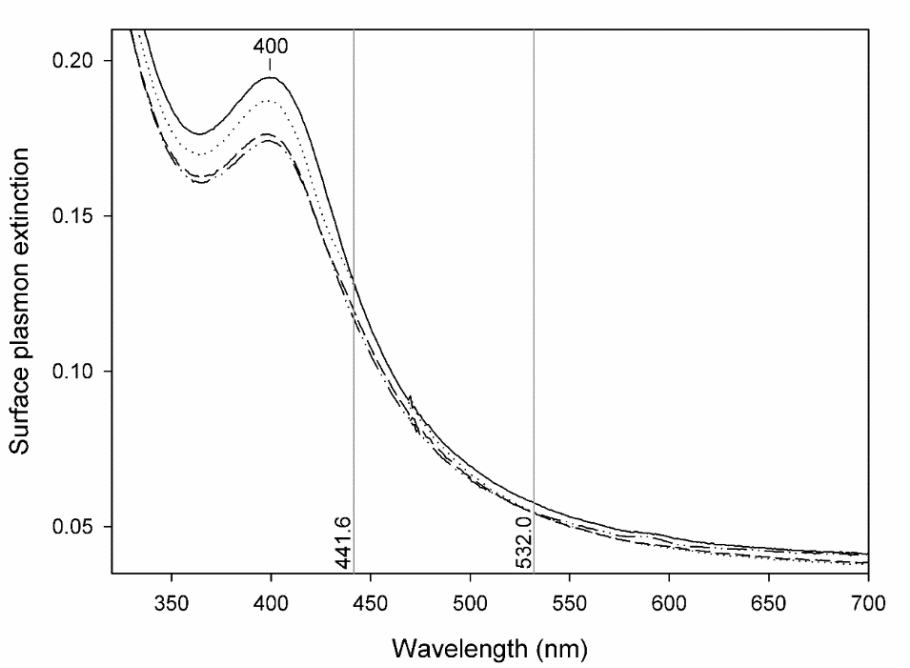

Fig. 4.12: Surface plasmon extinction spectra of PEG2-AgNPs suspension: NPs alone (solid line), with 1×10^{-7} M H_2TMPyP (dotted line), with 1×10^{-7} M H_2TMPyP and 0.01 M NaCl (dashed line), and with 1×10^{-7} M H_2TMPyP and 0.01 M NaCl after 6 days (dot-and-dashed line).

First, accessibility of the PEG-AgNP surface for cationic porphyrins H_2TMPyP and H_2TMAP were studied. Fig. 4.13 and Fig. 4.14 show spectra of 1×10^{-7} M H_2TMPyP in PEG1-Ag and PEG2-Ag colloidal suspension, respectively, and their evolution within six days after addition of NaCl. Sketches with assumed interaction of porphyrin with the PEG-AgNP for each spectrum are presented below the spectra. Spectral markers of the free-base, Ag+ and Ag(0) metallation forms are labeled I, II and III, respectively. For the values of the marker band wavelengths see the manuscript [V]. The evolution of SERRS response was different for PEG1-Ag and PEG2-Ag suspensions. At first, almost no SERRS signal was observed from PEG1-AgNPs. This improved significantly thanks to addition of NaCl. The difference in intensity is connected with surface accessibility for porphyrins. In comparison, no influence of NaCl on the intensity of SERRS was observed for PEG2-AgNPs. We suggest that chlorides influence the structure of the PEG1 polymer coating, thus increasing the accessibility of the Ag surface for H_2TMPyP. The addition of chlorides led to appearance of the metallation by Ag(0), which has been observed by other authors previously [90]. The concentration 0.01 M NaCl was sufficient to observe this effect. Overall, the metallation seems to be faster for PEG2-AgNPs as the free-base marker disappears in both cases in 2 days; however for PEG1-AgNPs a downshifted band 314 cm^{-1} appears which we attributed to the interaction between porphyrin macrocycle and the propionylamino moiety of PEG1. These results show that depending on the surface accessibility and interaction with the coating, porphyrin may adopt a parallel

or perpendicular orientation to the Ag NP surface, allowing or preventing porphyrin core metallation (see the schemes in Fig. 4.13 and Fig. 4.14).

The time evolution of SERRS spectra after addition of chlorides was studied for another cationic porphyrin - H_2TMAP. Different adsorption kinetics was observed for PEG1 and PEG2 coating. In the case of PEG2 coating, rapid metallation with Ag(0) occured, whereas in the case of PEG1 with the propionylamino group, porphyrin stayed free-base for a longer time with gradual metallation to Ag(0) form. We therefore suppose that a majority of porphyrin molecules passes freely through the PEG2 coating to the Ag surface where it adsorbes and is metallated, whereas for PEG1-Ag colloidal suspension it is hindered by the PEG coating. Unlike in the case of H_2TMPyP, shift of the free-base marker to shorter wavelengths was not observed, which is supposedly caused by the larger side groups of H_2TMAP hindering interaction of the core nitrogen atoms with propionylamino group of PEG1. Again we infer that in case of PEG2-AgNPs the porphyrins can access the Ag surface in parallel orientation and become metallated while for PEG1-AgNPs they are hindered by the coating and mostly adopt a perpendicular orientation towards the Ag surface.

To evaluate the effect of concentration on porphyrin adsorption and SERRS, spectra in a concentration range 10^{-6}–10^{-9} M recorded one day after NaCl addition were compared. Metallation was more efficient at lower porphyrin concentrations than at higher concentrations. Such behaviour was also observed for H_2TMPyP on the ion-free surface of laser-ablated Ag NPs, in contrast to citrate- and borohydride-reduced colloids where the ratio of metallated molecules increases with concentration, which was explained by a need to win the competition for adsorption on the Ag surface against the anions present after the reduction step of the colloid preparation [85]. The similarity to the laser-ablated Ag NPs indicates that the Ag surface of the PEG-SH-coated AgNPs can be considered as ion-free (one might recall that they were dialyzed against distilled water) therefore on the Ag the porphyrin molecules do not have to compete with other molecules for the adsorption. The absence of competition against anions for binding to the Ag surface could be an advantage for analytes having low affinity to Ag.

From the sensitivity point of view, PEG2-AgNPs were more efficient than PEG1-Ag NPs. The lowest detection limit of ca. 10^{-9} M was obtained with cationic porphyrin H_2TMPyP on PEG2-AgNPs. The same detection was obtained for CuTMPyP using the conventional borohydride-reduced Ag NPs obtained for the same excitation [109]. This quantitative comparison with bare nonaggregated NPs indicates that for the analytes able to diffuse through it, the PEG coating does not necessarily lead to a dramatic loss of the analyte adsorption sites on the Ag NP surface.

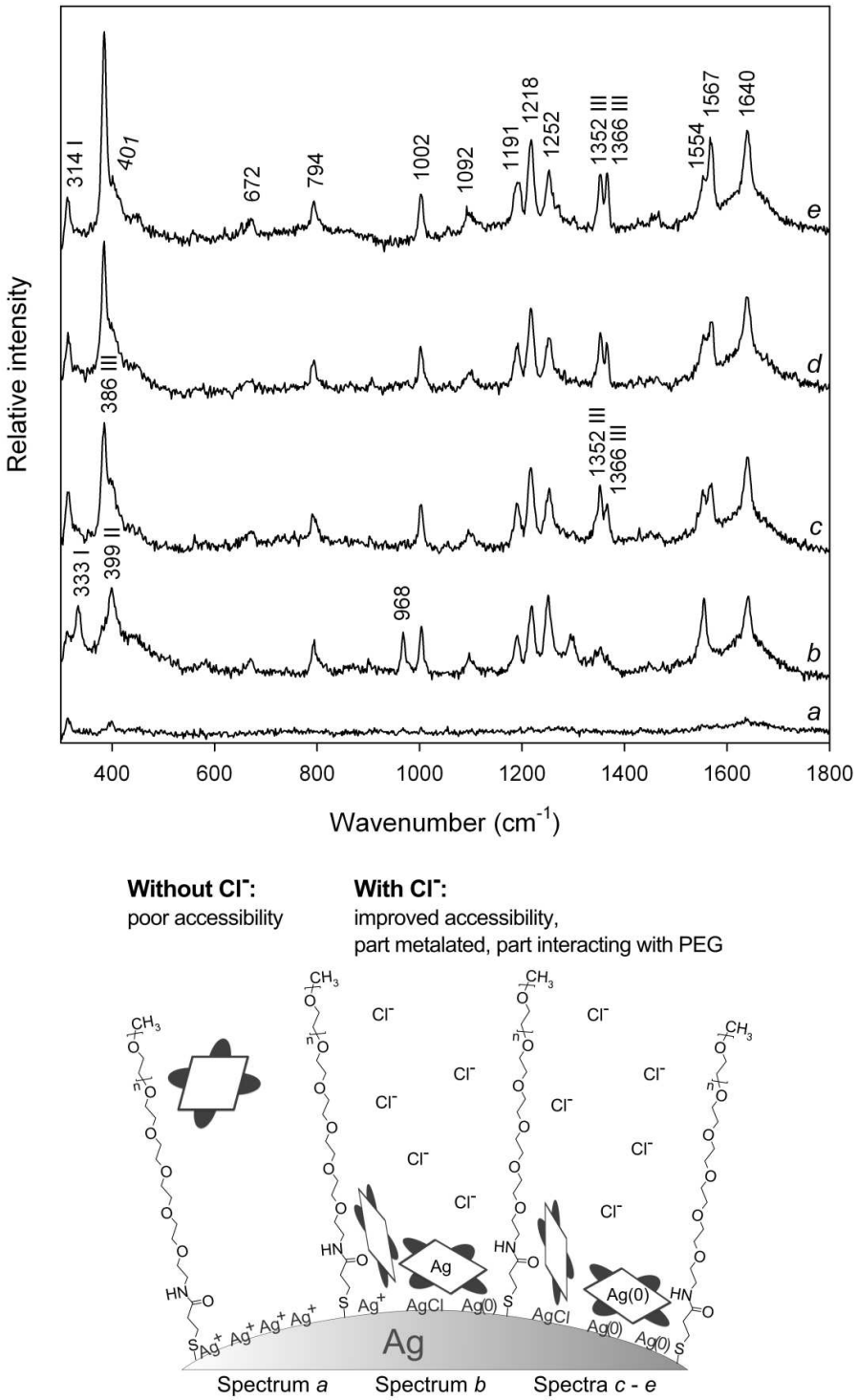

Fig. 4.13: Top: SERRS spectra obtained from 1×10^{-7} M H_2TMPyP adsorbed on PEG1-AgNPs before and after addition of NaCl (0.01 M): (a) no NaCl, (b) with NaCl, (c) with NaCl – 2 days, (d) with NaCl – 3 days, (e) with NaCl – 6 days. Relevant spectral features of porphyrin metallation forms are marked I-III. **Bottom:** Scheme showing possible adsorption of porphyrin metallation forms on PEG1-AgNPs.

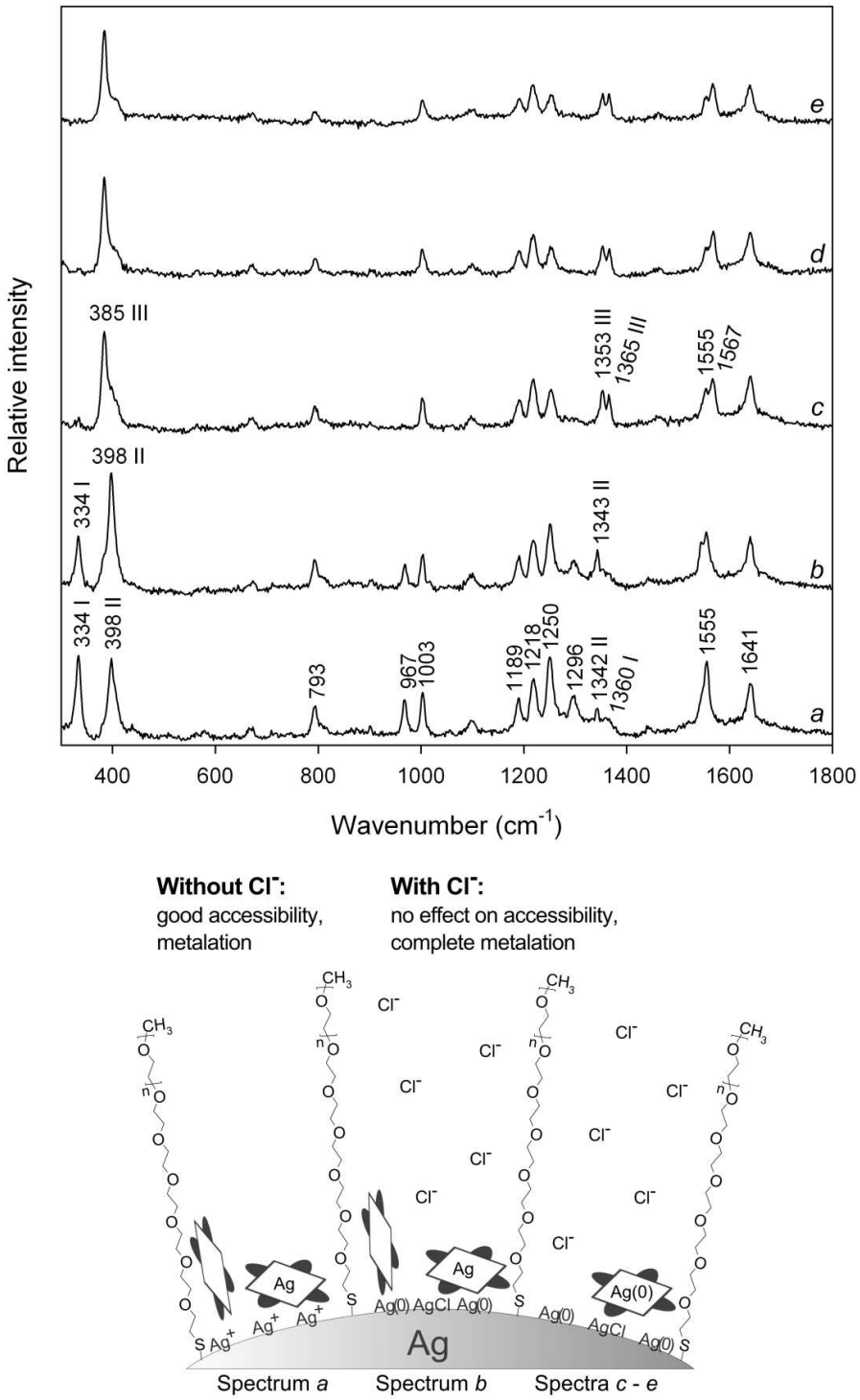

Fig. 4.14: Top: SERRS spectra obtained from 1×10^{-7} M H_2TMPyP adsorbed on PEG2-AgNPs before and after addition of NaCl (0.01 M): (a) no NaCl, (b) with NaCl, (c) with NaCl – 1 day, (d) with NaCl – 2 days, (e) with NaCl – 6 days. Relevant spectral features of porphyrin metallation forms are marked I-III. **Bottom:** Scheme showing possible adsorption of porphyrin metallation forms on PEG2-AgNPs.

SERRS detection was less sensitive for anionic and neutral porphyrins than for cationic ones. It appears that the accessibility of the PEGylated Ag surface is lower for noncationic porphyrins. Nevertheless, SERRS spectra of anionic and neutral porphyrins with a satisfactory signal-to-noise ratio were obtained for the concentration 1×10^{-6} M after addition of NaCl as shown in Fig. 4.15.

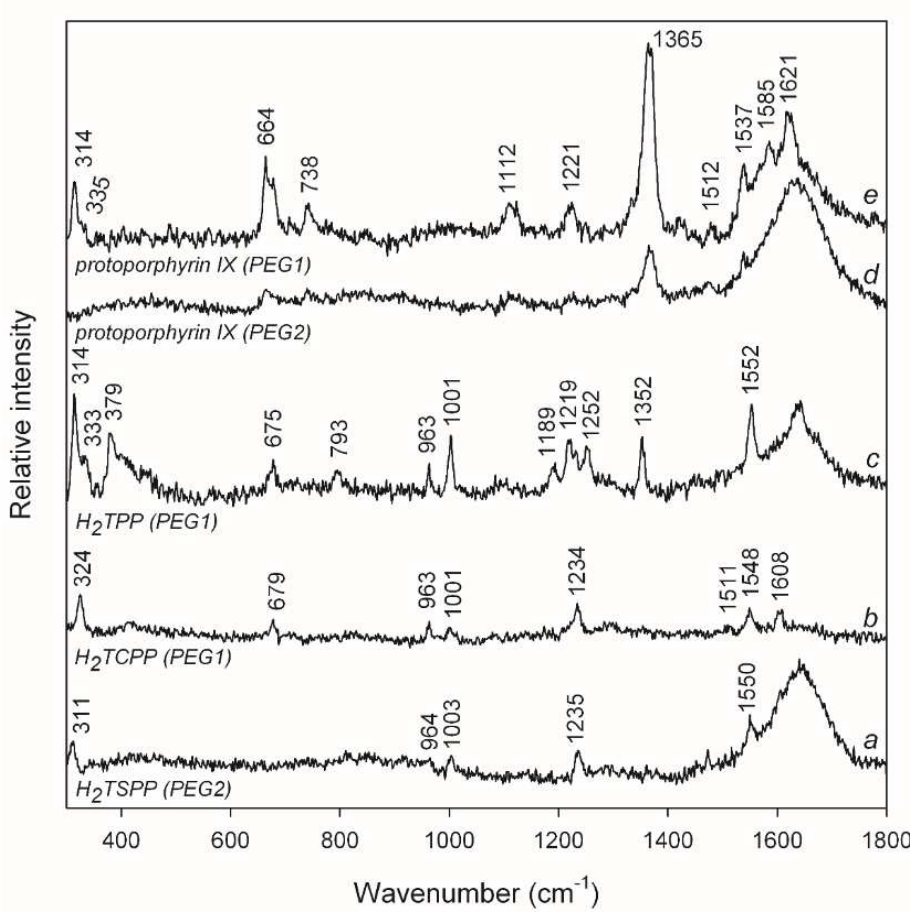

Fig. 4.15: SERRS spectra of non-cationic porphyrins obtained from PEG1-Ag- or PEG2-AgNPs (approx. 1×10^{-6} M porphyrin and 0.01 M NaCl), accumulation time 5 s×60 (except the spectrum b which was accumulated 1 s×60).

As a last experiment in our Czech-French MOBILITY project we tried to obtain SERS spectra of H_2TMPyP from cells incubated with a mixture of PEGylated Ag colloidal suspension with H_2TMPyP. The HeLa carcinoma cells were used. The cells readily uptake the PEGylated Ag NPs as seen in the Fig. 4.16. SERS experiment was performed with 488.0 nm excitation. Unfortunately, a strong fluorescence was observed in the majority of aquired spectra, only sometimes with some distinguishable Raman peaks of H_2TMPyP. It confirmed the presence of H_2TMPyP inside the cells, but it was impossible to prove that our spectra are SERS spectra rather than RRS ones. Since the project was not prolonged we were not able to continue these experiments.

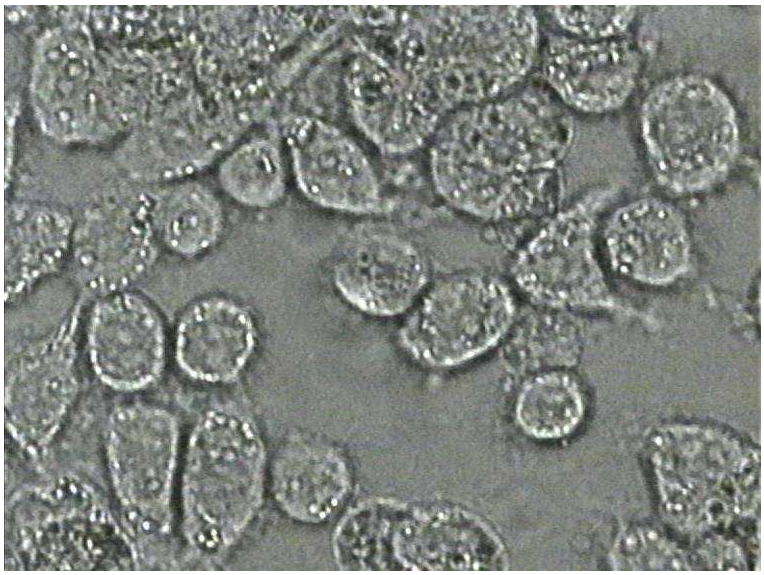

Fig. 4.16: White light image of HeLa cancer cells with PEG-AgNPs/H_2TMPyP.

4.3 Ordered nanostructures

4.3.1 Gold and silver film over nanospheres (FON) substrates

The FON substrates used in this thesis were composed of polystyrene spheres of 253 nm in diameter covered with 20 nm of silver or gold by magnetron sputtering. They were prepared for us by Lucie Štolcová at the Faculty of Nuclear Sciences and Physical Engineering, Czech Technical University in Prague. The preparation procedure is described in the Experimental in chapter 3.2.7. The ordered monolayer of PS spheres before coating is shown in Fig. 4.17. SPE spectra of one Au- and one AgFON substrates are shown in Fig. 4.18. Both 514.5 nm and 632.8 nm laser lines lie in the plasmon resonance band of AgFON surface. On the other hand, only the 632.8 nm line is in resonance with the plasmon band of AuFON surface. Porphyrin H_2TMPyP was used as the test molecule for SE(R)RS experiments.

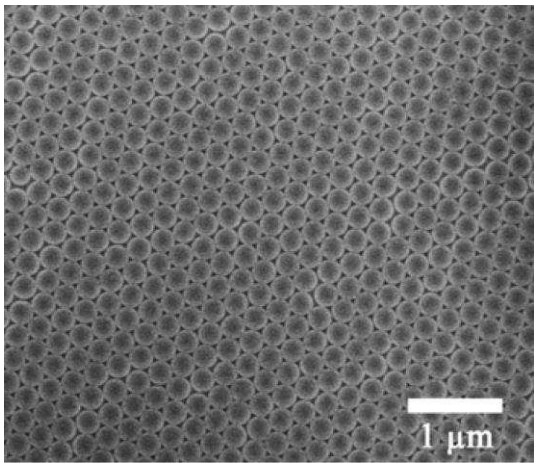

Fig. 4.17: SEM image of closely packed PS spheres of 253 nm diameter before coating with metal. Reprinted from [110].

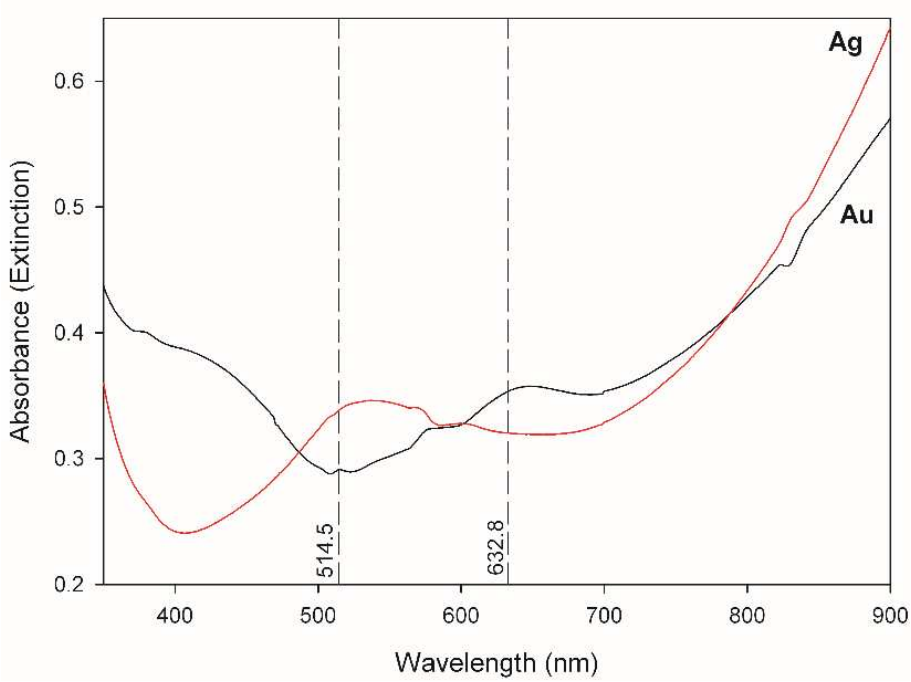

Fig. 4.18: SPE spectra of an Au- and AgFON substrates.

4.3.1.1 AgFON

AgFON substrates were covered with aqueous solution of H_2TMPyP. The solution contained 10% of ethanol in order to decrease surface tension which in the case of pure water was prone to tear the FON surface. Nevertheless, even so small parts of the surface got ripped off. FONs were immersed for 1 hour, then dried with air.
SERS spectra were measured by Raman microspectrometer with excitations 632.8 nm and 514.5 nm and objective ×100. No signal of H_2TMPyP was detected even for the highest concentration 1×10^{-7} M using either excitation. On the other hand, some spurious spectral bands are present (see Fig. 4.19). The strong peaks around 1000 cm^{-1} probably belong to styrene from PS spheres [111, 112].

The concentration was increased to 2×10^{-7} M and 2×10^{-6} M, the substrates were immersed into the H_2TMPyP solutions for 16 hours. In the case of AgFON SERRS spectra of H_2TMPyP were obtained for both concentrations with the excitation line 514.5 nm (see Fig. 4.20 and Fig. 4.21). With the laser line 632.8 nm no recognizable spectrum of H_2TMPyP was detected. The reason can be, first, that the green excitation is nearer the plasmon resonance maximum and, secondly, that it is in resonance with the absorption of H_2TMPyP and therefore produces surface-enhanced resonance Raman scattering. The applied intensities were either 0.02 mW or 0.2 mW. For the lower intensity, there was too little signal compared to the noise and accumulation of the signal did not improve it. For the higher intensity, spurious bands appeared originating in decomposition of species present on the AgFON surface. The best way for obtaining spectra was using the higher intensity and slightly defocusing the laser beam off the sample.

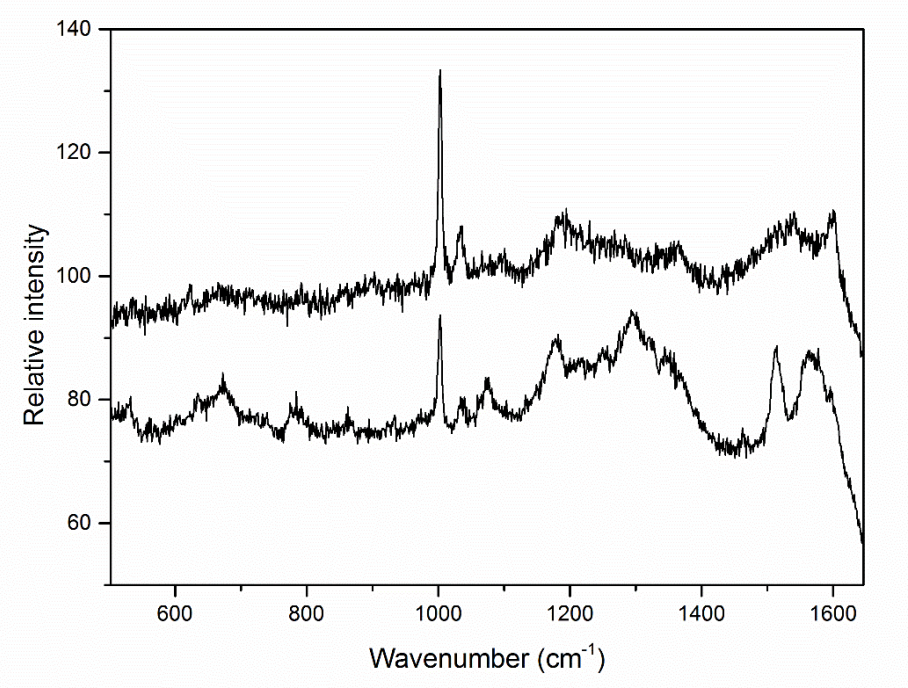

Fig. 4.19: Spectra measured from AgFON immersed in 1×10^{-7} M H_2TMPyP.

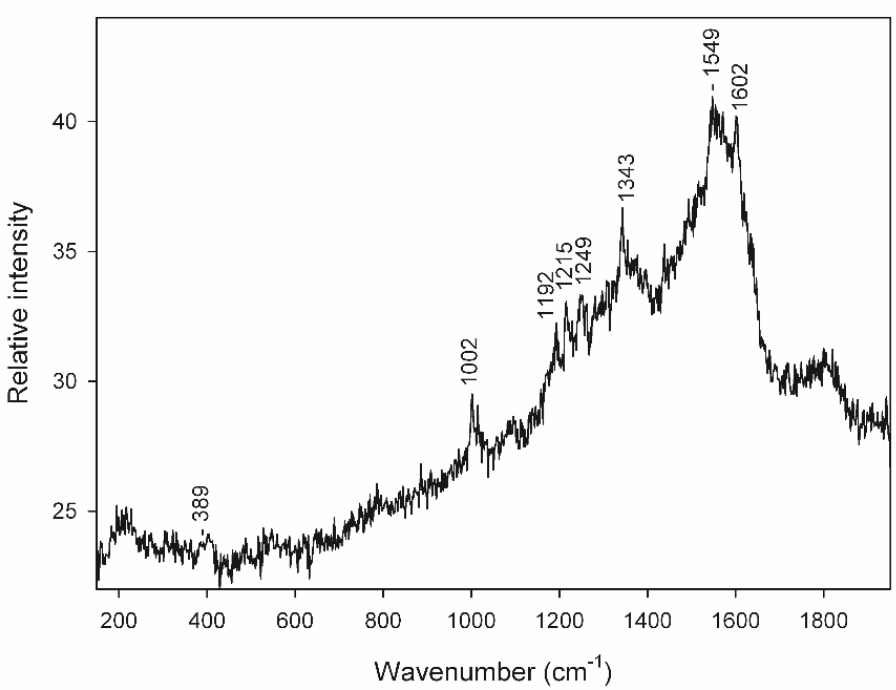

Fig. 4.20: SERRS spectrum of 2×10^{-7} M TMPyP from AgFON, excitation 514.5 nm, 0.02 mW, acquisition time 1s×50.

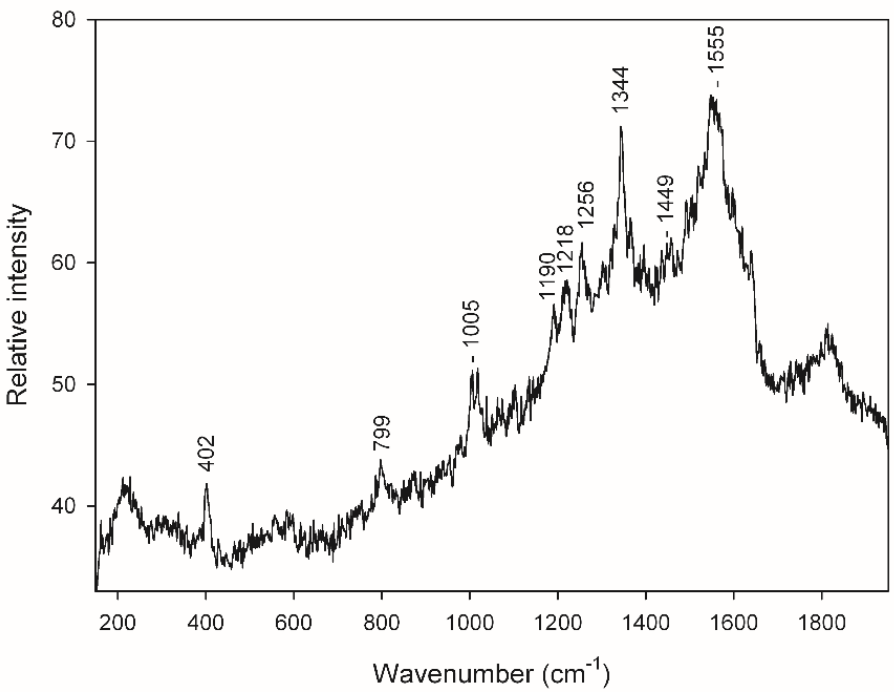

Fig. 4.21: SERRS spectrum of 2×10^{-6} M TMPyP from AgFON, excitation 514.5 nm, 0.2 mW, acquisition time 1s×30.

In the following experiment it was found out that acidifying the H_2TMPyP solution with HCl increases SERS signal. Freshly prepared FON substrates were immersed in aqueous solution, aqueous solutions with ethanol, resp. HCl with 1×10^{-7} M H_2TMPyP for 23 hours and then dried with air.

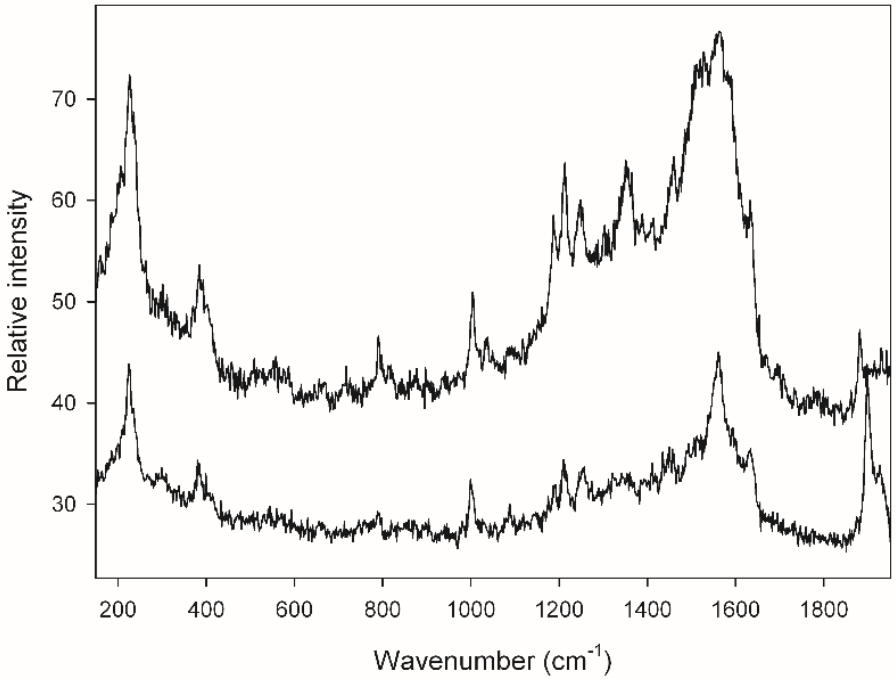

Fig. 4.22: SERRS spectra from AgFON, excitation 514.5 nm that was immersed in 1×10^{-7} M H_2TMPyP aqueous solution with addition of HCl, 0.02 mW, acquisition time 1s×30.

In contrast to water solution and solution with ethanol used under the same conditions, in the case of acidic solution the spectra of 1×10^{-7} M H_2TMPyP were detected from AgFON using excitation 514.5 nm (see Fig. 4.22).

4.3.1.2 AuFON

The samples were prepared identically to AgFON only using Au instead of Ag. In the case of AuFON, it was reasonable to use just the excitation 632.8 nm. Recognizable spectra of H_2TMPyP were obtained only for the soaking concentration 2×10^{-6} M (immersion time 16 h). In contrast to AgFON the spurious bands were not present much, although the signal decreased with time of illumination here as well. Spectra could be very reproducibly obtained from different spots as demonstrated by the Fig. 4.23.

No spectra of H_2TMPyP were detected for the concentration 1×10^{-7} M even with the addition of HCl (excitation 632.8 nm).

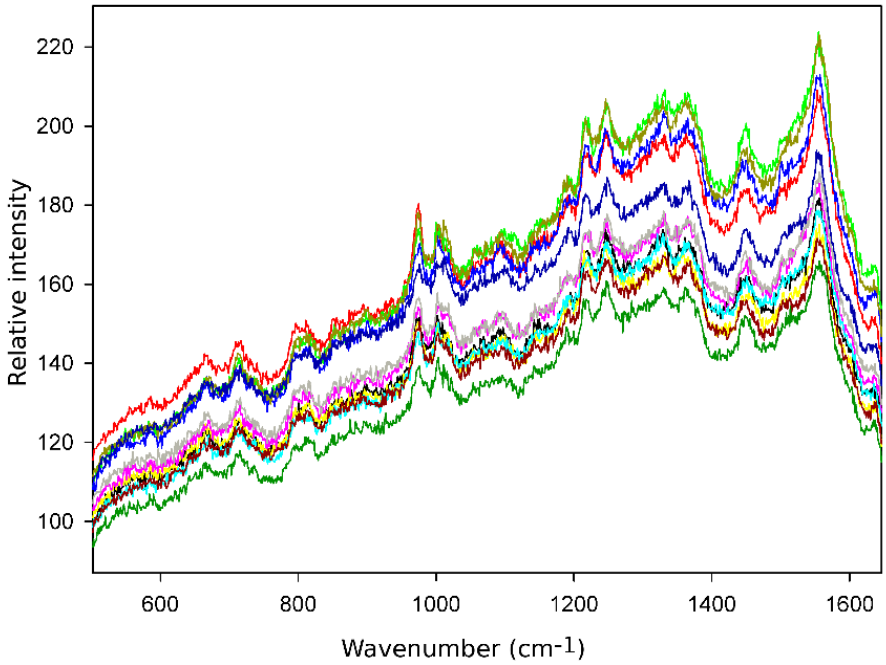

Fig. 4.23: SERS spectra of 2×10^{-6} M H_2TMPyP from different spots of AuFON illustrating spectral reproducibility over a substrate, 12 different spots, 633 nm, 0.065 mW, 1×60 s.

4.3.2 Silver-coated insect wings

4.3.2.1 Cicada wings

Wings of a specimen of cicada Cryptotympana aquila were coated by electroless silver plating by RNDr. Jan Proška at the Faculty of Nuclear Sciences and Physical Engineering, Czech Technical University in Prague. Comparison of the uncoated and coated structure of the cicada wing as viewed by SEM is shown in Fig. 4.24 and a more detailed image capturing silver grains on the individual cones in Fig. 4.25.

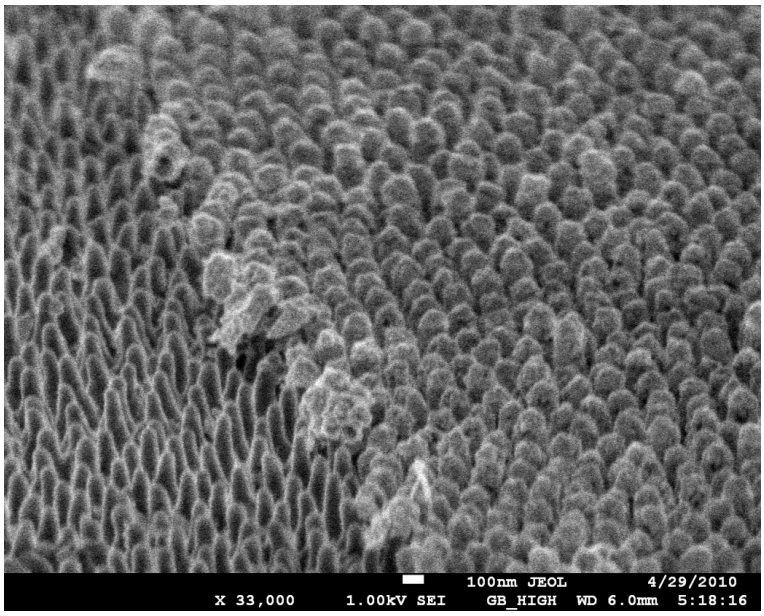

Fig. 4.24: SEM image of a partly silver-coated cicada wing. Nanopillars without silver capping can be seen in the left part of the picture and arrays of the silver-coated nanopillar tips in the right side of the picture.

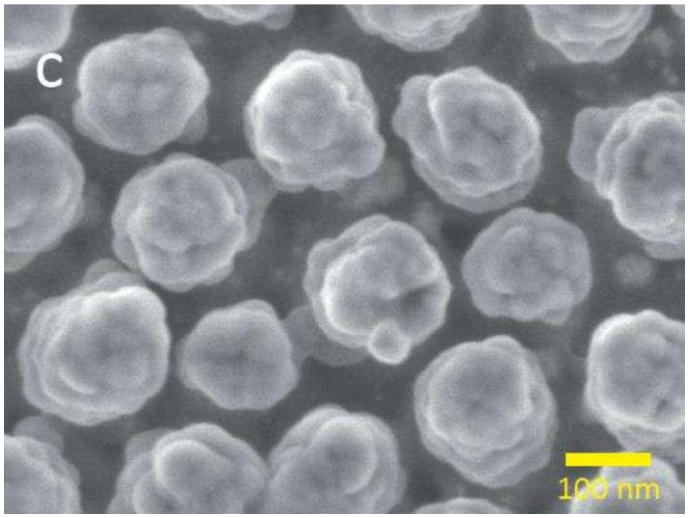

Fig. 4.25: SEM top view of a silver-coated cicada nanopillars.

A silver-coated cicada wing was cut into rectangles on which droplets (ca. 8 µl) of H_2TMPyP water solution were dropped. The surface of silver-coated structure of cicada wing is hydrophobic causing the water solution drop maintain a spherical shape and dry into a small circle. Spectra were measured by the Raman microspectrometer using an ultra long working distance (ULWD) objective (magnification ×50) and excitation 514.5 nm.

Reproducible good-quality SERRS spectra were obtained from all measured spots of the dried drop with H_2TMPyP concentration 1×10^{-6} M (see Fig. 4.26) and 1×10^{-8} M (see Fig. 4.27).

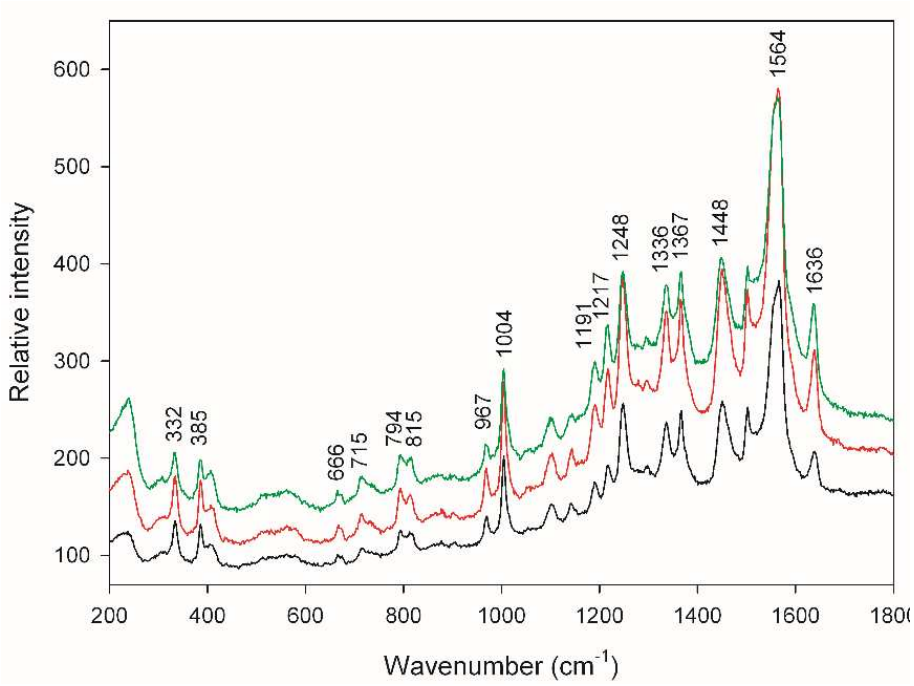

Fig. 4.26: SERRS spectra TMPyP measured from from different spots of a 1×10^{-6} M H_2TMPyP dried drop on a silver-coated cicada wing, excitation 514.5 nm, laser power 0.02 mW, acquisition time 1s×60.

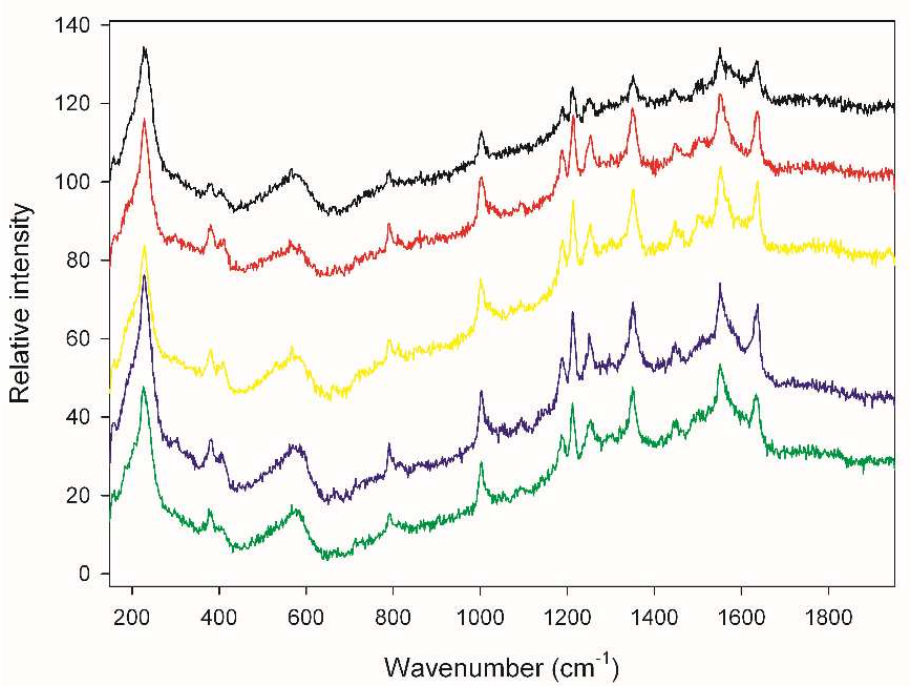

Fig. 4.27: SERRS spectra of TMPyP measured from different spots of 1×10^{-8} M H_2TMPyP dried drop on silver-coated cicada wing, excitation 514.5 nm, laser power 0.02 mW, acquisition time 3s×60.

H_2TMPyP solution with addition of ethanol (20%) for better wettability of the cicada wing structure were also tested. Droplets with ethanol can lose its contact line, spread and dry into on a larger area than droplets of water solution of the same volume.

Considering that, the signal should be lower from the droplet with ethanol because the analyte is spread on a larger area. This led to lower signal compared to the water drop where the analyte spread on a smaller area. On other occasions the drop with ethanol maintained the spherical shape and the resulting signal was of similar intensity as the signal from aqueous suspension droplet (see Fig. 4.28). Unlike the FON substrates water drop cannot damage the underlying structure therefore we recommend that ethanol does not have to be added into the solution.

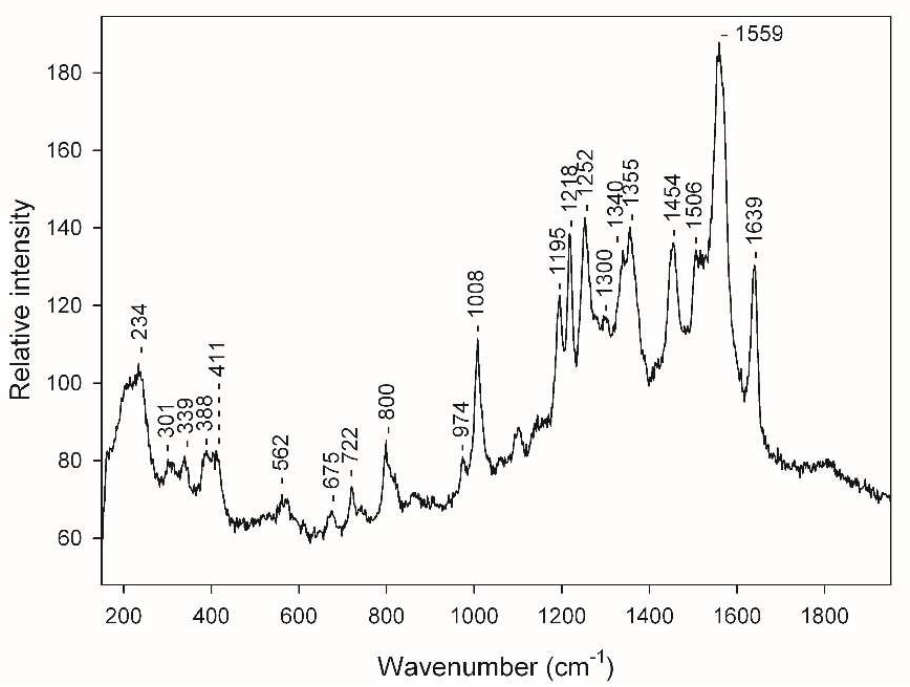

Fig. 4.28: SERRS spectrum of TMPyP from a dried drop of 1×10^{-6} M H_2TMPyP aqueous solution with 20% of ethanol, excitation 514.5 nm, laser power 0.02 mW, acquisiton times 1s×30.

In a next experiment, cicada wings covered with 40 nm of Ag by magnetron sputtering were used as the SERS substrate. SERS of 1×10^{-7} M and 1×10^{-6} M TMPyP and TMAP was measured with both 514.5 nm and 632.8 nm. Again ULWD objective with magnification ×50 was used.

Good quality SERRS spectra were acquired for both TMPyP and TMAP at the concentration 1×10^{-6} M with the excitation 514.5 nm. The ten times lower concentration gave worse, although still identifiable, SERRS spectra for both porphyrins.

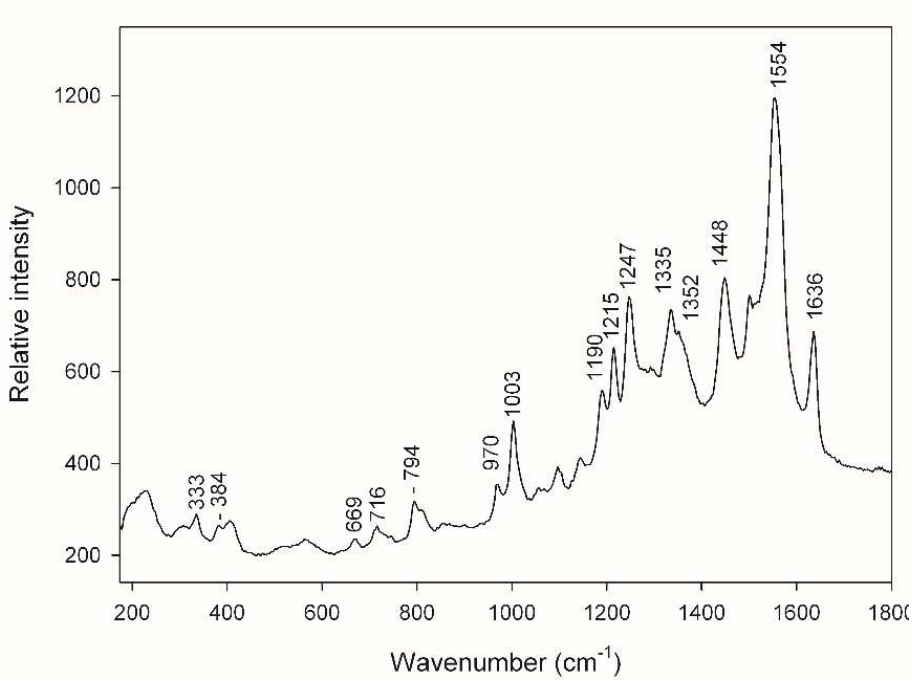

Fig. 4.29: SERRS spectrum of TMPyP measured from a dried drop of 1×10^{-6} M H_2TMPyP concentration on a cicada wing Ag-covered by magnetron sputtering, excitation 514.5 nm, laser power 0.02 mW, acquisition time 1s×30.

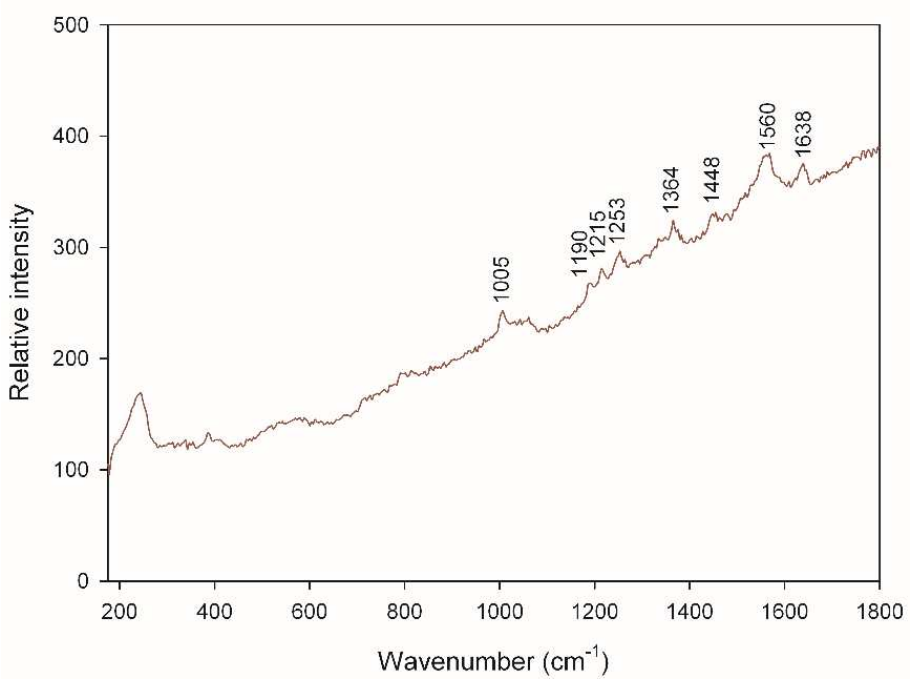

Fig. 4.30: SERRS spectrum of TMPyP measured from a dried drop of 1×10^{-7} M H_2TMPyP concentration on a cicada wing Ag-covered by magnetron sputtering, excitation 514.5 nm, laser power 0.02 mW, acquisition time 1s×30.

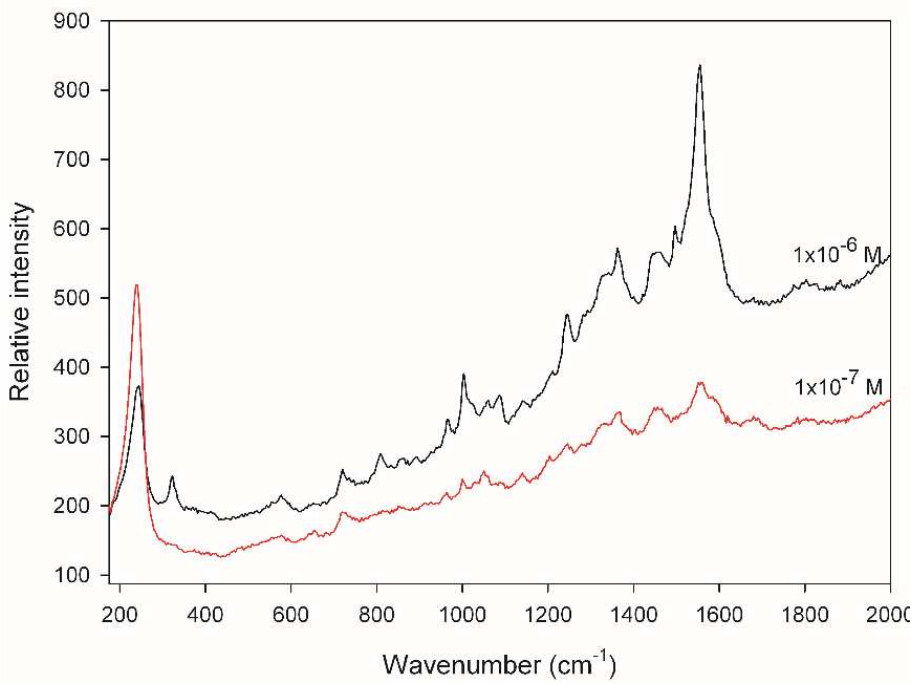

Fig. 4.31: SERRS spectrum of TMAP measured from a dried drop of 1×10^{-6} M and 1×10^{-7} M H_2TMAP concentration on a cicada wing Ag-covered by magnetron sputtering, excitation 514.5 nm, laser power 0.02 mW, acquisition time 1s×30.

With the excitation 632.8 nm good SERS spectra were obtained only for 1×10^{-6} M TMPyP (see Fig. 4.32). The lower concentrations were impossible to detect. The reason is probably that the red laser line lies further from the plasmon resonance of the Ag structure.

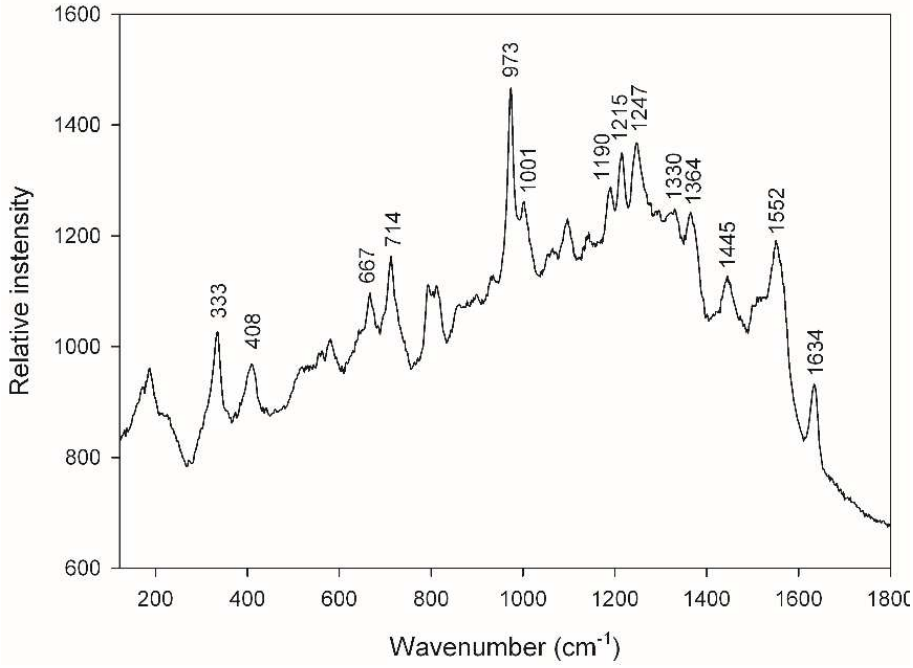

Fig. 4.32: SERS spectrum of TMPyP measured from a dried drop of 1×10^{-6} M H_2TMPyP concentration on a cicada wing Ag-covered by magnetron sputtering, excitation 632.8 nm, laser power 0.02 mW, acquisition time 1s×30.

Good SERS spectra of TMPyP were obtained also for a Ag-coated cicada wing covered with a less than 2nm layer of Au added by magnetron sputtering. This time the wavelength 632.8 nm was used besides 514.5 nm for excitation because of the gold layer in which the surface plasmons could be excited by this wavelength. The obtained SE(R)RS spectra are shown in Fig. 4.33.

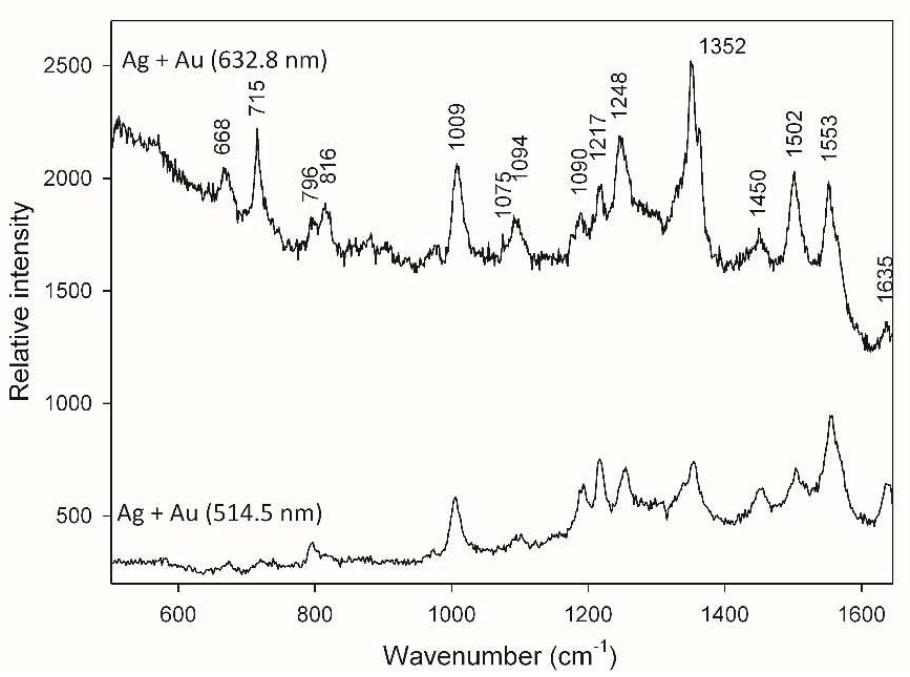

Fig. 4.33: SE(R)RS spectra of 1×10^{-6} M TMPyP obtained a dried aqueous drop on Ag-coated cicada wing with a layer of Au, excitation 514.5 nm, 0.2 mW, 1s and excitation 632.8 nm, 0.07 mW, 1s.

4.3.2.2 Butterfly wings

Wings of butterflies are divided into scales with nanostructure which can be also successfully used as SERS substrates. We measured SERRS spectra of TMPyP from wings of the butterfly species Papilio palinurus coated by electroless silver plating like the cicada wings. SEM image of the Ag-coated wing is in Fig. 4.34. Spectra were again acquired from dried drop of H_2TMPyP aqueous solution by Raman microspectrometer with ULWD ×50 objective and excitation 514.5 nm. Spectra from dried drops with 1×10^{-6} M TMPyP are shown in Fig. 4.35.

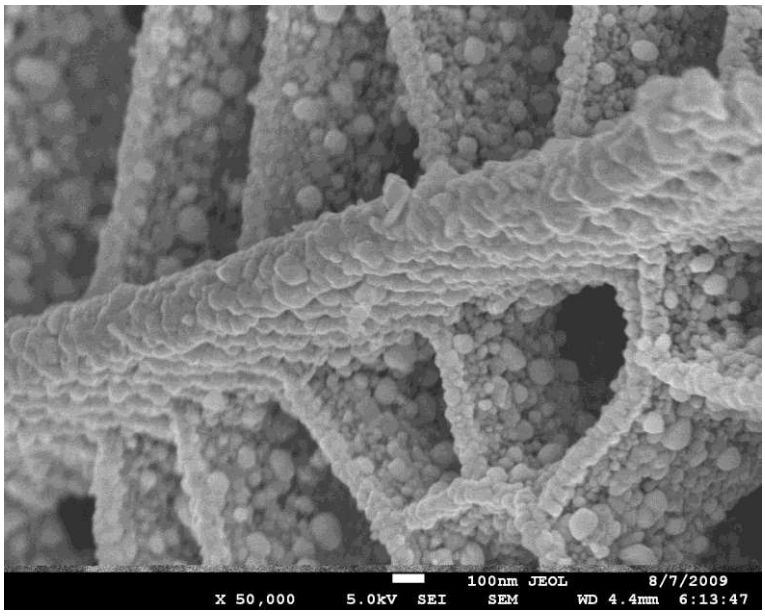

Fig. 4.34: SEM image of silver-coated butterfly wing scale.

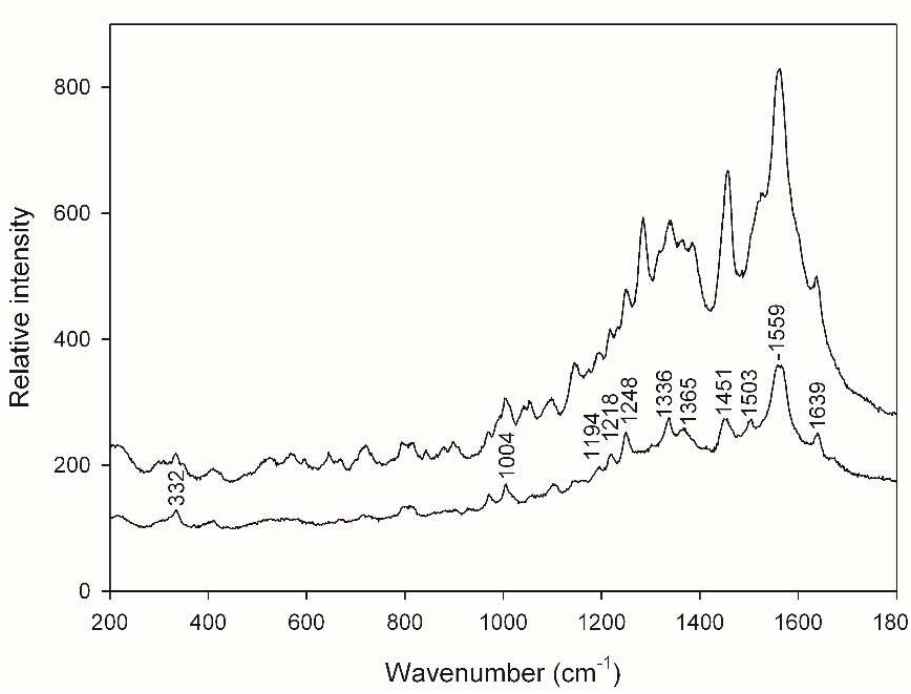

Fig. 4.35: SERRS spectra of 1×10^{-6} M TMPyP, excitation 514.5 nm (laser power on the sample 0.02mW), accumulation time 1×60s.

5 Conclusions

This thesis examined the application of surface-enhanced Raman microspectroscopy for study of biomolecules and biological systems.

The porphyrin derivative 5,10,15,20-tetrakis(1-methyl-4-pyridyl)porphyrin (H_2TMPyP) was the dominant probe molecule. It was used to test all of the substrates available in this thesis: Au- and AgNPs immobilized via organosilane, AgNPs immobilized by drying, PEGylated AgNPs, FON and silver-coated insect wings. The lowest detected concetration was generally about 1×10^{-8} M with the exception of Ag- and AuFON where only 2×10^{-7} M was achieved and the NPs immobilized by drying where the LOD was calculated as 1×10^{-10} M. Nevertheless, in the case of dried NPs the disadvantage is irreproducibility of the porphyrin spectra caused by different ratio of the free-base and metallated forms at different spots. In contrast, highly reproducible SERS spectra were obtained from the ordered substrates – AuFON (that produced more reproducible spectra than AgFON) and Ag-coated insect wings.

The AgNPs immobilized by drying of the colloidal solution/probe mixture gave the best detection limits, thanks to creation of "hot spots" by the aggregation with the adsorbate and less frequent occurrence of spurious bands due to the absence of organosilane. 1×10^{-5} M tryptophan solution, 2×10^{-7} M DSPC and 3×10^{-7} M DMTAP, which is about five orders of magnitude lower than that for conventional Raman spectroscopy from lipid suspension. The SERS spectra of lipids were slightly perturbed by the adsorption on the metal surface and drying compared to their Raman spectra from solution.

In cooperation with J. Gautier and I. Chourpa under a MOBILITY project a thorough study of porphyrin adsorption on PEGylated Ag NPs was done by means of classical macro-Raman spectrometer. The best SERS spectra were acquired for the cationic porphyrins (the lowest detection limit of ca. 10^{-9} M was obtained with cationic porphyrin H_2TMPyP on PEG2-AgNPs.), SERS spectra of other porphyrins were detected in about two orders of magnitude higher concentration. The metallation of free-base porphyrins was used to identify the accessibility of the Ag NP surface coated by PEG polymers. The polar functional group on one of the used PEG polymers interacted with the porphyrins and reduced the accessiblitiy of the metal for cationic porphyrins causing preservation of the free-base form on one hand, but on the other hand a lower SERS signal. To sum it up, the accessibility of the surface depended on the chemical properties of both the polymer and the porphyrine species.

The SERS experiments with HeLa cells proved the applicability of PEG-NPs with H_2TMPyP for intracellular studies.

SERS signal can be influenced by change in the ionic strength or pH of the system. For example, addition of 0.1 M NaCl induced Ag(0) sites on the Ag surface and thus favored the metallation of porphyrins to the Ag(0) metallation form. The Ag(0)-TMPyP spectral markers were also present in the spectra from dried Ag NP drops where NaCl was present from the reducer in the preparation of the colloidal NPs. Another example is acidifying of H_2TMPyP solution by HCl which led to increased SERS signal from AgFON.

In coclusion, the used solid SERS substrates all achieved a very good sensitivity in detection of the probe biomolecules. The ordered SERS substrates – AuFON and Ag-coated natural templates (insect wings) proved the best reproducibility of all substrates.

6 Bibliography

[1] C. V. Raman, R. S. Krishnan, A new type of secondary radiation, Nature **121** (1928), 501–502.

[2] C. V. Raman, R. S. Krishnan, A change of wave-length in light scattering, Nature **121** (1928), 619–619.

[3] G. S. Landsberg, L. I. Mandelstam, New phenomenon in scattering of light (preliminary report), Journal of the Russian Physico-Chemical Society, Physics Section **60** (1928), 335.

[4] A. Smekal, Zur Quantentheorie der Dispersion, Die Naturwissenschaften **11** (1923), 873–875.

[5] G. Placzek, Rayleigh-Streuung und Raman-Effekt, Handbuch der Radiologie **6** (1934), 205.

[6] K. Kneipp, H. Kneipp, I. Itzkan, R. R. Dasari, M. S. Feld, Surface-enhanced Raman scattering and biophysics, J. Phys.: Condens. Matter **14** (2002), R597–R624.

[7] R. Aroca, Surface-enhanced vibrational spectroscopy, John Wiley and Sons Ltd, Chichester, 2006.

[8] M. Dendisová, P. Žvátora, P. Matějka, Ramanova spektrometrie, pokyny k úloze č. 5 Laboratoře analytické chemie II (LACHII), http://old.vscht.cz/anl/lach2/

[9] by Danh, In: English Wikipedia, CC BY-SA 3.0, [29.7.2017] https://commons.wikimedia.org/w/index.php?curid=12565861

[10] M. Fleischmann, P. J. Hendra, A. J. McQuillan, Raman spectra of pyridine adsorbed at a silver electrode, Chem. Phys. Lett. **26** (1974), 163–166.

[11] D. J. Jeanmaire, R. P. Van Duyne, Surface Raman spectroelectrochemistry. 1. Heterocyclic, aromatic, and aliphatic-amines adsorbed on anodized silver electrode, J. Electroanal. Chem. **84** (1977), 1–20.

[12] M. G. Albrecht, J. A. Creighton, Anomalously intense Raman-spectra of pyridine at a silver electrode, J. Am. Chem. Soc. **99** (1977), 5215–5217.

[13] A. Pinczuk, E. Burstein, Raman Scattering from InSb surfaces at photon energies near the E 1 energy gap, Phys. Rev. Lett. **21** (1968), 1073.

[14] M. R. Philpott, Effect of surface plasmons on transitions in molecules, J. Chem. Phys. **62** (1975), 1812–1817.

[15] M. Moskovits, Surface roughness and the enhanced intensity of Raman scattering by molecules adsorbed on metals, J. Chem. Phys. **69** (1978), 4159–4168.

[16] M. Moskovits, How the localized surface plasmon became linked with surface-enhanced Raman spectroscopy, Notes Rec. Roy. Soc. (2012) 66, 195–203.

[17] M. Moskovits, Surface-enhanced Raman spectroscopy: a brief retrospective, J. Raman Spectrosc. **36** (2005), 485–496.

[18] P. L. Stiles, J. A. Dieringer, N. C. Shah, R. P. Van Duyne, Surface-enhanced Raman spectroscopy, Annu. Rev. Anal. Chem. **1** (2008), 601–626.

[19] K. Kneipp, M. Moskovits, H. Kneipp (eds.), Surface-enhanced Raman scattering: Physics and applications, Series: Topics in applied physics **103**, Springer-Verlag Berlin Heidelberg, 2006.

[20] E. C. Le Ru, P. G. Etchegoin, Principles of Surface-enhanced Raman Spectroscopy and Related Plasmonic Effects, Elsevier, Amsterdam, 2009.

[21] M. Procházka, Surface-Enhanced Raman Spectroscopy: Bioanalytical, Biomolecular and Medical Applications, Springer International Publishing, Switzerland, 2016.

[22] E. A. Stern, R. A. Ferrell, Surface plasma oscillations of a degenerate electron gas, Phys. Rev. **120** (1960), 130.

[23] S. L. Cunningham, A. A. Maradudin, R. F. Wallis, Effect of a charge layer on the surface plasmon polariton dispersion curve, Phys. Rev. B **10** (1974), 3342.

[24] U. Kreibig, P. Zacharias, Surface plasmon resonances in small spherical silver and gold particles, Z. Phys. **231** (1970), 128.

[25] G. Mie, Beitrage zur Optik truber Medien, speziell kolloidaler Metallosungen, Ann. Phys. **330** (1908), 377-445.

[26] M. Moskovits, Surface-enhanced spectroscopy, Rev. Mod. Phys. **57** (1985), 783–826.

[27] T. Dörfer, M. Schmitt, J. Popp, Deep-UV surface-enhanced Raman scattering, J. Raman Spectrosc. **38** (2007) 1379–1382.

[28] H. Xu, J. Aizpurua, M. Käll, P. Apell, Electromagnetic contributions to single-molecule sensitivity in surface-enhanced Raman scattering, Phys. Rev. E **62** (2000), 4318–4324.

[29] H. Xu, M. Käll, Polarization-Dependent Surface-Enhanced Raman Spectroscopy of Isolated Silver Nanoaggregates, Chem. Phys. Chem. **4** (2003), 1001–1005.

[30] A. Otto, The ‘chemical’ (electronic) contribution to surface-enhanced Raman scattering, J. Raman Spectrosc. **36** (2005), 497–509.

[31] A. Campion, P. Kambhampati, Surface-enhanced Raman scattering, Chem. Soc. Rev. **27** (1998), 241–250.

[32] K. Kneipp, Y. Wang, H. Kneipp, L. T. Perelman, I. Itzkan, R. R. Dasari, M. S. Feld, Single molecule detection using surface-enhanced Raman scattering (SERS), Phys. Rev. Lett. **78** (1997), 1667–1670.

[33] Z.-Q. Tian, B. Ren, D.-Y. Wu, Surface-Enhanced Raman Scattering: From Noble to Transition Metals and from Rough Surfaces to Ordered Nanostructures, J. Phys. Chem. B **106** (2002), 1463–1483.

[34] X. M. Lin, Y. Cui, Y. H. Xu, B. Ren, Z. Q. Tian, Surface-enhanced Raman spectroscopy: substrate-related issues. Anal. Bioanal. Chem **394** (2009), 1729–1745.

[35] M. Fan, G. F. S. Andrade, A. G. Brolo, A review on the fabrication of substrates for surface enhanced Raman spectroscopy and their applications in analytical chemistry. Anal. Chim. Acta **693** (2011), 7–25.

[36] M. Jahn, S. Patze, I. Hidi, R. Knipper, A. Radu, A. Mühlig, S. Yüksel, V. Peksa, K. Weber, T. Mayerhöfer, D. Cialla-May, J. Popp, Plasmonic nanostructures for surface enhanced spectroscopic methods, Analyst **141** (2016), 756–793.

[37] J. A. Creighton, C. G. Blatchford, M. G. Albrecht, Plasma reosnance enhancement of Raman scattering by pyridine adsorbed on silver and gold sol particles of size comparable to the excitation wavelength, J. Chem. Soc. Faraday Trans. **75** (1979), 790–798.

[38] P. C. Lee, D. Meisel, Adsorption and surface-enhanced Raman of dyes on silver and gold sols, J. Phys. Chem. **86** (1982), 3391–3395.

[39] N. Leopold, B. Lendl, A new method for fast preparation of highly surface-enhanced Raman scattering (SERS) active silver colloids at room temperature by reduction of silver nitrate with hydroxylamine hydrochloride, J. Phys. Chem. B **107** (2003), 5723–5727.

[40] I. A. Larmour, K. Faulds, D. Graham, SERS activity and stability of the most frequently used silver colloids, J. Raman Spectrosc. **43** (2012), 202–206.

[41] T. K. Sau, C. J. Murphy, Room Temperature, High-Yield Synthesis of Multiple Shapes of Gold Nanoparticles in Aqueous Solution, J. Am. Chem. Soc. **126** (2004), 8648–8649.

[42] Z. Q. Tian, B. Ren, J. F. Li, Z. L. Yang, Expanding generality of surface-enhanced Raman spectroscopy with borrowing SERS activity strategy, Chem. Commun. **34** (2007), 3514–3534.

[43] I. Srnová-Šloufová, F. Lednický, A. Gemperle, J. Gemperlová, Core− shell (Ag) Au bimetallic nanoparticles: Analysis of transmission electron microscopy images, Langmuir **16** (2000), 9928–9935.

[44] S. J. Oldenburg, J. B. Jackson, S. L. Westcott, N. J. Halas, Infrared extinction properties of gold nanoshells, Appl. Phys. Lett. **75** (1999), 2897–2899.

[45] D. H. Everett, Basic Principles of Colloid Science, The Royal Society of Chemistry, London, 1988.

[46] I. Chourpa, F. H. Lei, P. Dubois, M. Manfait, G. D. Sockalingum, Intracellular applications of analytical SERS spectroscopy and multispectral imaging, Chem. Soc. Rev. **37** (2008), 993–1000.

[47] J. V. Jokerst, T. Lobovkina, R. N. Zare, S. S. Gambhir, Nanoparticle PEGylation for Imaging and Therapy, Nanomedicine **6** (2011), 715−728.

[48] C. Luo, Y. Zhang, X. Zeng, Y. Zeng, Y. Wang, The Role of Poly(ethylene Glycol) in the Formation of Silver Nanoparticles, J. Colloid Interface Sci. **288** (2005), 444−448.

[49] D. P. Lankveld, R. G. Rayavarapu, P. Krystek, A. G. Oomen, H. W. Verharen, T. G. van Leeuwen, W. H. De Jong, S. Manohar, Blood Clearance and Tissue Distribution of PEGylated and Non-PEGylated Gold Nanorods after Intravenous Administration in Rats, Nanomedicine **6** (2011), 339−349.

[50] L. Bo, W. Yang, M. Chen, J. Gao, Q. Xue, Simple and 'Green' Synthesis of Polymer-Based Silver Colloids and Their Antibacterial Properties, Chem. Biodiversity **6** (2009), 111−116.

[51] A. Shkilnyy, M. Soucé, P. Dubois, F. Warmont, M.-L. Saboungi, I. Chourpa, Poly(ethylene Glycol)-Stabilized Silver Nanoparticles for Bioanalytical Applications of SERS Spectroscopy, Analyst **134** (2009), 1868−1872.

[52] M. V. Canamares, J. V. Garcia-Ramos, J. D. Gomez-Varga, C. Domingo, S. Sanchez-Cortes, Comparative study of the morphology, aggregation, adherence to glass, and surface-enhanced Raman scattering activity of silver nanoparticles prepared by chemical reduction of Ag+ using citrate and hydroxylamine, Langmuir **21** (2005), 8546−8553.

[53] R. D. Deegan, O. Bakajin, T. F. Dupont, G. Huber, S. R. Nagel, T. A. Witten, Capillary flow as the cause of ring stains from dried liquid drops, Nature **389** (1997), 827–829.

[54] J.-Y. Jung, Y. W. Kim, J. Y. Yoo, Behavior of particles in an evaporating didisperse colloid droplet on a hydrophilic surface, Anal. Chem. **81** (2009), 8256–8259.

[55] G. V. Pavan Kumar, B. A. Ashok Reddy, M. Arif, T. K. Kundu, C. Narayana, Surface-enhanced Raman scattering studies of human transcriptional coactivator p300, J. Phys. Chem. B **110** (2006), 16787–16792.

[56] N. Hajduková, M. Procházka, J. Štěpánek, M. Špírková, Chemically reduced and laser-ablated gold nanoparticles immobilized to silanized glass plates: Preparation, characterization and SERS spectral testing, Colloids and Surfaces A: Physicochem. Eng. Aspects **301** (2007), 264–270.

[57] N. Hajduková, M. Procházka, P. Molnár, J. Štěpánek, SERRS of free-base porphyrins on immobilized metal gold and silver nanoparticles, Vibrational Spectr. **48** (2008), 142–147.

[58] M. Fan, A. G. Brolo, Silver nanoparticles self assembly as SERS substrates with near single molecule detection limit, Phys. Chem. Chem. Phys. **11** (2009), 7381–7389.

[59] K. R. Brown, M. J. Natan, Hydroxylamine seeding of colloidal Au nanoparticles in solution and on surfaces, Langmuir **14** (1998), 726–728.

[60] V. Joseph, M. Gensler, S. Seifert, U. Gernert, J. P. Rabe, J. Kneipp, Nanoscopic Properties and Application of Mix-and-Match Plasmonic Surfaces for Microscopic SERS, J. Phys. Chem. C **116** (2012), 6859−6865.

[61] R.G. Freeman, K.C. Grabar, K.J. Allison, R.M. Bright, J.A. Davis, M.A. Jackson, P.C. Smith, D.G. Walter, M.J. Natan, Self-assembled metal colloid monolayers: an approach to SERS substrates, Science **267** (1995), 1629–1632.

[62] G. Chumanov, K. Sokolov, B. W. Gregory, T. M. Cotton, Colloidal metal-films as a substrate for surface-enhanced spectroscopy, J. Phys. Chem. **99** (1995), 9466–9471.

[63] C. D. Keating, M. D. Musick, M. H. Keefe, M. J. Natan, Kinetics and thermodynamics of Au colloid monolayer self-assembly – Undergraduate experiments in surface and nanomaterials chemistry, J. Chem. Educ. **76** (1999), 949–955.

[64] L. G. Olson, Y.-S. Lo, T. P. Beebe Jr., J. M. Harris, Characterization of silanemodified immobilized gold colloids as a substrate for surface-enhanced Raman spectroscopy, Anal. Chem. **73** (2001), 4268–4276.

[65] F. Toderas, M. Baia, L. Baia, S. Astilean, Controlling gold nanoparticle assemblies for efficient surface-enhanced Raman scattering and localized surface plasmon resonance sensors, Nanotechnology **18** (2007), 255702.

[66] M. Fan, A. G. Brolo, Self-assembled Au nanoparticles as substrates for surfaceenhanced vibrational spectroscopy: optimization and electrochemical stability, Chem. Phys. Chem. **9** (2008), 1899–1907.

[67] T. Makiabadi, A. Bouvree, V. Le Nader, H. Terrisse, G. Louarn, Preparation, optimization, and characterization of SERS sensor substrates based on twodimensional structures of gold colloid, Plasmonics **5** (2010), 21–29.

[68] M. Kahl, E. Voges, S. Kostrewa, C. Viets, W. Hill, Periodically structured metallic substrates for SERS, Sensors and Actuators B: Chemical **51** (1998) 285–291.

[69] J.-L. Yao, J. Tang, D.-Y. Wu, D.-M. Sun, K.-H. Xue, B. Ren, B.-W. Mao, Z.-Q. Tian, Surface enhanced Raman scattering from transition metal nano-wire array and the theoretical consideration, Surf. Sci. **514** (2002), 108–116.

[70] C. Schönenberger, B. M. I. van der Zande, L. G. J. Fokkink, M. Henny, C. Schmid, M. Krüger, A. Bachtold, R. Huber, H. Birk, U. Staufer, Template synthesis of nanowires in porous polycarbonate membranes: electrochemistry and morphology, J. Phys. Chem. B **101** (1997), 5497–5505.

[71] J. C. Hulteen, R. P. Van Duyne, Nanosphere lithography: A materials general fabrication process for periodic particle array surfaces, J. Vac. Sci. Technol. A **13** (1995), 1553–1558.

[72] C. L. Haynes, R. P. Van Duyne, Nanosphere lithography: a versatile nanofabrication tool for studies of size-dependent nanoparticle optics, J. Phys. Chem. B **105** (2001), 5599–5611.

[73] D.-Y. Wu, J.-F. Li, B. Ren, Z.-Q. Tian, Electrochemical surface-enhanced Raman spectroscopy of nanostructures, Chem. Soc. Rev. **37** (2008), 1025–1041.

[74] L. Štolcová, J. Proška, M. Procházka, Hexagonally ordered gold semishells as tunable SERS substrates, In: Proceedings of Nanocon, Brno, 2012, pp. 225–229.

[75] L. A. Dick, A. D. McFarland, C. L. Haynes, R. P. Van Duyne, Metal Film over Nanosphere (MFON) Electrodes for Surface-Enhanced Raman Spectroscopy (SERS): Improvements in Surface Nanostructure Stability and Suppression of Irreversible Loss, J. Phys. Chem. B **106** (2002), 853–860.

[76] A. Kosiorek, W. Kandulski, P. Chudzinski, K. Kempa, M. Giersig, Shadow nanosphere lithography: Simulation and experiment, Nano Lett. **4** (2004), 1359–1363.

[77] O. Lyandres, N. C. Shah, C. R. Yonzon, J. T. Walsh, M. R. Glucksberg, R. P. Van Duyne, Real-time glucose sensing by surface-enhanced Raman spectroscopy in bovine plasma facilitated by a mixed decanethiol/mercaptohexanol partition layer, Anal. Chem. **77** (2005), 6134–6139.

[78] V. Peksa, M. Jahn, L. Štolcová, V. Schulz, J. Proška, M. Procházka, K. Weber, D. Cialla-May, J. Popp, Quantitative SERS Analysis of Azorubine (E 122) in Sweet Drinks, Anal. Chem. **87** (2015), 2840–2844.

[79] G. Zhang, J. Zhang, G. Xie, Z. Liu, H. Shao, Cicada wings: a stamp from nature for nanoimprint lithography, Small **2** (2006), 1440-1443.

[80] N. L. Garrett, P. Vukusic, F. Ogrin, E. Sirotkin, P. Winlove, J. Moger, Spectroscopy on the wing: Naturally inspired SERS substrates for biochemical analysis, J. Biophotonics **2** (2009), 157–166.

[81] Y. Tan, X. Zang, J. Gu, D. Liu, S. Zhu, H. Su, C. Feng, Q. Liu, W. Ming Lau, W.-J. Moon, D. Zhang, Morphological Effects on Surface-Enhanced Raman Scattering from Silver Butterfly Wing Scales Synthesized via Photoreduction, Langmuir **27** (2011), 11742–11746.

[82] Y. Tan, J. Gu, L. Xu, X. Zang, D. Liu, W. Zhang, Q. Liu, S. Zhu, H. Su, C. Feng, G. Fan, D. Zhang, High-Density Hotspots Engineered by Naturally Piled-Up Subwavelength Structures in Three-Dimensional Copper Butterfly Wing Scales for Surface-Enhanced Raman Scattering Detection, Adv. Funct. Mater. **22** (2012), 1578–1585.

[83] P. R. Stoddart, P. J. Cadusch, T. M. Boyce, R. M. Erasmus, J. D. Comins, Optical properties of chitin: Surface-enhanced Raman scattering substrates based on antireection structures on cicada wings, Nanotechnology **17** (2006), 680–686.

[84] G. Kostovski, D. J. White, A. Mitchell, M. W. Austin, P. R. Stoddart, Nanoimprinted optical fibres: Biotemplated nanostructures for SERS sensing. Biosens. Bioelectron. **24** (2009), 1531–1535.

[85] M. Procházka, J. Štěpánek, P.-Y. Turpin, J. Bok, Drastically different porphyrin adsorption and metallation processes in chemically prepared and laser-ablated SERS-active silver colloidal substrates, J. Phys. Chem. B **106** (2002), 1543–1549.

[86] M. Procházka, P.-Y. Turpin, J. Štěpánek, J. Bok, Metallation kinetics of a free base porphyrin in surface-enhanced resonance Raman scattering active Ag colloid system as a probe of porphyrin–nucleic acids interaction, J. Mol. Struct. **482–483** (1999), 221–224.

[87] P. Šmejkal, B. Vlčková, M. Procházka, P. Mojzeš, J. Pfleger, Testing anionic spacers by SERRS (surface-enhanced resonance Raman scattering) of a cationic free-base porphyrin in systems with laser-ablated Ag colloids, Vib. Spectrosc. **19** (1999), 243–247.

[88] P. Šmejkal, B. Vlčková, M. Procházka, P. Mojzeš, J. Pfleger, SERRS spectra of cationic free-base porphyrin species adsorbed on laser ablated Ag colloids modified by mercaptoacetate spacers, J. Mol. Struct. **482-483** (1999), 225–229.

[89] J. Hanzlíková, M. Procházka, J. Štěpánek, J. Bok, V. Baumruk, P. Anzenbacher Jr., Metallation of 5,10,15,20-Tetrakis(1-methyl-4-pyridyl)porphyrin in Silver

Colloids Studied via Time Dependence of Surface-Enhanced Resonance Raman Spectra, J. Raman Spectrosc. **29** (1998), 575−584.

[90] I. Šloufová, K. Šišková, B. Vlčková, J. Štěpánek, SERS-activating effect of chlorides on borate-stabilized silver nanoparticles: formation of new reduced adsorption sites and induced nanoparticle fusion, Phys.Chem. Chem. Phys. **10** (2008), 2233–2242.

[91] Tryptophan, In: English Wikipedia [29.7.2017], https://en.wikipedia.org/wiki/Tryptophan

[92] C.-H. Chuang, Y.-T. Chen, Raman scattering of L-tryptophan enhanced by surface plasmon of silver nanoparticles: vibrational assignment and structural determination, J. Raman Spectrosc. **40** (2009), 150–156.

[93] A. Kandakkathara, I. Utkin, R. Fedosejevs, Surface-enhanced Raman scattering (SERS) detection of low concentrations of tryptophan amino acid in silver colloid, Applied Spectroscopy **65** (2011), 507–513.

[94] D. Liu, Y. K. Song, Cationic liposome-mediated transfection in vivo, Gene Ther. Mol. Biol. **2** (1998), 59–68.

[95] I. W. Levin, In: Advances in Infrared and Raman Spectroscopy Vol. 11, R. J. H. Clark, R. E. Hester (eds.), Wiley Heyden, Chichester, 1984, p.1.

[96] T. M. Cotton, J.-H. Kim, G. D. Chumanov, Application of surface-enhanced Raman spectroscopy to biological systems, J. Raman Spectrosc. **22** (1991), 729–742.

[97] A. M. Ahern, R. L. Garrell, Insitu photoreduced silver-nitrate as a substrate for surface-enhanced Raman-spectroscopy, Anal. Chem. **59** (1987), 2813-2816.

[98] I. Šloufová-Srnová, B. Vlčková, Two-dimensional assembling of Au nanoparticles mediated by tetrapyridylporphine molecules, Nano Lett. **2** (2002), 121-125.

[99] T. P. Ang, W. S. Chin, Dodecanethiol-Protected Copper/Silver Bimetallic Nanoclusters and Their Surface Properties, J. Phys. Chem. B **109** (2005), 22228-22236.

[100] A. Carrouée, E. Allard-Vannier, S. Même, F. Szeremeta, J.-C. Beloeil, I. Chourpa, Sensitive Trimodal Magnetic Resonance Imaging-Surface-Enhanced Resonance Raman Scattering-Fluorescence Detection of Cancer Cells with Stable Magneto-Plasmonic Nanoprobes, Anal. Chem. **87** (2015), 11233−11241.

[101] L. Štolcová, J. Proška, F. Novotný, M. Procházka, I. Richter, Periodic arrays of metal nanobowls as SERS- active substrates, In: Conference proceedings Nanocon, Brno, 2011.

[102] P. Šimáková, Study of biomolecules by surface-enhanced Raman microspectroscopy, master thesis, MFF UK, Praha, 2009. (Czech)

[103] A. Kudelski, Some aspects of SERS temporal fluctuations: analysis of the most intense spectra of hydrogenated amorphous carbon deposited on silver, J. Ram. Spectrosc. **38** (2007), 1494-1499.

[104] E. C. Le Ru, E. Blackie, M. Meyer, P. G. Etchegoin, Surface enhanced Raman scattering enhancement factors: a comprehensive study, J. Phys. Chem. C **111** (2007) 13794-13803.

[105] P. Šimáková, Adsorption-desorption properties of porphyrins on metal nanosurfaces, bachelor thesis, MFF UK, Praha, 2007. (Czech)

[106] V. Thomsen, D. Schatzlein, D. Mercuro, Limits of detection in spectroscopy, Spectroscopy **18** (2003), 112-114.

[107] E. R. Malinowski, Factor Analysis in Chemistry, Wiley, New York, 1991.

[108] M. Procházka, B. Vlčková, J. Štěpánek, and P. Y. Turpin, Probing of porphyrin surface chemistry in systems with laser-ablated Ag nanoparticle hydrosol: role of thiosulfate anions, Langmuir **21** (2005), 2956–2962.

[109] M. Procházka, P. Mojzeš, B. Vlčková, P.-Y. Turpin, Surface-Enhanced Resonance Raman Scattering from Copper(II) 5,10,15,20-tetrakis(1-methyl-4-pyridyl)porphyrin Adsorbed on Aggregated and Nonaggregated Silver Colloids, J. Phys. Chem. B **101** (1997), 3161–3167.

[110] L. Štolcová, J. Proška, M. Procházka, Rationally designed SERS substrates for the ultrasensitive detection of biologically important compounds, In: Conference Proceedings Nanocon, Brno, 2013, pp. 659-664.

[111] A. Palm, Raman spectrum of polystyrene, J. Phys. Chem. **55** (1951), 1320–1324.

[112] J. R. Anema, A. G. Brolo, A. Felten, C. Bittencourt, Surface-enhanced Raman scattering from polystyrene on gold clusters, J. Raman Spectrosc. **41** (2010), 745–751.

List of Abbreviations

AEF	analytical enhancement factor
AFM	atomic force microscopy
CCD	charge-coupled device
CT	charge transfer
DCDR	drop coating deposition Raman
DLS	dynamic light scattering
DMSO	dimethylsulfoxide
DMTAP	1,2-dimyristoyl-3-trimethylammonium-propane
DSPC	1,2-distearoyl-sn-glycero-3-phosphocholine
EBL	electron beam lithography
EF	enhancement factor
FA	factor analysis
FIB	focused ion beam
FON	film-over-nanospheres
FWHM	full width at high maximum
HOMO	highest occupied molecular orbital
IR	infrared
LOD	limit of detection
LSP	localized surface plasomon
LSPP	localized surface plasmon-polariton
LSPR	localized surface plasmon resonance
LUMO	lowest unoccupied molecular orbital
NIR	near infrared
NL	nanolithography
NP	nanoparticle
NSL	nanosphere lithography
PEG	polyethylene glycol
PS	polystyrene
RRS	resonance Raman scattering
RS	Raman scattering
SAM	self-assembled monolayer
SEM	scanning electron microscopy
SERRS	surface-enhanced resonance Raman scattering
SERS	surface-enhanced Raman scattering
SP	surface plasmon
SPE	surface plasmon extinction
SPP	surface plasmon-polariton
TMAP	5,10,15,20-tetrakis(4-trimethylammoniophenyl)-21H,23H-porphine

TMPyP	5,10,15,20-tetrakis(1-methyl-4-pyridyl)porphyrin
ULWD	ultra long working distance
UV	ultraviolet
VIS	visible

List of Conference Contributions

P. Šimáková, M. Procházka: SERRS microspectroscopy of porphyrins on Ag immobilized nanoparticles, poster, 30th European Congress of Molecular Spectroscopy, Florence, Italy, August 29 – September 3, 2010, abstract in Book of abstracts, M. Becucci, C. Gellini, V. Schettino, (eds.), p. 227.

P. Šimáková, M. Procházka, E. Kočišová: SERS microspectroscopy of biomolecules on dried Ag colloidal drops, poster, 14th European Conference on the Spectroscopy of Biological Molecules, Coimbra, Portugal, August 29 – September 3, 2011.

P. Šimáková, L. Štolcová, M. Procházka, J. Proška: SERS of porphyrins from regular metal nanostructures, poster, 31st European Congress on Molecular Spectroscopy, August 26 – 31, 2012, Cluj-Napoca, Romania, Book of abstracts, K. Nagy-Póra, V. Chis, S. Astilean, O. Cozar (eds.), p. 238.

P. Šimáková, M. Procházka, L. Štolcová, F. Novotný, J. Proška: SERS spectra of porphyrins measured on silver substrates prepared by biotemplating, poster, 7th International Conference on Advanced Vibrational Spectroscopy, Kobe, Japan, August 25 – 30, 2013.

List of Papers

Papers which are part of the thesis:

P. Šimáková, M. Procházka: SERRS microspectroscopy of porphyrins on Ag immobilized nanoparticles, J. Mol. Struct. **993** (2011), 425–427.
*Author´s contribution: all experimental work, writin*g of the paper.

M. Procházka, P. Šimáková, N. Hajduková-Šmídová: SE(R)RS microspectroscopy of porphyrins on immobilized Au nanoparticles: Testing spectral sensitivity and reproducibility, Colloids Surf. A: Physicochem. Eng. Aspects **402** (2012), 24-28.
Author´s contribution: part of the experimental work.

P. Šimáková, M. Procházka, E. Kočišová: SERS microspectroscopy of biomolecules on dried Ag colloidal drops, Spectroscopy: An International Journal **27** (2012), 449-453.
*Author´s contribution: all experime*ntal work, writing major part of the paper.

Published also in a book:
M.P. Marques, L.B. de Carvalho, and P.I. Haris (eds.), Spectroscopy of Biological Molecules: Proceedings from the 14th European Conference on the Spectroscopy of Biological Molecules 2011. Vol. 7. IOS Press, 2013, p. 171-175.

P. Šimáková, E. Kočišová, M. Procházka: Sensitive Raman spectroscopy of lipids based on drop deposition using DCDR and SERS, J. Raman Spectrosc. **44** (2013), 1479–1482.
Author´s contribution: major part of the experimental work, preparation of the figures, partly writing the paper.

P. Šimáková, J. Gautier, M. Procházka, K. Hervé-Aubert, I. Chourpa: Polyethylene-glycol-stabilized Ag nanoparticles for surface-enhanced Raman scattering spectroscopy: Ag surface accessibility studied using metallation of free-base porphyrins, J. Phys. Chem. C **118** (2014), 7690–7697.
Author´s contribution: experimental work in collaboration with J. Gautier,
preparation of the figures, partly writing the paper.

Other papers of the author:

K. Herynková, M. Šlechta, P. Šimáková, A. Fučíková, O. Cibulka, Agglomeration of Luminescent Porous Silicon Nanoparticles in Colloidal Solutions, Nanoscale Res. Lett. **11** (2016), 367.

K. Herynková, C. Vorkötter, P. Šimáková, J. Benedikt, O. Cibulka, Structural and luminescence properties of silicon nanocrystals in colloidal solutions for bio-applications, Phys. Status Solidi A **213** (2016), 2873-2878.

Supplements

[I] P. Šimáková, M. Procházka
SERRS microspectroscopy of porphyrins on Ag immobilized nanoparticles
J. Mol. Struct. **993** (2011), 425–427

[II] M. Procházka, P. Šimáková, N. Hajduková-Šmídová
SE(R)RS microspectroscopy of porphyrins on immobilized Au nanoparticles: Testing spectral sensitivity and reproducibility
Colloids Surf. A: Physicochem. Eng. Aspects **402** (2012), 24-28

[III] P. Šimáková, M. Procházka, E. Kočišová
SERS microspectroscopy of biomolecules on dried Ag colloidal drops
Spectroscopy: An International Journal **27** (2012), 449-453

[IV] P. Šimáková, E. Kočišová, M. Procházka
Sensitive Raman spectroscopy of lipids based on drop deposition using DCDR and SERS
J. Raman Spectrosc. **44** (2013), 1479–1482

[V] P. Šimáková, J. Gautier, M. Procházka, K. Hervé-Aubert, I. Chourpa
Polyethylene-glycol-stabilized Ag nanoparticles for surface-enhanced Raman scattering spectroscopy: Ag surface accessibility studied using metallation of free-base porphyrins
J. Phys. Chem. C **118** (2014), 7690–7697

Supplement [I]

P. Šimáková, M. Procházka, SERRS microspectroscopy of porphyrins on Ag immobilized nanoparticles, J. Mol. Struct. **993** (2011), 425–427.

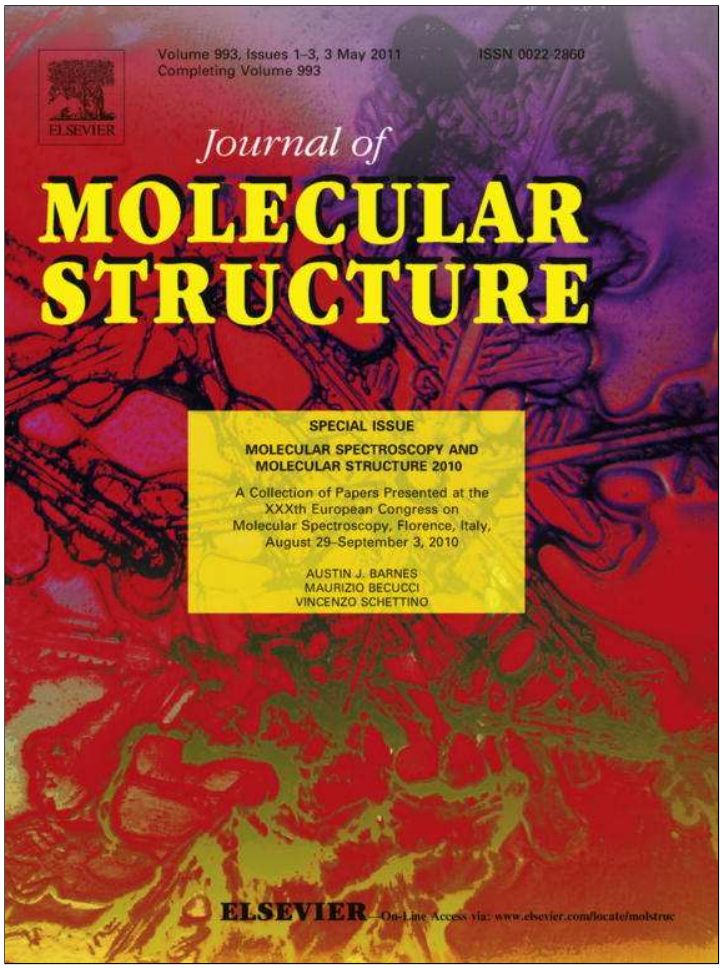

Journal of Molecular Structure 993 (2011) 425–427

Contents lists available at ScienceDirect

Journal of Molecular Structure

journal homepage: www.elsevier.com/locate/molstruc

SERRS microspectroscopy of porphyrins on Ag immobilized nanoparticles

Petra Šimáková *, Marek Procházka

Charles University, Faculty of Mathematics and Physics, Institute of Physics, Ke Karlovu 5, CZ-121 16 Prague 2, Czech Republic

ARTICLE INFO

Article history:
Available online 23 December 2010

Keywords:
SERS
Porphyrin
Ag immobilized nanoparticles
Raman microspectroscopy

ABSTRACT

SERRS spectra of cationic 5,10,15,20-tetrakis(1-methyl-4-pyridyl)porphyrin (TMPyP) on Ag nanoparticles immobilized to glass *via* silane or by drying were measured using confocal Raman microspectrometer. The limit of detection (LOD) of TMPyP on Ag silanized glass plates was $\sim 1 \times 10^{-8}$ M, but spectra suffered from presence of spurious bands originating from carbon species mainly as a result of thermal decomposition of silane. Ag colloid/TMPyP drops dried on glass show better spectra and fewer spurious bands for the same TMPyP concentration compared to the silanized surfaces. Dried drops form a ring in the edge part of the drop containing high enhancing sites (big aggregates with some 'hot spots') providing high SERRS signal of TMPyP in extremely short acquisition times (1 s). Despite the problems with spurious bands, Raman microspectroscopy from immobilized Ag colloidal nanoparticles improves SERS sensitivity and reproducibility in comparison to macro-Raman measurements in Ag colloidal solution.

1. Introduction

Porphyrins are important biomolecules and their derivatives are or can potentially be applied in photodynamic therapy of cancer, antiviral treatment, specific sensing of DNA sequences, selective cleavage of nucleic acids, etc. Surface-enhanced (resonance) Raman scattering (SE(R)RS) spectroscopy is a very sensitive method of Raman spectroscopy that provides enhanced Raman signal for molecules adsorbed on rough metal surfaces [1]. Porphyrins exhibit strong SE(R)RS signal and therefore can be used for testing of the properties of SERS-active surfaces.

In SERS spectroscopy metal colloidal solutions are the most frequently used substrates due to their cheap and simple preparation, but their chemical instability and irreproducibility of spectral measurements are serious drawbacks for their use in analytical applications. Furthermore, in the case of free-base porphyrins, metalation process (incorporation of a metal ion from the surface into the porphyrin core) is observed [2,3].

Higher spectral reproducibility can be achieved by immobilization of the metal colloidal nanoparticles on a solid substrate. One way to do that is to attach colloidal nanoparticles to glass slides *via* a self-assembled monolayer of organosilanes [4]. Using porphyrins as testing molecules, the preparation procedure was improved for gold [5] and for silver nanoparticles [6,7] where it was surprisingly found out that in this case metalation of free-base porphyrin by silver does not occur. SERS limits of detection were determined for porphyrins of different charge on gold and silver substrates using macro-Raman [6]. Another possibility is to use colloidal nanoparticles immobilized directly on glass prepared by drying of a colloid or colloid/analyte droplet on a glass substrate [8,9]. During evaporation the 'coffee ring effect' [10] causes formation of a ring at the contact line of the drop containing most of the nanoparticles [11]. Aggregation of the nanoparticles upon drying leads to creation of fractal-like structures with 'hot spots' with high SERS enhancement [8]. For example, SERS spectra of proteins were measured from the ring [12].

This contribution is devoted to SERRS microspectroscopy of cationic 5,10,15,20-tetrakis(1-methyl-4-pyridyl)porphyrin (TMPyP) on immobilized silver colloidal nanoparticles. Silver colloidal nanoparticles attached to glass slides *via* silane and by drying were used. Objectives of this work were to compare these two types of immobilized silver nanoparticle systems in terms of SERS sensitivity and reproducibility.

2. Experimental

Deionized water of a specific resistance of 18 MΩ cm was used for all preparations. HNO_3 (65%), H_2SO_4 (96%), H_2O_2 (30%), HCl (35%) and NaOH were purchased from Lachema, Brno, Czech Republic. $AgNO_3$, $NaBH_4$, 3-aminopropyltrimethoxysilane (APTMS, 97%), methanol (99.8%) and free-base 5,10,15,20-tetrakis(1-methyl-4-pyridyl)porphyrin salt were obtained from Sigma–Aldrich. All glassware was cleaned with 'piranha' solution (four parts H_2SO_4, one part H_2O_2) to remove organic compounds and then with diluted HNO_3 (one part HNO_3, one part deionized water) to remove silver and finally rinsed with deionized water.

Borohydride-reduced colloid was prepared by reduction of $AgNO_3$ by $NaBH_4$ according to [13]. To prepare Ag nanoparticles

* Corresponding author. Tel.: +420 221911463; fax: +420 224922797.
E-mail addresses: simakova@karlov.mff.cuni.cz (P. Šimáková), prochaz@karlov.mff.cuni.cz (M. Procházka).

0022-2860/$ - see front matter © 2010 Elsevier B.V. All rights reserved.
doi:10.1016/j.molstruc.2010.12.037

immobilized by silanization on glass, clean glass plates (1 × 2 cm) were immersed into 10% solution of APTMS in methanol for 30 min [6]. After silanization, the substrates were rinsed several times with methanol and deionized water to remove unbound silane that could cause colloid aggregation. After that, the substrates were soaked separately (to prevent destroying of a whole set) in vials with 1 ml of borohydride-reduced silver colloid for 6 h and rinsed with deionized water. In spite of using this optimized preparation procedure, the preparation of Ag surfaces is successful for only about 60% of the substrates (i.e., for example, six surfaces out of 10 were suitable for SERS while four were not because the colloid aggregated in contact with the silanized substrate and subsequently settled at the bottom and therefore not enough nanoparticles attached to the substrate) [6]. For SERRS measurements the best substrates with the highest surface plasmon extinction monitored by UV/VIS absorption spectroscopy were chosen.

In the case of Ag nanoparticles immobilized by silane, SERS systems were prepared by dipping of the Ag substrate into TMPyP solution of the desired concentration for 15 min and then directly measured. In the case of dried drops, TMPyP was added to Ag colloid to obtain the desired TMPyP concentration and ~2 μl of Ag colloid/TMPyP mixture were dropped by pipette on a clean glass plate. The droplet was then left to dry at room temperature for approximately 45 min and then SERRS spectra were measured.

SERRS spectra were recorded at room temperature by a confocal micro-Raman spectrometer LabRam HR800 (Horiba Jobin Yvon) equipped with a nitrogen-cooled CCD detector and a 600 grooves/mm spectrograph. 514.5 nm excitation line of an Ar^+ laser (Melles Griot, power ~0.2 or 0.02 mW at the sample) and 100 × (NA 0.9) objective were used.

3. Results and discussion

Fig. 1 shows examples of SERRS spectra for three different TMPyP concentrations measured from different spots of two Ag substrates prepared by silanization. The acquisition times were 2 × 60 s for the upper spectrum (1×10^{-6} M) and 5 × 12 s for the other spectra. Problems occurred with accumulation of the signal because of the TMPyP signal decrease and presence of spurious bands. The decrease of the SERRS signal of TMPyP was probably caused by thermal decomposition and/or thermal desorption of TMPyP. Intensity and signal-to-noise ratio are strongly affected by this process and in some cases longer acquisition time does not lead to a better spectrum (Fig. 1). The spurious bands are fluctuating narrow bands in the spectral region 1200–1700 cm^{-1} and/or two broad bands with maxima at ~1350 cm^{-1} and ~1580 cm^{-1} that could not be assigned to TMPyP. Examples of these bands are shown in Fig. 2a. They were measured from the same spot in time intervals of approximately 1 min. We assign them according to the literature [14] to vibrations of amorphous carbon (~1350 cm^{-1} and ~1580 cm^{-1}) and other carbon species originating in thermal decomposition of compounds present on the surface due to the intense laser irradiation. To judge the contribution of TMPyP to the spurious bands, Raman spectra from a bare Ag surface were measured (Fig. 2b). Spurious bands of the same character were observed in this case as well, which means that they cannot come only from thermal decomposition of TMPyP. They probably originate mainly in thermal decomposition of silane because we observed much less spurious bands on Ag nanoparticles immobilized by drying. We found out that these problems cannot be significantly reduced by changing experimental parameters, including defocused laser beam, lower laser power and shorter acquisition times.

The limit of detection (LOD) of TMPyP was determined from dependence of SERRS spectra on concentration as ~1×10^{-8} M (data not shown). It was done by extrapolation to concentration for which the intensity of the strongest TMPyP band at

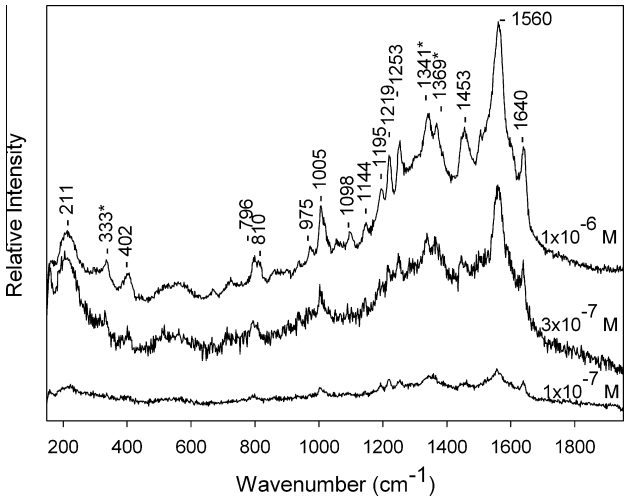

Fig. 1. SERRS spectra of various TMPyP concentrations measured from Ag nanoparticles immobilized on a glass plate by silane: 1×10^{-7} M (~0.02 mW at the sample, 5 × 12 s), 3×10^{-7} M (~0.2 mW at the sample, 5 × 12 s) 1×10^{-6} M (~0.2 mW at the sample, 2 × 60 s), free-base markers labeled with an asterisk.

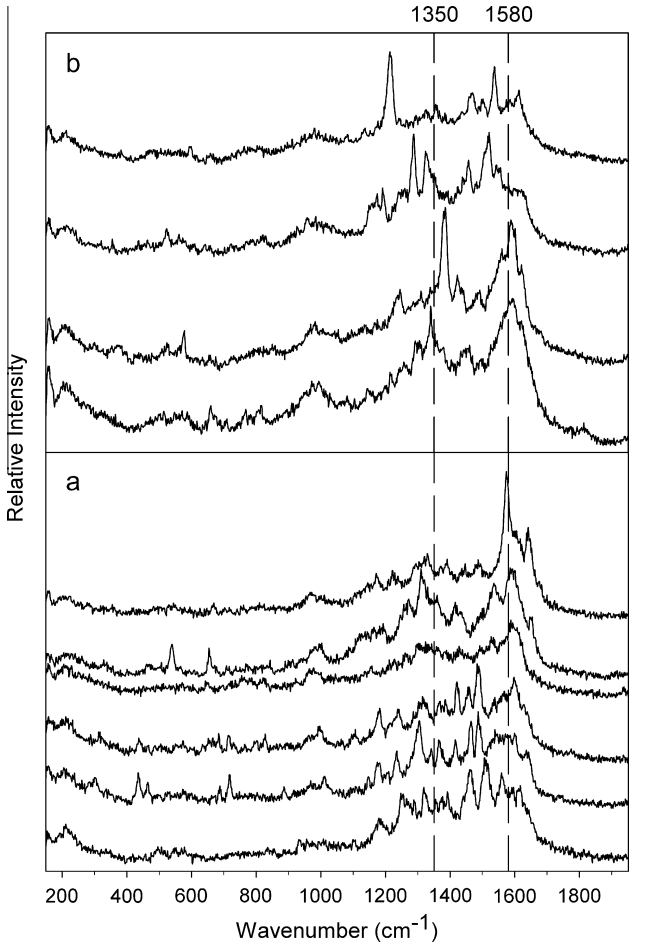

Fig. 2. SERS spectra with spurious bands measured from Ag nanoparticles immobilized on a glass plate by silane (a) with 1×10^{-6} M TMPyP (~0.2 mW at the sample, 2 s, all spectra from one spot) and (b) bare Ag surface (~0.2 mW at the sample, 2 s, upper three spectra from one spot). Time increases from bottom to top for spectra measured from one spot.

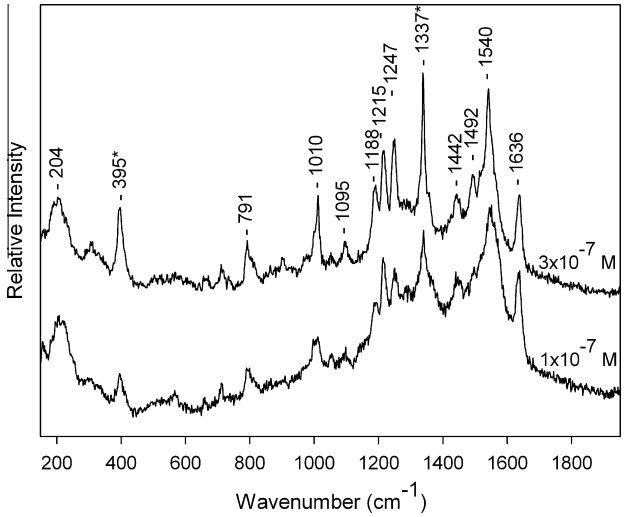

Fig. 3. SERRS spectra of TMPyP (1×10^{-7} M and 3×10^{-7} M) measured from dried Ag colloid/TMPyP drops (~0.2 mW at the sample, 1 s), metalation markers labeled with an asterisk.

~1556 cm^{-1} exceeds triple of the blank signal standard deviation [15]. Only one substrate was used because reproducibility of SERRS spectra from different spots within a substrate is better than between two substrates. LOD of TMPyP measured by macro-Raman using the same excitation wavelength was determined as 3×10^{-9} M [6]. Despite the problems with spurious bands and worse LOD, Raman microspectroscopy brings certain advantages compared to the macro-Raman: higher spatial resolution, no signal of glass, shorter acquisition times and the possibility of spectral mapping.

In accordance with measurements done using macro-Raman [7], we observed that in contrast to silver colloidal solution [2] TMPyP on Ag silanized glass retains its unperturbed free-base form since only free-base markers 333, 1341 + 1369 cm^{-1} [2] are present (labeled with an asterisk in Fig. 1). Our explanation is that some silane molecules could be moved from the glass to the metal surface during the Ag nanoparticles immobilization and after TMPyP adsorption could act as a spacer [6].

SERRS spectra of TMPyP were measured from dried Ag colloid/TMPyP drops on glass slides. We used a lower-than-coverage (1×10^{-7} M) and a higher-than-coverage (3×10^{-7} M) TMPyP concentration [3]. A ring of aggregates similar to that in the 'coffee ring effect' was formed for both concentrations, when the droplet was dropped carefully on a clean glass plate. Examples of SERRS spectra of TMPyP obtained from the rings are shown in Fig. 3. Compared to the SERRS spectra of TMPyP of the same concentrations measured from the Ag nanoparticles immobilized by silanization (see Fig. 1) spurious bands were negligible and the TMPyP spectra are more intense with better signal-to-noise ratio. In addition to that, the acquisition time was only 1 s. High SERRS enhancement is due to the presence of big aggregates probably containing some 'hot spots'. In contrast to Ag silanized substrates, in the case of dried drops metalation of TMPyP occurs as can be seen from the presence of metalation markers: 395 and 1337 cm^{-1} [2] (labeled with an asterisk in Fig. 3), so spectra of free-base porphyrin cannot be obtained.

4. Conclusions

Ag nanoparticles immobilized on glass *via* silane and by drying were compared as substrates for SERS microspectroscopy of TMPyP. In the case of Ag nanoparticles immobilized *via* silane, detection limit of the testing biomolecule (TMPyP) was $\sim 1 \times 10^{-8}$ M. Dried drops of Ag colloid/TMPyP form a ring in the edge part of the drop which contains high enhancing sites (big aggregates with some 'hot spots') providing better SERRS signal of TMPyP in short acquisition times (1 s) for the same TMPyP concentrations compared with the Ag silanized substrates. Comparison of the two immobilization methods shows that Ag nanoparticles immobilized *via* silane are less sensitive, but allow obtaining SERRS spectra of TMPyP in the unperturbed free-base form. A better LOD could be achieved if the spurious bands of carbon species frequently observed in the SERRS spectra and originating mainly from decomposition of silane due to laser irradiation could be avoided. Drying method provides better sensitivity and less spurious bands, but the inhomogeneity of dried drops leads to high spectral irreproducibility.

In conclusion, combination of the immobilized Ag colloidal nanoparticles with confocal Raman microspectrometer improves SERS sensitivity and reproducibility in comparison to macro-Raman measurements in Ag colloidal solution.

Acknowledgments

The work was supported by the Grants SVV-2010-261 304 and MSM0021620835.

References

[1] M. Fleischmann, P.J. Hendra, A.J. McQuillan, Chem. Phys. Lett. 26 (1974) 163.
[2] J. Hanzlíková, M. Procházka, J. Štěpánek, V. Baumruk, J. Bok, P. Anzenbacher Jr., J. Raman Spectrosc. 29 (1998) 575.
[3] M. Procházka, J. Štěpánek, P.-Y. Turpin, J. Bok, J. Phys. Chem. B 106 (2002) 1543.
[4] C.D. Keating, M.D. Musick, M.H. Keefe, M.J. Natan, J. Chem. Educ. 76 (1999) 949.
[5] N. Hajduková, M. Procházka, J. Štěpánek, M. Špírková, Colloids Surf. A: Physicochem. Eng. Asp. 301 (2007) 264.
[6] N. Hajduková, M. Procházka, P. Molnár, J. Štěpánek, Vib. Spectrosc. 48 (2008) 142.
[7] P. Molnár, M. Procházka, J. Raman Spectrosc. 38 (2007) 799.
[8] E.C. Le Ru, P.G. Etchegoin, Principles of Surface-enhanced Raman Spectroscopy and Related Plasmonic Effects, Elsevier, Amsterdam, 2009.
[9] M.V. Cañamares, J.V. Garcia-Ramos, J.D. Gómez-Varga, C. Domingo, S. Sanchez-Cortes, Langmuir 21 (2005) 8546.
[10] R.D. Deegan, O. Bakajin, T.F. Dupont, G. Huber, S.R. Nagel, T.A. Witten, Nature 389 (1997) 827.
[11] J.-Y. Jung, Y.W. Kim, J.Y. Yoo, Anal. Chem. 81 (2009) 8256.
[12] G.V. Pavan Kumar, B.A. Ashok Reddy, M. Arif, T.K. Kundu, C. Narayana, J. Phys. Chem. B 110 (2006) 16787.
[13] B. Vlčková, P. Matějka, J. Šimonová, K. Čermáková, P. Pančoška, V. Baumruk, J. Phys. Chem. 97 (1993) 9719.
[14] A. Kudelski, J. Raman Spectrosc. 38 (2007) 1494.
[15] V. Thomsen, D. Schatzlein, D. Mercuro, Spectroscopy 18 (2003) 112.

Supplement [II]

M. Procházka, P. Šimáková, N. Hajduková-Šmídová: SE(R)RS microspectroscopy of porphyrins on immobilized Au nanoparticles: Testing spectral sensitivity and reproducibility, Colloids Surf. A: Physicochem. Eng. Aspects **402** (2012), 24-28.

Colloids and Surfaces A: Physicochem. Eng. Aspects 402 (2012) 24–28

Contents lists available at SciVerse ScienceDirect

Colloids and Surfaces A: Physicochemical and Engineering Aspects

journal homepage: www.elsevier.com/locate/colsurfa

SE(R)RS microspectroscopy of porphyrins on immobilized Au nanoparticles: Testing spectral sensitivity and reproducibility

Marek Procházka*, Petra Šimáková, Natália Hajduková-Šmídová

Charles University, Faculty of Mathematics and Physics, Institute of Physics, Ke Karlovu 5, CZ-121 16 Prague 2, Czech Republic

ARTICLE INFO

Article history:
Received 6 January 2012
Received in revised form 28 February 2012
Accepted 13 March 2012
Available online 20 March 2012

Keywords:
SERS
Immobilized Au nanoparticles
Porphyrin
Reproducibility
LOD

ABSTRACT

Although surface-enhanced (resonance) Raman scattering SE(R)RS spectroscopy is currently employed as a (bio)analytical technique, designing and optimizing of cheaply and easily available SERS-active substrates are still in progress. In this paper, we tested SERS substrates prepared by immobilization of Au colloidal nanoparticles via aminosilane on glass from the point of view of their spectral sensitivity and reproducibility. This preparation procedure is easy, cheap and provides uniform SERS substrates on a large scale. We measured SE(R)RS spectra of free-base cationic 5,10,15,20-tetrakis(1-methyl-4-pyridyl)porphyrin (TMPyP) as a testing biomolecule using a confocal Raman microspectrometer and two excitation wavelengths (514.5 and 632.8 nm). SERS microspectroscopy had several advantages in comparison to macro-Raman technique: namely the possibility of spectral mapping over the surface, shorter collection times and the absence of strong Raman bands from the glass support. Analytical enhancement factor (AEF) of Au substrates between 10^5 and 10^6 and limits of detection (LOD) of TMPyP $\sim 5 \times 10^{-8}$ M were determined. Excellent spectral reproducibility of Au substrates (relative standard deviation of signal ~15%) was proved. Immobilized Au colloidal nanoparticles can be therefore considered as suitable substrates for SE(R)RS (bio)analytical applications.

1. Introduction

Interaction of metal nanostructures with electromagnetic radiation of different wavelengths can enhance electromagnetic field depending on the nanostructure and its resonance. In the case of surface-enhanced Raman scattering (SERS), interaction of light with noble metal nanostructures produces large amplification of the electromagnetic field through excitations generally known as plasmon resonances and Raman scattering of adsorbed molecule is enhanced by a factor above 10^5 [1]. Besides this electromagnetic enhancement, chemical enhancement originating from charge transfer between the molecule and the surface takes place in specific cases. The most commonly used metals are silver and gold because both have suitable plasmon resonance frequencies to give effective enhancement with visible excitation [1]. Although gold nanoparticles provide generally lower SERS enhancement than silver ones, they are particularly attractive for biological and biomedical applications because of their long-term stability and biocompatibility [2].

Although recent advances have turned SERS into an extremely sensitive analytical technique for small quantities of molecules (even single molecule) [3], the employed SERS-active substrates are often a serious drawback for routine analytical applications. For these purposes, the substrate should not only be uniform, stable and providing reproducible spectroscopic results but also easily available. Metal colloidal nanoparticles are the most frequent SERS substrates due to their cheap and simple preparation [4], but they suffer from chemical instability and spectral irreproducibility. This problem can be overcome by assembling the nanoparticles into two-dimensional array structures using a self-assembled monolayer (SAM) of bifunctional silane [5,6]. 3-Aminopropyltrimethoxysilane (APTMS) is routinely used to produce stable and highly SERS-active surfaces with regular and uniform distribution of Au nanoparticles [7–12]. Although SERS spectra of different molecules, including pyridylethylen [5], mercaptoundecanol [6], aminothiophenol [9], hydroxythiophenol [10], benzoic acid [11], and crystal violet [8], have been reported, biomolecular applications of these substrates are rare. We previously studied cationic and anionic porphyrins on such substrates using a classical (macro) Raman spectrometer [13,14]. Although manipulation with samples is not easy (reflection geometry has to be used) and SERS spectra of porphyrins are overlapped by a strong Raman signal from the glass support, low limits of detection (LOD) of porphyrins including TMPyP ($3–5 \times 10^{-8}$ M) and excellent spectral reproducibility were obtained [14].

In this paper, we turned our attention to SERS microspectroscopy of free-base 5,10,15,20-tetrakis(1-methyl-4-pyridyl)porphyrin (TMPyP) adsorbed on immobilized Au

* Corresponding author. Tel.: +420 221911474; fax: +420 224922797.
E-mail address: prochaz@karlov.mff.cuni.cz (M. Procházka).

0927-7757/$ – see front matter © 2012 Elsevier B.V. All rights reserved.
doi:10.1016/j.colsurfa.2012.03.012

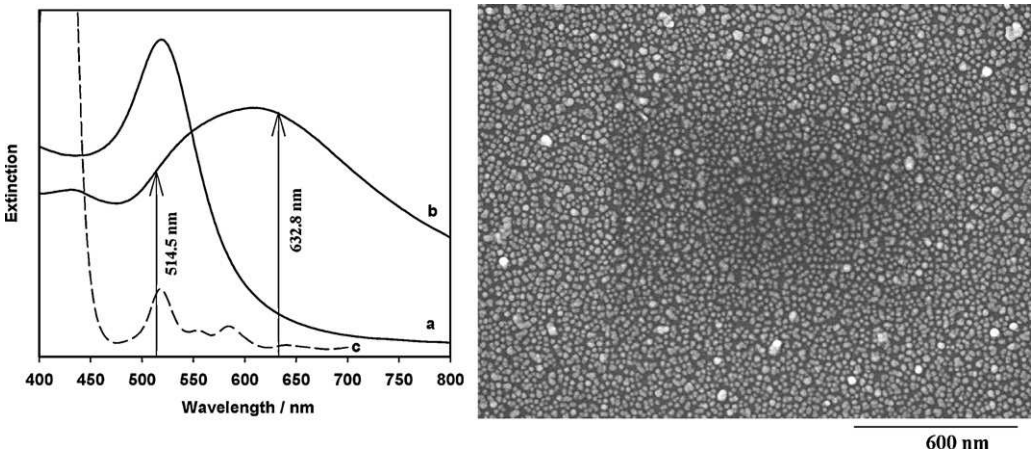

Fig. 1. Left: SPE spectra of the parent Au colloidal solution (a), Au substrate (b) and electronic absorption spectrum of TMPyP solution (c). Excitation wavelengths are marked by arrows. Right: Typical SEM image of Au substrate.

nanoparticles using an integrated Raman microspectrometer with two excitation wavelengths (514.5 nm and 632.8 nm). The 514.5 nm excitation falls into the maximum of electronic absorption Q-band of TMPyP at ~518 nm (Fig. 1) and thus, in this case, spectra of TMPyP are surface-enhanced resonance Raman scattering (SERRS) spectra. We determined the analytical enhancement factor (AEF) of our Au substrates and the limit of detection (LOD) of TMPyP for both excitation wavelengths and compared the LODs with our macro-SERS results [13,14]. Confocal Raman microspectrometer provides the possibility of spectral mapping over the surface giving us information about uniformity and spectral reproducibility of the SERS substrate as well as allowing us to selectively detect the signal from highly enhancing sites ("hot spots"). On the other hand, the focused laser beam in the case of micro-Raman set-up can cause decomposition of the adsorbate and/or of another surface species and consequently "spurious" Raman bands can appear in the spectra [15].

2. Experimental

2.1. Chemicals and glassware cleaning

Deionized water of a specific resistance of 18 MΩcm was used for all preparations. H_2SO_4 (96%), H_2O_2 (30%), HCl (35%) and HNO_3 (65%) were obtained from Lachema. $HAuCl_4$, sodium citrate, methanol (99.8%), 3-aminopropyltrimethoxysilane (APTMS, 97%) and free-base 5,10,15,20-tetrakis(1-methyl-4-pyridyl)porphyrin (TMPyP, tetra-p-tosylate salt) were purchased from Sigma–Aldrich.

All glassware was cleaned using "piranha" solution (4 parts H_2SO_4, 1 part H_2O_2) to remove organics and then aqua regia (3 parts HCl, 1 part HNO_3) to remove metal particles.

2.2. Substrate and sample preparation

Au colloidal nanoparticles were prepared by reduction of $HAuCl_4$ by sodium citrate: 250 ml of 1 mM solution of $HAuCl_4$ was brought to a boil and then 25 ml of 38.8 mM solution of sodium citrate was added. Boiling continued for 15 min and then the solution was left to cool.

Preparation of Au silanized substrates is described in our previous paper [12]. Clean borosilicate glass slides (1 cm × 2 cm strips) were immersed into 10% solution of APTMS in methanol for 30 min. After silanization, the substrates were rinsed several times with methanol and then with water to remove unbound silane that could cause colloid aggregation when the substrate is put into it. Then each silanized substrate was dipped separately in a vertical position into a vial containing 1 ml of the colloidal suspension for 3–4 h. After that, they were rinsed again with water and left to dry at 100 °C for 10 min. Au nanoparticles are attached to glass slides by electrostatic interactions between the anions covering their surface and the positively charged amino groups of APTMS [7,8].

For SERS measurements, the Au substrate was placed into porphyrin aqueous solution for 20 min, then it was rinsed with deionized water and SE(R)RS spectrum was measured. 20 min soaking time was found to be optimal to obtain maximal SE(R)RS signal of TMPyP [13].

2.3. Instrumentation

Scanning electron microscopy (SEM) images of Au substrates were obtained using a Hitachi S5000 device.

Surface plasmon extinction (SPE) spectra of Au substrates and electronic absorption spectrum of TMPyP were recorded with a UV/VIS Perkin Elmer Lambda 12 spectrometer. The light spot at the sample was a line of ~9 mm length and ~1 mm width.

SE(R)RS spectra of TMPyP were recorded at room temperature with an integrated confocal Raman microscopic system LabRam HR800 (Horiba Jobin-Yvon) equipped with a 800-mm single spectrograph (600 g/mm holographic grating) and a nitrogen cooled CCD. The laser beam was focused using 100× objective to a spot of a diameter of ~1.2 μm. 632.8 nm excitation line of an internal He–Ne laser (laser power 0.065 mW at sample) and 514.5 nm excitation line of an Ar^+ laser (Melles Griot, laser power 0.19 mW at sample) were used. Accumulation times were 1 × 60 s for all spectra.

3. Results and discussion

Prepared Au substrates were characterized by SPE and SEM techniques. Typical SPE spectra of the parent Au colloidal solution and immobilized Au colloidal nanoparticles on glass are shown in Fig. 1, left. Au surfaces are grey-violet with a broad SPE spectrum between 500 and 800 nm. SPE spectrum is formed by two overlapping bands with maxima at 520–530 nm and 600–650 nm, but their ratio is slightly different from preparation to preparation [12,14]. The 520–530 nm extinction band is close to the extinction band of the parent colloidal solution and thus corresponds to isolated gold nanoparticles. The 600–650 nm one indicates an interaction between the neighbouring nanoparticles manifested by the red shift of the SPE maximum caused by plasmon resonance coupling. No change in the SPE spectrum was observed during storage or after adsorption of TMPyP. SEM image of Au substrates (see Fig. 1, right)

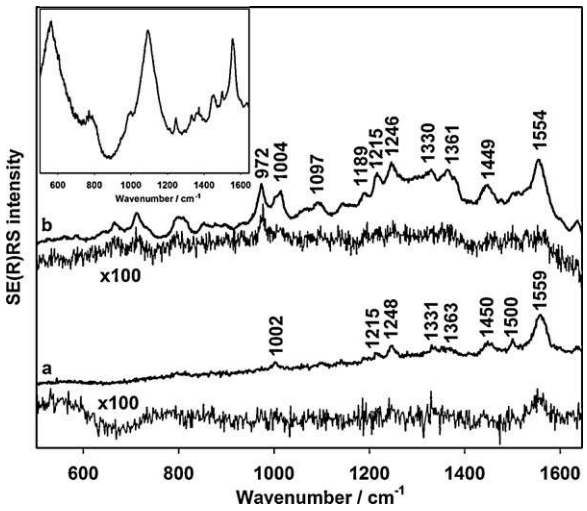

Fig. 2. SE(R)RS spectra of TMPyP adsorbed on Au substrate excited by 514.5 nm (a) and 632.8 nm (b) laser line. Top spectra are of 1×10^{-6} M TMPyP soaking concentration, bottom spectra of 6×10^{-8} M TMPyP soaking concentration. Inset: Rough SERRS spectrum of TMPyP (1×10^{-6} M soaking concentration) measured using macro-Raman spectrometer (see details in [14]), 514.5 nm excitation, 5×60 s accumulation time.

shows a compact coverage of glass by Au nanoparticles of diameters varying from ~30 to 100 nm and by small aggregates. Scanning the whole surface and comparing several samples indicate that our Au substrates are uniform and the preparation is highly reproducible.

Typical SE(R)RS spectra of TMPyP (1×10^{-6} M soaking concentration) adsorbed on Au substrate excited by 514.5 nm (a, top spectrum) and 632.8 nm (b, top spectrum) are shown in Fig. 2. Comparison of these spectra with Raman spectra of 1×10^{-3} M TMPyP measured without Au nanoparticles indicates that we obtained SE(R)RS spectra of TMPyP in the unperturbed free-base form (see doublet at ~1330 + 1360 cm^{-1}) [16,17]. This result is in agreement with the fact that TMPyP cannot be metalated by Au atoms [14]. Spectral changes in SE(R)RS spectra obtained using two different excitation lines originate from resonance effect in the case of 514.5 nm laser line. The 514.5 nm excitation falls into the maximum of electronic absorption Q-band of TMPyP at ~518 nm while the 632.8 nm excitation is out of electronic absorption of TMPyP (Fig. 1). Decomposition of the adsorbate on the metal surface has not been observed in our experimental conditions. However, if laser power higher than 0.2 mW is used, strong bands of amorphous carbon at ~1300–1600 cm^{-1} are seen for both excitation wavelengths.

Our results demonstrate significant advantages of confocal micro-Raman spectrometer in comparison to macro-Raman one. Crucial advantage is an absence of strong Raman spectrum of glass support which interferes with macro-SE(R)RS spectrum of TMPyP. Inset of Fig. 2 shows an example of rough SERRS spectrum of TMPyP (1×10^{-6} M soaking concentration) measured using macro-Raman set-up (see [14] for details) and 514.5 nm excitation and 5×60 s accumulation time. Lower part of the spectrum (500–1200 cm^{-1}) is overlapped by normal Raman spectrum of glass. Other advantages of micro-Raman set-up include at least 5 times shorter collection times (under our experimental conditions), easier manipulation with samples (reflection geometry has to be used in the case of macro-Raman experiment) and the possibility of spectral mapping over the substrate.

We tried to estimate analytical enhancement factor (AEF), a parameter suitable to display the analytical capability of a particular SERS substrate. The AEF is defined as the following equation considering the intensity ratio of SE(R)RS (I_{SERS}) and normal (resonance) Raman (I_{RS}) spectrum of TMPyP and the ratio of TMPyP concentrations in each experiment [1,18]:

$$\mathrm{AEF} = \frac{I_{SERS}/c_{SERS}}{I_{RS}/c_{RS}}$$

In our calculation, we used integral intensities of the strongest band at ~1555 cm^{-1} in SE(R)RS spectra of TMPyP (1×10^{-6} M soaking concentration) measured from Au substrates and in normal (resonance) Raman spectra of 1×10^{-3} M TMPyP measured without Au nanoparticles under the same experimental conditions. Since SE(R)RS intensities measured from different spectral points of Au substrates slightly differ, the intensity ratio I_{SERS}/I_{RS} varies between 10–20 and 50–250 for 514.5 nm and 632.8 nm excitations, respectively. Concentration c_{SERS} is the most critical approximation. It should be the concentration corresponding to the amount of TMPyP molecules adsorbed on Au substrate and providing the SE(R)RS signal. Using absorption spectroscopy it was possible to measure the decrease of TMPyP molecules from the soaking solution (after taking out the Au substrate) and thus determine the amount of TMPyP molecules adsorbed on the Au substrate. In our calculation, when 1×10^{-6} M TMPyP soaking concentration is used, the amount of adsorbed TMPyP is ~10^{14} molecules/cm^2. It represents ~1×10^{-7} M concentration in solution which corresponds to submonolayer coverage of metal colloidal nanoparticles [17]. Finally, the AEF values for TMPyP on our Au substrates were estimated as ~10^5 and ~10^6 for 514.5 nm and 632.8 nm excitation, respectively. This result is consistent with theoretically predicted and experimentally proved SERS enhancement of Au nanoparticles [1,9].

SERS sensitivity of the Au substrates for TMPyP was characterized by limit of detection (LOD) of TMPyP. We measured SE(R)RS spectra of TMPyP of soaking concentrations between 1×10^{-5} M and 6×10^{-8} M. Typical SE(R)RS spectra of TMPyP (6×10^{-8} M soaking concentration) adsorbed on Au substrate excited by 514.5 nm (a, bottom spectrum) and 632.8 nm (b, bottom spectrum) are shown in Fig. 2. The LOD was determined by extrapolation to the concentration for which the intensity of the strongest porphyrin band at ~1555 cm^{-1} exceeds the triple of the blank signal standard deviation [19]. The LODs of TMPyP on our Au substrates are 6.5×10^{-8} M and 4.0×10^{-8} M soaking concentrations for 514.5 nm and 632.8 nm excitation, respectively. The LODs are comparable to the values obtained previously for TMPyP on the same Au substrates but using a classical macro-Raman spectrometer (LOD is 5×10^{-8} M at 514.5 nm excitation) [14].

Uniformity and spectral reproducibility of Au substrates in mm-scale was studied by measurement of TMPyP spectra from several

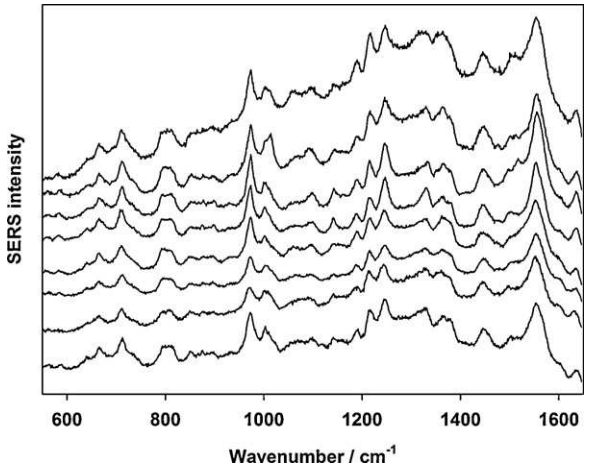

Fig. 3. Eight spectra of TMPyP measured from several random places of one Au substrate, 5×10^{-6} M TMPyP soaking concentration, 632.8 nm excitation.

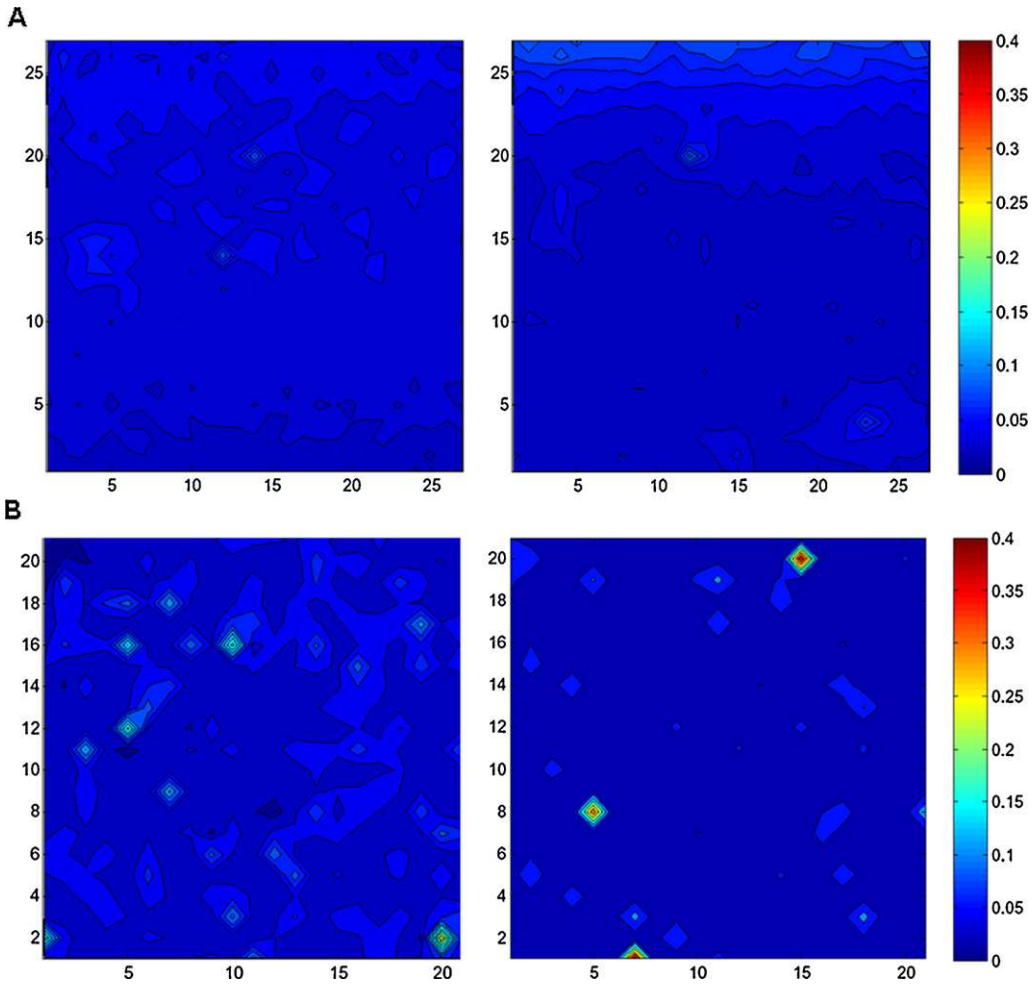

Fig. 4. Spectral maps of TMPyP (1×10^{-6} M soaking concentration) on Au substrate: excitation 514.5 nm (A) and 632.8 nm (B), 20 μm (left) and 2 μm (right) steps between mapping points. Numbers on the axes represent the mapping points; the scale represents the relative intensity. (Color figure is available on the web version of the article.)

random places of the substrate. Fig. 3 shows such eight spectra measured from one substrate with 632.8 nm excitation. Relative standard deviation (RSD) of signal is 15.3%. In the μm-scale, we carried out spectral mapping of the Au surface. Fig. 4 shows examples of spectral maps of SE(R)RS spectra of TMPyP (1×10^{-6} M soaking concentration) with 20 and 2 μm steps between mapping points for both excitations. The obtained sets of spectra were treated by an in-house developed software including baseline correction and factor analysis (FA) [17,20]. "Singular value decomposition" FA algorithm provides a set of orthonormal subspectra S_j and weights W_j, and a set of scores V_{ij} representing the relative presence of the S_j subspectrum in each experimental spectrum Y_i. A particular experimental spectrum $Y_i(\nu)$ can then be approximated as:

$$Y_i(\nu) = \sum_{j=1}^{M} W_j V_{ij} S_j(\nu)$$

The first subspectrum S_1 is a weighted average of the experimental spectra reflecting changes of the overall intensity, while the second subspectrum S_2 can be considered as a difference spectrum reflecting the spectral changes. In our maps, the SE(R)RS intensity in each mapping point is represented by the corresponding coefficient of the first subspectrum of the FA. The advantage of this approach is that it is a rapid and precise way to analyze intensity of huge set of spectra. The results demonstrate that only slight intensity variation is observed for 514.5 nm excitation. In the case of 632.8 nm excitation, spectral reproducibility is not so good, the intensity jumps 5–10 times in a few points. We suggest that by using the 632.8 nm excitation, some aggregates of Au nanoparticles containing "hot spots" are excited.

We can summarize that spectral mapping over the surface of our Au substrates shows excellent spectral reproducibility in mm-scale (relative standard deviation of signal ~15%). Worse spectral reproducibility in μm-scale is caused by selective excitation of "hot spots" in some spectral points. Practical implementations of SE(R)RS detection are expected to rely on substrate architectures which are uniform over at least square millimeter-sized areas. Uniformity of SERS substrates given by RSD ~15% is sufficient for this purpose. Moreover, immobilization of Au colloidal nanoparticles via aminosilane to glass support is an easy and cheap way to fabricate SERS-active substrates on a large scale. Thus, such substrates can be considered as suitable for SE(R)RS (bio)analytical applications.

4. Conclusions

SERS-active substrates were prepared by immobilization of Au colloidal nanoparticles via aminosilane on glass and characterized by SPE and SEM techniques. This preparation procedure leads to easy and cheap fabrication of uniform SERS substrates on a large scale. SERS sensitivity and spectral reproducibility of Au substrates were investigated using free-base 5,10,15,20-tetrakis (1-methyl-4-pyridyl)porphyrin (TMPyP). SE(R)RS spectra of TMPyP were measured by a confocal Raman microspectrometer with two

different excitation wavelengths (514.5 nm and 632.8 nm). Both excitations provide good SE(R)RS spectra of TMPyP, the analytical enhancement factor (AEF) of Au substrates was found to be between 10^5 and 10^6 and the limits of detection (LOD) of TMPyP $\sim 5 \times 10^{-8}$ M in soaking solution. Spectral measurement over the Au surface proved their excellent spectral reproducibility (relative standard deviation of signal ~15%). Confocal micro-Raman spectrometer shows significant advantages in comparison to macro-Raman one including shorter collection times and the absence of strong Raman bands of the glass support. Thus, SERS microspectroscopy using immobilized Au colloidal nanoparticles can be considered as suitable approach for SE(R)RS (bio)analytical applications.

Acknowledgements

We thank Břetislav Šmíd for performing of SEM images at the National Institute for Materials Science (NIMS), Tsukuba, Japan. Financial supports from the Czech Science Foundation (P205/12/G118) and Ministry of Education, Youth and Sports of the Czech Republic (project Barrande 7AMB12FR023) are gratefully acknowledged.

References

[1] E.C. Le Ru, P.G. Etchegoin, Principles of Surface-enhanced Raman Spectroscopy and Related Plasmonic Effects, Elsevier, Amsterdam, 2009.
[2] S. Link, M.A. El-Sayed, Optical properties and ultrafast dynamics of metallic nanocrystals, Annu. Rev. Phys. Chem. 54 (2003) 331–366.
[3] Surface-enhanced Raman scattering: physics and applications, in: K. Kneipp, M. Moskovits, H. Kneipp (Eds.), Topics in Applied Physics, vol. 103, Springer-Verlag, Berlin Heidelberg, 2006.
[4] R.F. Aroca, R.A. Alvarez-Puebla, N. Pieczonka, S. Sanchez-Cortes, J.V. Garcia-Ramos, Surface-enhanced Raman scattering on colloidal nanostructures, Adv. Colloid Interface Sci. 116 (2005) 45–61.
[5] R.G. Freeman, K.C. Grabar, K.J. Allison, R.M. Bright, J.A. Davis, A.P. Guthrie, M.B. Hommer, M.A. Jackson, P.C. Smith, D.G. Walter, M.J. Natan, Self-assembled metal colloid nanolayers—an approach to SERS substrates, Science 267 (1995) 1629–1632.
[6] G. Chumanov, K. Sokolov, B.W. Gregory, T.M. Cotton, Colloidal metal-films as a substrate for surface-enhanced spectroscopy, J. Phys. Chem. 99 (1995) 9466–9471.
[7] C.D. Keating, M.D. Musick, M.H. Keefe, M.J. Natan, Kinetics and thermodynamics of Au colloid monolayer self-assembly, J. Chem. Educ. 76 (1999) 949–955.
[8] T. Makiabadi, A. Bouvree, V. Le Nader, H. Terrisse, G. Louarn, Preparation, optimization and characterization of SERS sensor substrates based on two-dimensional structures of gold colloid, Plasmonics 5 (2010) 21–29.
[9] F. Toderas, M. Baia, L. Baia, S. Astilean, Controlling gold nanoparticle assemblies for efficient surface-enhanced Raman scattering and localized surface plasmon resonance sensors, Nanotechnology 18 (2007) 255702.
[10] M. Fan, A.G. Brolo, Self-assembled Au nanoparticles as substrates for surface-enhanced vibrational spectroscopy: optimization and electrochemical stability, Chem. Phys. Chem. 9 (2008) 1899–1907.
[11] L.G. Olson, Y.S. Lo, T.P. Beebe, J.M. Harris, Characterization of silane-modified immobilized gold colloids as a substrate for surface-enhanced Raman spectroscopy, Anal. Chem. 73 (2001) 4268–4276.
[12] N. Hajduková, M. Procházka, J. Štěpánek, M. Špírková, Chemically reduced and laser-ablated gold nanoparticles immobilized to silanized glass plates: preparation, characterization and SERS spectral testing, Colloid Surf. A: Physicochem. Eng. Asp. 301 (2007) 264–270.
[13] M. Procházka, N. Hajduková, J. Štěpánek, Surface-enhanced resonance Raman scattering of porphyrins on gold nanoparticles attached to silanized glass plates, Biopolymers 82 (2006) 390–393.
[14] N. Hajduková, M. Procházka, P. Molnár, J. Štěpánek, SERRS of free-base porphyrins on immobilized metal gold and silver nanoparticles, Vib. Spectrosc. 48 (2008) 142–147.
[15] P. Šimáková, M. Procházka, SERRS microspectroscopy of porphyrins on Ag immobilized nanoparticles, J. Mol. Struct. 993 (2011) 425–427.
[16] M. Procházka, P.-Y. Turpin, J. Štěpánek, B. Vlčková, SERRS of free base porphyrin in laser-ablated colloids: evidence for three different spectral porphyrin forms, J. Raman Spectrosc. 33 (2002) 758–760.
[17] M. Procházka, J. Štěpánek, P.-Y. Turpin, J. Bok, Drastically different porphyrin adsorption and metalation processes in chemically prepared and laser-ablated SERS-active silver colloidal substrates, J. Phys. Chem. B 106 (2002) 1543–1549.
[18] E.C. Le Ru, E. Blackie, M. Meyer, P.G. Etchegoin, Surface enhanced Raman scattering enhancement factors: a comprehensive study, J. Phys. Chem. C 111 (2007) 13794–13803.
[19] V. Thomsen, D. Schatzlein, D. Mercuro, Limits of detection in spectroscopy, Spectroscopy 18 (2003) 112–114.
[20] E.R. Malinowski, Factor Analysis in Chemistry, Wiley, New York, 1991.

Supplement [III]

P. Šimáková, M. Procházka, E. Kočišová: SERS microspectroscopy of biomolecules on dried Ag colloidal drops, Spectroscopy: An International Journal **27** (2012), 449-453.

Hindawi Publishing Corporation
Spectroscopy: An International Journal
Volume 27 (2012), Issue 5-6, Pages 449–453
doi:10.1155/2012/393847

SERS Microspectroscopy of Biomolecules on Dried Ag Colloidal Drops

P. Šimáková, M. Procházka, and E. Kočišová

Institute of Physics, Faculty of Mathematics and Physics, Charles University, Ke Karlovu 5, 121 16 Prague 2, Czech Republic

Correspondence should be addressed to P. Šimáková, simakova@karlov.mff.cuni.cz

Abstract. We report the application of dried Ag hydroxylamine-reduced colloidal drops to surface-enhanced (resonance) Raman scattering (SE(R)RS) study of biomolecules using Raman microspectroscopy. 5,10,15,20-tetrakis(1-methyl-4-pyridyl)porphyrin (TMPyP), amino acid tryptophan, and phospholipid 1,2-distearoyl-*sn*-glycero-3-phosphocholine (DSPC) served as testing biomolecules. Ag colloid/biomolecule drop dried on glass support forms a ring in the edge part of the drop in which almost all nanoparticles are clustered. This specific drying process promotes adsorption of the studied biomolecules in highly enhancing sites ("hot spots") as well as concentrates them in the ring. We were able to obtain SE(R)RS spectra from the ring that cannot be acquired directly from Ag colloidal solutions (SERRS spectrum of 1×10^{-10} M TMPyP by 1 s accumulation time, SERS spectrum of 2×10^{-7} M DSPC). Despite the spectral irreproducibility and problems with spurious bands in some cases, SERS microspectroscopy of studied biomolecules using dried Ag colloid/adsorbate systems improves SERS applicability and sensitivity in comparison to measurements directly from Ag colloidal solution.

Keywords: SERS, Ag colloidal nanoparticles, porphyrin, tryptophan, phosphatidylcholine

1. Introduction

Surface-enhanced Raman scattering (SERS) spectroscopy is a very useful detection and analytical technique thanks to the enhancement of Raman scattering for molecules adsorbed on rough metal surfaces [1, 2]. The enhancement is usually up to 10^6, but selective excitation of extremely high-enhancing sites ("hot spots") can give SERS enhancement of the order of 10^{12} allowing even single-molecule detection [1, 2].

Silver and gold colloidal suspensions prepared by chemical reduction still belong to popular SERS-active substrates because of their simple and cheap preparation and sufficient SERS enhancement. Drawbacks of colloidal solutions are their low spectral reproducibility due to the colloid aggregation which generally increases SERS enhancement, but is very difficult to control [2]. Moreover, the diffusion of aggregates in the solution causes signal fluctuations. More stable SERS substrates can be obtained by immobilization of colloidal nanoparticles on glass *via* silane [3, 4] or by drying [2, 4, 5]. In the latter case, during the evaporation of a colloidal or colloid/adsorbate drop on glass surface the "coffee ring effect" [6] causes formation of a ring at the contact line of the drop containing most of the nanoparticles.

Aggregation of the nanoparticles upon drying can create fractal-like aggregates with "hot spots" [2]. One can expect that drying promotes adsorption of the studied compound in such highly enhancing sites as well as concentrates it in the ring. Although dried drops are neither uniform nor reproducible substrates [2], SERS measurement from the ring can bring some advantages in comparison to measurement directly from the colloidal solution.

In this contribution we report the application of dried Ag hydroxylamine-reduced colloidal drops to SE(R)RS study of biomolecules using Raman microspectrometer. We chose 5,10,15,20-tetrakis(1-methyl-4-pyridyl)porphyrin (TMPyP), amino acid tryptophan, and phospholipid distearoylphosphatidylcholine (DSPC) as testing biomolecules.

2. Experimental

$AgNO_3$, $NH_2OH{\cdot}HCl$, NaOH, 5,10,15,20-tetrakis(1-methyl-4-pyridyl)porphyrin (TMPyP) and L-tryptophan were purchased from Sigma-Aldrich and 1,2-distearoyl-*sn*-glycero-3-phosphocholine (DSPC) from Avanti Polar Lipids, Inc. Deionized water of a specific resistance of 18 MΩcm was used. Liposomes of ∼400 nm in diameter were prepared by extrusion of 1 mg/mL (1.3 mM) DSPC water suspension through a polycarbonate membrane filter of the LiposoFast-Basic apparatus (Avestin, Inc.) [7].

Ag colloid was prepared by reduction of $AgNO_3$ by hydroxylamine hydrochloride [8] according to protocol used in [5]. Aqueous solution of the biomolecules was mixed with Ag colloid to obtain the desired concentration and ∼2 μL of the colloid/biomolecule mixture was dropped by pipette on a clean glass slide (cleaned with diluted HNO_3 and ethanol). The drop was left to dry at room temperature for approximately 45 min.

SE(R)RS spectra were recorded by a confocal Raman microspectrometer LabRam HR800 (Horiba Jobin Yvon) equipped with a 600 grooves/mm grating and a nitrogen-cooled CCD detector. Objectives (100x, NA = 0.9 or 50x, NA = 0.7) provided 1-2 μm laser spot on the sample. Excitation lines 514.5 nm of an Ar^+ laser (Melles Griot, power ∼0.19 mW at the sample) and 632.8 nm of an internal He-Ne laser (∼0.07 mW at the sample) were used. Spectra were collected at room temperature (20°C). Microscopic images of the dried drops were taken by the built-in digital camera using objectives 5x and 50x.

3. Results and Discussion

Ag colloid mixed with TMPyP, tryptophan, or DSPC dropped carefully on clean glass surface forms a ring in the edge part of the drop in which almost all nanoparticles are clustered. An example of such structure is shown in Figure 1 for the Ag hydroxylamine-reduced colloid with TMPyP (1×10^{-7} M concentration). The ring consists of big aggregates of colloidal nanoparticles and crystals of NaCl coming from the colloid preparation. Formation of a clearly distinguishable ring was observed for various TMPyP concentrations, that is, for different aggregation states of the colloid, including strongly aggregated (1×10^{-6} M) and nonaggregated (1×10^{-9} M and lower) Ag colloid/TMPyP systems, although the ring had different width for each particular TMPyP concentration.

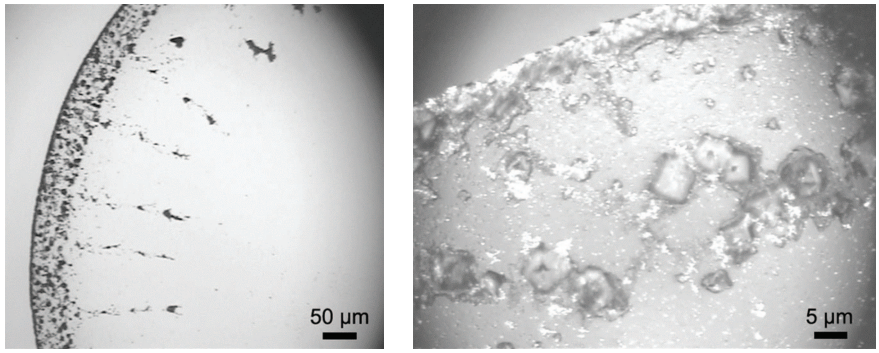

(a) (b)

Figure 1: Optical microscope images of a dried Ag hydroxylamine-reduced colloid/TMPyP drop with 1×10^{-7} M TMPyP concentration: edge part of the drop (a) and detail of the ring (b).

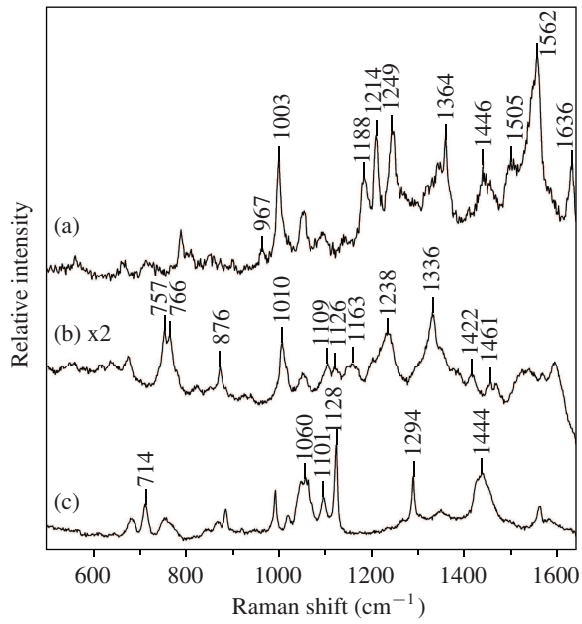

Figure 2: Examples of SE(R)RS spectra obtained from the dried Ag colloid/biomolecule drops with (a) 1×10^{-7} M TMPyP (514.5-nm excitation, 1 s), (b) 1×10^{-5} M tryptophan (632.8-nm excitation, 1 s $\times$ 60) and (c) 2×10^{-6} M (1.7×10^{-3} mg/mL) DSPC (632.8-nm excitation, 5 s $\times$ 40).

TMPyP is a suitable molecule for SERS because it provides high SERS signal owing to its structure and positive charge which helps adsorption on the Ag nanoparticles surrounded by negative ions. We measured the concentration dependence of SERRS spectra of TMPyP at 514.5 nm excitation in the concentration range 1×10^{-6} M–1×10^{-10} M and 1 s accumulation time (it is resonance Raman scattering because the excitation falls into an absorption Q-band of TMPyP). An example of the SERRS spectrum of 1×10^{-8} M TMPyP is demonstrated in Figure 2 (spectrum (a)). It shows signs of metalation

(bands at 1364 cm^{-1} and 1562 cm^{-1}), belonging to a metalation form in which Ag(0) atoms (probably induced by chlorides present in the colloid from the reduction agent) are incorporated into the porphyrin macrocycles [9]. Spectral features of TMPyP (marked in the spectrum (a) on Figure 2) were observed for all studied TMPyP concentrations (even for 1×10^{-10} M) although some other bands not assigned to TMPyP can be seen. These spurious spectral bands (fluctuating narrow bands in the spectral region 1200–1700 cm^{-1} and/or two broad bands with maxima at ~1350 cm^{-1} and ~1580 cm^{-1}) come from carbon species contamination and/or burning of the sample [4]. However, in the case of dried drops, problems with spurious bands were negligible compared to Ag nanoparticles immobilized by silane [4]. We have to emphasize that SERRS spectra of such low TMPyP concentrations (1×10^{-10} M detected even by 1 s accumulation time) cannot be measured directly from Ag colloidal solution.

SERS spectra of tryptophan obtained using Ag colloids have been reported in the literature recently [10–12], but the results significantly differ from each other. Such discrepancy can be explained by particular experimental conditions (pH, used Ag colloid and its activation, mode of adsorption, and consequently orientation of tryptophan on the surface, etc.). We measured SERS spectra of 1×10^{-5} M tryptophan at 632.8-nm excitation. An example is spectrum (b) in Figure 2. We have to note that our SERS spectra of tryptophan are completely different than that obtained by Aliaga et al. [10] from the same SERS system (dried hydroxylamine-reduced Ag colloid/tryptophan drop) but in good agreement with Raman spectra measured from Ag colloidal solutions [11, 12] and solid powder [12]. In Figure 2, spectrum (b), only spectral bands that can be surely assigned to tryptophan are marked [12]. We note that some spurious bands caused by burning of the sample might occur at certain spots and/or using higher laser power.

SERS studies of lipids using Ag colloidal solutions have not been reported up to now. Presence of both positive and negative charges on lipid heads makes adsorption of lipids on colloidal nanoparticles difficult. Moreover, long lipid chains could hinder nanoparticles aggregation. We were able to obtain SERS spectra of DSPC in 2×10^{-6} M and 2×10^{-7} M concentrations from dried Ag colloidal drops using 632.8 nm excitation. DSPC was prepared in the form of liposomes which are spherical lipid bilayers and represent a good model of biological membranes. An example of the SERS spectrum of DSPC in 2×10^{-6} M concentration with marked spectral bands of the phospholipid is shown in Figure 2 (spectrum (c)). Spectral features agree with those of normal Raman spectra of phosphatidylcholine [7, 13] although some spurious bands occurred. No SERS spectra of DSPC were obtained directly from Ag colloidal solution at the same concentration.

4. Conclusions

Ag hydroxylamine-reduced colloid/biomolecule drop dropped carefully on clean glass surface forms a ring in the edge part of the drop in which almost all nanoparticles are clustered. It seems that drying process promotes adsorption of some analytes (e.g. lipids) on Ag nanoparticles and "hot spots" providing enormous SERS enhancement are created inside the ring. Thus, using this structure, SE(R)RS spectra that cannot be acquired directly from Ag colloidal solutions (e.g. 1×10^{-10} M TMPyP by 1 s accumulation time, phospholipid DSPC) were obtained. Despite the spectral irreproducibility and problems with spurious bands in some cases, SERS microspectroscopy of studied biomolecules using dried Ag colloid/adsorbate systems improves SERS applicability and sensitivity in comparison to measurements directly from Ag colloidal solution.

Acknowledgments

The work was supported by grants of the Ministry of Education, Youth and Sports (SVV 265 304) and of the Czech Science Foundation (P208/10/0941).

References

[1] *Surface-Enhanced Raman Scattering: Physics and Applications*, K. Kneipp, M. Moskovits, and H. Kneipp, Eds., vol. 103 of *Topics in Applied Physics*, Springer, Berlin, Germany, 2006.

[2] E. C. Le Ru and P. G. Etchegoin, *Principles of Surface-Enhanced Raman Spectroscopy and Related Plasmonic Effects*, Elsevier, Amsterdam, The Netherlands, 2009.

[3] C. D. Keating, M. D. Musick, M. H. Keefe, and M. J. Natan, "Kinetics and thermodynamics of Au colloid monolayer self-assembly undergraduate experiments in surface and nanomaterials chemistry," *Journal of Chemical Education*, vol. 76, no. 7, pp. 949–955, 1999.

[4] P. Šimáková and M. Procházka, "SERRS microspectroscopy of porphyrins on Ag immobilized nanoparticles," *Journal of Molecular Structure*, vol. 993, no. 1-3, pp. 425–427, 2011.

[5] M. V. Cañamares, J. V. Garcia-Ramos, J. D. Gómez-Varga, C. Domingo, and S. Sanchez-Cortes, "Comparative study of the morphology, aggregation, adherence to glass, and surface-enhanced Raman scattering activity of silver nanoparticles prepared by chemical reduction of Ag^{+} using citrate and hydroxylamine," *Langmuir*, vol. 21, no. 18, pp. 8546–8553, 2005.

[6] R. D. Deegan, O. Bakajin, T. F. Dupont, G. Huber, S. R. Nagel, and T. A. Witten, "Capillary flow as the cause of ring stains from dried liquid drops," *Nature*, vol. 389, no. 6653, pp. 827–829, 1997.

[7] E. Kočišová and M. Procházka, "Drop-coating deposition Raman spectroscopy of liposomes," *Journal of Raman Spectroscopy*, vol. 42, no. 8, pp. 1606–1610, 2011.

[8] N. Leopold and B. Lendl, "A new method for fast preparation of highly surface-enhanced Raman scattering (SERS) active silver colloids at room temperature by reduction of silver nitrate with hydroxylamine hydrochloride," *Journal of Physical Chemistry B*, vol. 107, no. 24, pp. 5723–5727, 2003.

[9] M. Procházka, B. Vlčková, J. Štěpánek, and P. Y. Turpin, "Probing of porphyrin surface chemistry in systems with laser-ablated Ag nanoparticle hydrosol: role of thiosulfate anions," *Langmuir*, vol. 21, no. 7, pp. 2956–2962, 2005.

[10] A. E. Aliaga, I. Osorio-Román, P. Leyton et al., "Surface-enhanced Raman scattering study of L-tryptophan," *Journal of Raman Spectroscopy*, vol. 40, no. 2, pp. 164–169, 2009.

[11] A. Kandakkathara, I. Utkin, and R. Fedosejevs, "Surface-enhanced Raman scattering (SERS) detection of low concentrations of tryptophan amino acid in silver colloid," *Applied Spectroscopy*, vol. 65, no. 5, pp. 507–513, 2011.

[12] C.-H. Chuang and Y.-T. Chen, "Raman scattering of L-tryptophan enhanced by surface plasmon of silver nanoparticles: vibrational assignment and structural determination," *Journal of Raman Spectroscopy*, vol. 40, no. 2, pp. 150–156, 2009.

[13] I. W. Levin, "Vibrational spectroscopy of membrane assemblies," in *Advances in Infrared and Raman Spectroscopy*, R. J. H. Clark and R. E. Heste, Eds., vol. 11, Wiley Heyden, Chichester, UK, 1984.

Supplement [IV]

P. Šimáková, E. Kočišová, M. Procházka: Sensitive Raman spectroscopy of lipids based on drop deposition using DCDR and SERS, J. Raman Spectrosc. **44** (2013), 1479–1482.

Research article

Journal of RAMAN SPECTROSCOPY

Received: 1 May 2013 Revised: 12 July 2013 Accepted: 14 July 2013 Published online in Wiley Online Library: 15 August 2013

(wileyonlinelibrary.com) DOI 10.1002/jrs.4364

Sensitive Raman spectroscopy of lipids based on drop deposition using DCDR and SERS

Petra Šimáková, Eva Kočišová and Marek Procházka*

Raman spectroscopy is widely used for study of lipids and membrane models. A severe limitation of this technique lies in the low Raman cross section requiring high sample concentrations. We report sensitive detection of synthetic 1,2-dimyristoyl-3-trimethylammonium-propane (DMTAP) lipid employing two Raman techniques with improved sensitivity: drop coating deposition Raman (DCDR) and surface-enhanced Raman scattering (SERS) spectroscopies. DCDR provided well-reproducible DMTAP spectra without considerable loss of its solution properties if measured from the 'coffee ring' pattern of a drop dried on a SpectRIM™ plate. DMTAP was detected at ~10 μM initial solution concentration, which is about three orders of magnitude lower than that for conventional Raman spectroscopy. Moreover, SERS spectra from dried ring of Ag hydrosol/DMTAP system were obtained down to ~0.3 μM DMTAP concentration, which means that sensitivity of SERS is about five orders of magnitude higher than that of conventional Raman spectroscopy. In contrast to the DCDR technique, good SERS spectra of DMTAP were obtained only from some spots of the ring containing big nanoparticle aggregates, and the structural properties of DMTAP were significantly perturbed by adsorption on the Ag nanoparticles. Copyright © 2013 John Wiley & Sons, Ltd.

Keywords: Raman scattering; DCDR; SERS; lipid; Ag nanoparticles

Introduction

Lipids are major structural components of cell membranes. Raman spectroscopy is a widely used optical vibrational technique to study biological molecules including lipid suspensions and membrane models.[1] Frequency, intensity and line-width of vibrational bands are extremely sensitive to structural alterations, packing constraints and mobility of polar head groups as well as of hydrocarbon chain moieties. The C–H stretching vibrations in the 2800–3100 cm^{-1} region reflect the order/disorder properties of the lipids.[1] Determination of the I_{2850}/I_{2880} and I_{2935}/I_{2880} intensity ratios can be used to distinguish between the ordered gel and the disordered liquid-crystalline phase of lipids: the lower the ratio, the higher the conformational order of the lipid hydrocarbon chains.[1] It characterizes phase transition from the ordered gel phase at low temperatures to the disordered liquid-crystalline phase at high temperatures.[1] Raman spectroscopy is particularly valuable when the observed spectral features in terms of conformation and structure of membranes can be quantitatively analyzed. It is possible only from Raman spectra with good signal-to-noise ratio obtained from 'bulk' samples at high concentration (~0.01–0.1 M). Better sensitivity is needed in some cases such as low concentrated samples in the presence of only a single membrane (bi)layer. Drop coating deposition Raman (DCDR) scattering and surface-enhanced Raman scattering (SERS) spectroscopies significantly improve sensitivity of Raman measurement although quantitative assessment is often difficult.

The DCDR method is based on deposition of a small drop of sample solution (several μl) on a special hydrophobic surface (e.g. Teflon-coated stainless steel, CaF_2 or polished metal).[2] Spontaneous drying leads to formation of a ring in the outer part of the droplet as a result of the so-called 'coffee ring' effect – an interplay of contact line pinning, solvent evaporation and the capillary flow.[3] Raman spectra are measured from the ring where the sample is concentrated. Moreover, impurities of different sizes can be partially separated this way.[4] Recently, Raman spectra of dried samples of proteins (~1 μM in the deposited solution)[5,6] and liposomes (~300 μM in the deposited solution)[7] were obtained. Apart from improved sensitivity, a big advantage of DCDR is that proteins and liposomes retain their solution properties.[5,7] Drying of the droplet on hydrophobic surface is not straightforward; it depends on both properties of the surface and the size, charge and initial concentration of deposited molecules. Up to now, formation of a compact, clearly distinguishable ring was reported for dried drops of amino acids and peptides,[8] proteins,[2,5,6] protein mixtures (human tears),[9] heme proteins,[10] oligosaccharides,[11] hyaluronic acid[12] and liposomes.[7,13–15]

SERS discovered in the 70s [16] provides a giant enhancement of Raman scattering for molecules in the close vicinity of certain rough metal surfaces. The enhancement factor is typically ~10^5–10^6, but selective excitation of extremely enhancing sites ('hot spots') can give SERS enhancement of ~10^{12} allowing even single molecule detection.[17,18] Due to the recent development of reproducible SERS-active nanosubstrates as well as new instrumentations, SERS has become a promising tool for bioanalytical applications.[17,19] Silver and gold nanoparticle hydrosols are commonly used SERS substrates for biomolecular studies despite their instability and poor spectral reproducibility due to the uncontrollable nanoparticle aggregation. Higher stability can be obtained by deposition and drying of the hydrosol on a clean glass surface.[20] Dried drops of Ag hydrosol or Ag hydrosol/adsorbate form ring patterns similar to DCDR samples, which

* *Correspondence to: Marek Procházka, Charles University in Prague, Faculty of Mathematics and Physics, Institute of Physics, Ke Karlovu 5, Prague 2, 121 16, Czech Republic.*
E-mail: prochaz@karlov.mff.cuni.cz

Charles University in Prague, Faculty of Mathematics and Physics, Institute of Physics, Ke Karlovu 5, Prague 2, 121 16, Czech Republic

was previously observed for charged polystyrene microsphere drops.[21] Although dried drops of metal nanoparticles are neither uniform nor reproducible substrates,[22,23] SERS measurement from the ring can bring some advantages in comparison to measurement directly from hydrosol.[24] Drying concentrates the sample in the ring and thus promotes adsorption of the studied compounds to nanoparticle surface as well as creates highly SERS enhancing sites ('hot spots').[22] SERS is a molecular specific effect and lipids belong to poorly SERS-active species.[25] Moreover, in SERS spectroscopy using metal nanoparticle hydrosols, long fatty acid chains may hinder nanoparticle aggregation necessary to achieve sufficient SERS enhancement. Presence of both a positive and a negative charge on the lipid (e.g. many phospholipids) makes adsorption of lipids on chemically prepared metal hydrosols difficult. Although some SERS studies were already reported on model lipid membranes including Langmuir–Blodgett monolayers, hybrid bilayers, vesicles and micelles,[25] SERS of lipids is a newly emerging area. Recently, we published SERS spectra of 1,2-distearoyl-*sn*-glycero-3-phosphocholine measured from Ag nanoparticles.[22]

In this paper, we report sensitive Raman detection of 1,2-dimyristoyl-3-trimethylammonium-propane (DMTAP) lipid using two Raman techniques: DCDR and SERS. DMTAP was chosen as a model cationic lipid suitable for this study since it possesses a cationic head (see Fig. 1). This feature should enable DMTAP adsorption onto the chemically prepared Ag nanoparticles with a negative surface potential. Cationic lipids including DMTAP can be also one of the components of biological membranes. Moreover, cationic lipids and liposomes have also been widely used as transfection vehicles to introduce a gene inside the cells, and *in vivo* cationic liposome-mediated transfection requires low detection limits of liposomes.[26]

Experimental

Synthetic DMTAP (chloride salt, M.W.=590.361) in powder (Avanti Polar Lipids, Inc.) was dissolved in pure chloroform. A weak jet of nitrogen gas was used to eliminate chloroform and to form a thin lipid film at the bottom of the flask. Deionized water was subsequently added to the flask and mixed to obtain a lipid suspension. Final lipid concentration in suspension was 1 mg/ml (1.7×10^{-3} M).

For our DCDR study, 2 μl of DMTAP suspension of a required concentration was dropped on a SpectRIM™ plate (Tienta Sciences, Inc.) and left to dry at room temperature for about 1 h. The plate is a hydrophobic surface made of polished stainless steel coated by 50 nm layer of Teflon. For SERS study, Ag hydrosol nanoparticles were prepared by reduction of $AgNO_3$ by hydroxylamine hydrochloride.[27] 2 μl of Ag hydrosol/DMTAP mixture was dropped on a microscope glass slide cleaned with diluted HNO_3 and ethanol. The drop was left to dry at room temperature for approximately 45 min. For Raman measurement from suspension, the 1 mg/ml aqueous DMTAP suspension was concentrated to approximately 10 mg/ml (1.7×10^{-2} M) in Concentrator 5301 (Eppendorf).

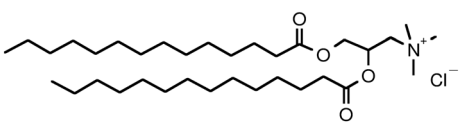

Figure 1. Chemical structure of 1, 2-dimyristoyl-3-trimethylammonium-propane (DMTAP).

All spectra were recorded by a confocal Raman microspectrometer LabRam HR800 (Horiba Jobin Yvon) equipped with a 600 grooves/mm grating and a nitrogen-cooled CCD detector. 632.8 nm excitation line of an internal He–Ne laser was used. Laser power at the sample was ~6 mW, ~3 mW and ~0.02–0.07 mW for solution, DCDR and SERS measurements, respectively. Objectives provided 1–2 μm laser spot at the sample. The objective 100× (NA = 0.9) was used for DCDR and SERS spectra acquisitions. White-light images of the dried drops were taken by the built-in digital camera using objectives 5× and 50×. Aqueous solution measurement was carried out using an immersion objective 100×. Spectra were collected at room temperature using 60 s accumulation time.

Results and discussion

The DCDR study started by drying of DMTAP drops of 1×10^{-3}–1×10^{-5} M initial solution concentrations deposited on SpectRIM™ plates. We found that, keeping the same drop volume, the result of the drying process depends on the concentration of DMTAP. Figure 2 shows white-light micro-images of dried drops at 210, 170 and 17 μM DMTAP initial solution concentrations. At 210 μM DMTAP concentration (Fig. 2A), the drop did not have a symmetric round shape, and some of the sample remained in its central part, but a 'coffee ring' pattern with ~20 μm diameter is clearly distinguishable on the edge of the drop. Deposition of less concentrated (100–200 μM) DMTAP samples led to formation of an incomplete dried drop but still with a ring pattern (Fig. 2B,C) that can be used for Raman measurements. More dilute DMTAP solutions (lower than 100 μM) formed a small dried pattern without a clear ring (Fig. 2D). Recently, this drying behavior was proposed as a universal 'solvent removal' method applicable to all samples in aqueous solutions deposited on (super)hydrophobic surfaces.[28]

Next, we acquired DMTAP spectra from the different dried patterns and compared them with a Raman spectrum from 17 mM aqueous suspension (see Fig. 3). The 1050–1150 cm^{-1} spectral region corresponds to C–C stretching vibrations sensitive to structural properties of the carbon backbone.[1,29,30] Broad bands in the 2800–3100 cm^{-1} region assigned to C–H stretching vibrational modes reflect the order/disorder characteristic of the tails.[1,29,30] The ~2850 cm^{-1} and ~2880 cm^{-1} bands are assigned

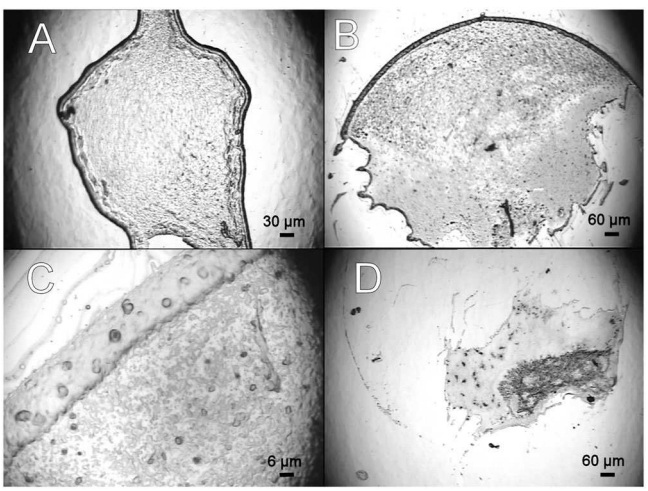

Figure 2. White-light micro-images of dried drops of DMTAP on a SpectRIM™ plate: (A) 210 μM, (B, C) 170 μM and (D) 17 μM initial solution concentration.

Journal of RAMAN SPECTROSCOPY

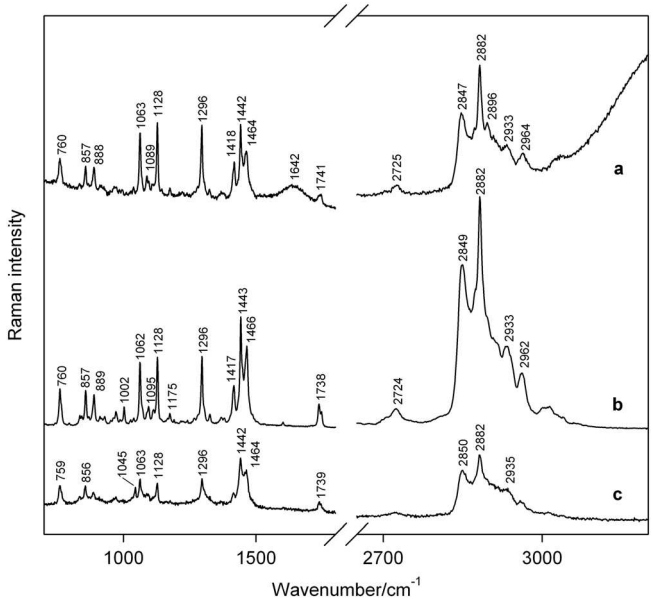

Figure 3. Raman spectra of DMTAP measured from: (a) aqueous suspension (17 mM concentration), (b) dried drop ring on a SpectRIM™ plate (210 μM initial solution concentration) and (c) dried pattern on a SpectRIM™ plate (17 μM initial solution concentration).

to acyl chain methylene C–H symmetric and anti-symmetric stretching, respectively, while ~2935 cm^{-1} band belongs to chain terminal methyl C–H symmetric stretching modes.[1,29,30] The I_{2850}/I_{2880} and I_{2935}/I_{2880} intensity ratios of DMTAP suspension spectrum (Fig. 3a) indicate a gel phase of DMTAP.[1] The same spectral features (band positions as well as relative intensity ratios) in Raman spectra of dried DMTAP (Fig. 3b) demonstrate that DMTAP holds its solution properties, including the phase, after drying. It confirms our previous conclusions for other lipids on DCDR plates.[7] There is no trace of remaining water (see water bands at 1642 and >3000 cm^{-1} in the solution spectrum, Fig. 3a) in the Raman spectra of dried DMTAP (Fig. 3b,c). The preservation of 'solution-like' spectral shape can be explained by formation of a glassy 'skin' at the surface of the ring.[5] It seems that DMTAP reproducibly retains its solution spectral features only if dried to a 'coffee ring' pattern, i.e. at DMTAP initial solution concentrations about 100 μM and higher (Fig. 3b). At lower concentrations when a small dried deposit is formed, the initial state of lipid starts to change, which can be seen from some spectral changes (e.g. decrease of 889, 1128 and 1417 cm^{-1} bands, increase of 1045 and 1464 cm^{-1} bands) although the lipid phase is still the gel one (Fig. 3c). The lowest detectable concentration of DMTAP deposited on a SpectRIM™ plate was ~8.5 μM (initial solution); however, in this case, spectra measured from different spots of the dried pattern significantly differed from each other, some of them showed spectral characteristics of the liquid-crystalline phase of DMTAP instead of the gel one.

SERS study of DMTAP was carried out using hydroxylamine-reduced Ag hydrosol nanoparticles. Ag hydrosol mixed with DMTAP dropped on a clean glass slide formed the 'coffee ring' pattern in the edge part of the drop in which almost all nanoparticles were accumulated (Fig. 4A). Apart from large aggregates, NaCl crystals coming from the hydrosol preparation are present (Fig. 4B). Clearly distinguishable rings of Ag hydrosol/DMTAP system were observed at DMTAP concentrations between 0.3 and 3 μM. In contrast to the DCDR technique, good SERS spectra

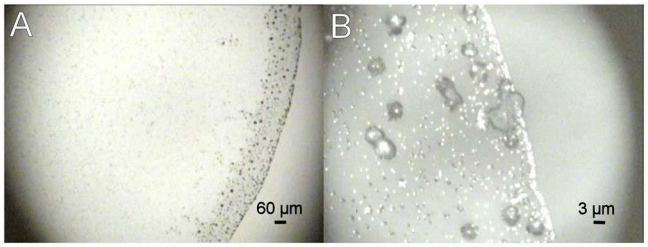

Figure 4. White-light micro-images of part (A) and detail of the ring (B) of Ag hydrosol/DMTAP (3 μM) drop dried on a clean glass slide.

of DMTAP can be obtained only from some spots of the ring containing big nanoparticle aggregates while other spots provide poor or no SERS signal. We note that spurious spectral bands (fluctuating narrow bands in the spectral region 1200–1700 cm^{-1} and two broad bands at ~1350 and ~1580 cm^{-1}) coming from carbon species contamination and/or burning of the sample[22] occurred in some spectra.

Figure 5 shows examples of the best SERS spectra of DMTAP measured at 3 μM (a) and 0.3 μM (b) concentrations. Both spectra contain spectral features of DMTAP (~762, 859, 890, 1068, 1087, 1128, 1298, 1436, 2850, 2873, 2914 and 2964 cm^{-1}). At 3 μM DMTAP concentration (Fig. 5a), SERS intensity ratio of the three bands between 1050 and 1150 cm^{-1} is similar to that of Raman spectrum of the DMTAP suspension (Fig. 3a) indicating that DMTAP carbon backbone is not affected by adsorption on Ag nanoparticles. In contrast to that, the C–H stretching vibration region at 2800–3100 cm^{-1} shows significant changes of order/disorder properties of CH_2 and CH_3 groups for both concentrations. At 0.3 μM DMTAP concentration, additional changes can be seen, e.g. decrease of 762 cm^{-1} band, strong increase of 1068 cm^{-1} band and decrease of 1127 cm^{-1} band (Fig. 5b). These changes demonstrate that also the structure of the carbon backbone is perturbed in this case. We can speculate about different orientation of DMTAP molecules on the surface for both concentrations: for higher one, the aliphatic chains are far from the Ag surface, but for lower one they lay on the surface, and thus backbone structure is strongly perturbed. In contrast to DCDR when a glassy 'skin' at the

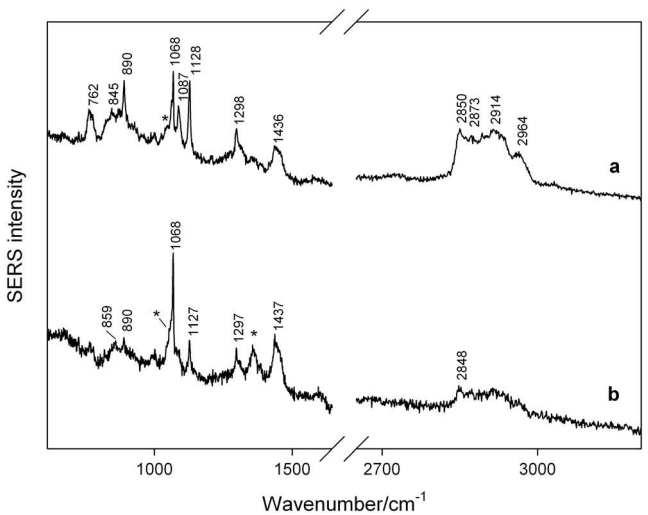

Figure 5. SERS spectra of DMTAP measured from the ring of Ag hydrosol/DMTAP mixture drop dried on a clean glass slide: (a) 3 μM and (b) 0.3 μM DMTAP concentration. Spectral features of Ag hydrosol are marked by an asterisk.

surface preserves 'solution-like' spectral shape of the dried sample, in the case of the dried Ag hydrosol/DMTAP drop, the lipid phases (pure order and disorder structures) are difficult to be considered. Spectral changes concerning 762 and 859 cm^{-1} bands assigned to the lipid head[1,29] indicate that DMTAP molecules are adsorbed on Ag nanoparticles *via* its head part. The 762 cm^{-1} bands belongs to the $\nu(N–CH_3)$ stretching vibration[1,29], and thus we suppose that nitrogen cation of lipid interacts with Ag nanoparticles. Additional bands coming from the anions present on the nanoparticle surface are marked by an asterisk (Fig. 5b). We can summarize that adsorption of DMTAP on Ag nanoparticles and the drying process significantly perturb structural properties of DMTAP.

Conclusions

We have demonstrated that both DCDR and SERS technique can be used to study DMTAP lipid samples at very low concentrations. Using DCDR, DMTAP was detected at ~10 μM initial solution concentration, which is about three orders of magnitude lower than that necessary for Raman measurement in lipid suspension. Up to this concentration, DCDR provided well-reproducible DMTAP spectra without considerable loss of its solution properties if measured from the 'coffee ring' pattern of a drop dried on a SpectRIM™ plate. The lowest detectable concentration of DMTAP was ~8.5 μM (initial solution), but in this case, DMTAP spectra substantially differ from that of solution. SERS spectra from dried Ag hydrosol/DMTAP drops can be obtained from concentrations down to ~0.3 μM, which is about five orders of magnitude lower than that for conventional Raman spectroscopy from lipid suspension. We suppose that DMTAP is adsorbed on Ag nanoparticles *via* its head part. The structural properties of DMTAP are significantly perturbed due to adsorption and the drying process. In contrast to DCDR technique, the drawback of SERS is poor reproducibility.

Acknowledgements

This work was supported by grants no. P205/12/G118 from the Czech Science Foundation and no. 267304 from the Charles University in Prague.

References

[1] I. W. Levin, in *Advances in Infrared and Raman Spectroscopy Volume 11*, (Eds: R. J. H. Clark, R. E. Hester), Wiley Heyden, Chichester, **1984**, p.1.
[2] D. Zhang, Y. Xie, M. F. Mrozek, C. Ortiz, V. J. Davisson, D. Ben-Amotz, *Anal. Chem.* **2003**, *75*, 5703.
[3] R. D. Deegan, O. Bakajin, T. F. Dupont, G. Huber, S. R. Nagel, T. A. Witten, *Nature* **1997**, *389*, 827.
[4] D. Zhang, M. F. Mrozek, Y. Xie, D. Ben-Amotz, *Appl. Spectrosc.* **2004**, *58*, 929.
[5] V. Kopecký Jr., V. Baumruk, *Vib. Spectrosc.* **2006**, *42*, 184.
[6] N. C. Dingari, G. L. Horowitz, J. W. Kang, R. R. Dasari, I. Barman, *PLoS ONE* **2012**, *7*, e32406.
[7] E. Kočišová, M. Procházka, *J. Raman Spectrosc.* **2011**, *42*, 1606.
[8] R. A. Halvorson, W. N. Leng, P. J. Vikesland, *Anal. Chem.* **2011**, *83*, 9273.
[9] J. Filik, N. Stone, *Anal. Chim. Acta* **2008**, *616*, 177.
[10] I. Barman, N. C. Dingari, J. W. Kang, G. L. Horowitz, R. R. Dasari, M. S. Feld, *Anal. Chem.* **2012**, *84*, 2474.
[11] M. F. Mrozek, D. Zhang, D. Ben-Amotz, *Carbohydr. Res.* **2004**, *339*, 141.
[12] K. A. Esmonde-White, S. V. Le Clair, B. J. Roessler, M. D. Morris, *Appl. Spectrosc.* **2008**, *62*, 503.
[13] E. Kočišová, A. Vodáková, M. Procházka, *Spectrosc. - Int. J.* **2012**, *27*, 349.
[14] E. Kočišová, A. Antalík, M. Procházka, *Chem. Phys. Lipids* **2013**, *172-173*, 1.
[15] E. Kočišová, M. Procházka, J. Štěpánek, P. Mojzeš, *Spectrosc. - Int. J.* **2010**, *24*, 197.
[16] M. Fleischmann, P. J. Hendra, A. McQuillan, *Chem. Phys. Lett.* **1974**, *26*, 163.
[17] K. Kneipp, M. Moskovits, H. Kneipp, *Surface-Enhanced Raman Scattering: Physics and Applications*, Springer, Berlin, **2006**.
[18] X. M. Qian, S. M. Nie, *Chem. Soc. Rev.* **2008**, *37*, 912.
[19] S. Schlücker (Ed.) *Surface Enhanced Raman Spectroscopy*: *Analytical, Biophysical and Life Science Applications*, Wiley-VCH, Weinheim, **2011**.
[20] M. V. Cañamares, J. V. Garcia-Ramos, J. D. Gómez-Varga, C. Domingo, S. Sanchez-Cortes, *Langmuir* **2005**, *21*, 8546.
[21] J.-Y. Jung, Y. W. Kim, J. Y. Yoo, *Anal. Chem.* **2009**, *81*, 8256.
[22] P. Šimáková, M. Procházka, E. Kočišová, *Spectrosc. - Int. J.* **2012**, *27*, 449.
[23] E. C. Le Ru, P. G. Etchegoin, *Principles of Surface-Enhanced Raman Spectroscopy and Related Plasmonic Effects*, Elsevier, Amsterdam, **2009**.
[24] P. Šimáková, M. Procházka, *J. Mol. Struct.* **2011**, *993*, 425.
[25] T. M. Cotton, J.-H. Kim, G. D. Chumanov, J. Raman *Spectrosc.* **1991**, *22*, 729.
[26] D. Liu, Y. K. Song, *Gene Ther. Mol. Biol.* **1998**, *2*, 59.
[27] N. Leopold, B. Lendl, *J. Phys. Chem. B* **2003**, *107*, 5723.
[28] I. A. Larmour, J. P. E. D. Gray, S. E. J. Bell, *Spectroscopy Europe* **2009**, *21*, 6.
[29] B. P. Gaber, W. L. Peticolas, *Biochim. Biophys. Acta* **1977**, *465*, 260.
[30] R. K. Bista, R. F. Bruch, A. M. Covington, *J. Raman. Spectrosc.* **2009**, *40*, 463.

Supplement [V]

P. Šimáková, J. Gautier, M. Procházka, K. Hervé-Aubert, I. Chourpa: Polyethylene-glycol-stabilized Ag nanoparticles for surface-enhanced Raman scattering spectroscopy: Ag surface accessibility studied using metalation of free-base porphyrins, J. Phys. Chem. C **118** (2014), 7690–7697.

THE JOURNAL OF PHYSICAL CHEMISTRY C

Article

pubs.acs.org/JPCC

Polyethylene-glycol-Stabilized Ag Nanoparticles for Surface-Enhanced Raman Scattering Spectroscopy: Ag Surface Accessibility Studied Using Metalation of Free-Base Porphyrins

Petra Šimáková,[†] Juliette Gautier,[‡,§] Marek Procházka,*[,†] Katel Hervé-Aubert,[‡] and Igor Chourpa[‡]

[†]Charles University in Prague, Faculty of Mathematics and Physics, Institute of Physics, Ke Karlovu 5, Prague 2, 121 16, Czech Republic

[‡]Université François-Rabelais de Tours, Nanomédicaments et Nanosondes EA 6295, Faculté de Pharmacie, 31 avenue Monge, 37200 Tours, France

Supporting Information

ABSTRACT: Silver nanoparticles (Ag NPs) stabilized with a permeable layer of long-chain polyethylene glycol (PEG) represent a new generation of surface-enhanced Raman scattering (SERS) substrates for bioanalytical applications. This paper will shed light on their efficiency in the SERS detection of biomolecules. Two types of thiol-terminated PEG (average molecular weight 5000 g/mol) were used. Metalation of free-base porphyrins (10^{-9}–10^{-6} M) of different size and charge was employed as the probe of accessibility of the Ag-PEG NP surface. The influence of NaCl (0.01 M) on the system was examined. The metalation was significantly decreased by the interaction of porphyrins with propionylamino groups of PEG1, while no interaction with the neutral chain of PEG2 was observed. Sterical hindrance of the porphyrin side groups seemed to cause a rather perpendicular porphyrin orientation on both types of Ag-PEG NP surfaces, inhibiting the metalation. Moreover, chloride anions influenced the structure of the polymer coating and improved the porphyrin accessibility on the Ag-PEG1 NPs. Finally, the studied Ag-PEG NPs remained isolated even after addition of porphyrins and chlorides, therefore being favorable for SERS applications inside the living cells.

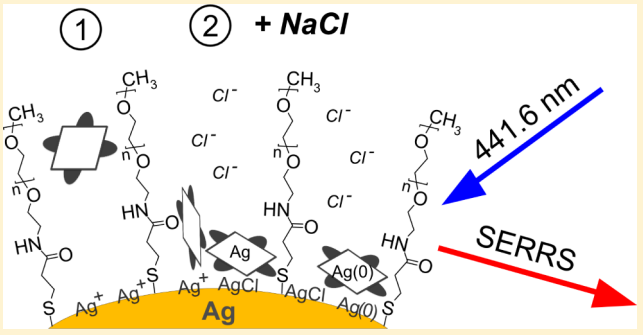

1. INTRODUCTION

Surface-enhanced Raman scattering (SERS) spectroscopy is a sensitive and selective analytical method based on a giant (above 10^6) enhancement of Raman signal for molecules adsorbed on suitably roughened metal (usually Ag or Au) surfaces.[1] Due to the recent development of new SERS-active substrates, labeling and derivatization chemistry, in addition to new instrumentations, SERS has become a promising tool for a wide range of applications, including bioanalytical and in vivo studies.[2−5]

Most of the bioanalytical SERS applications involve Ag or Au colloidal nanoparticles (NPs) prepared by conventional chemical reduction of metal salt.[6] Although isolated NPs can be used to obtain SERS spectra, aggregated NPs (upon the addition of aggregation agents or the analyte itself) usually give higher SERS enhancement due to the coupling of plasmon resonances in the interparticle junctions (so-called hot spots).[1] On the other hand, controlling the size and the aggregation state of the NPs to the degree necessary to obtain reproducible SERS enhancement is difficult. This is particularly problematic for SERS measurements with living cells.[5] The bare Ag and Au NPs aggregate rapidly and precipitate in the cell culture medium or intracellular environment. Maintaining the NPs well dispersed during their incubation to cells is important for their transportation through the cell membrane and their fate inside the cell. Isolated NPs should be less perturbing and should have a more homogeneous intracellular distribution which is crucial for SERS spectral mapping of cells.[5]

Coating the Ag and Au NP surfaces with a polymer layer such as polyethylene glycol (PEG) can protect them effectively from aggregation in vitro and in vivo as well as from being captured by the immune system in vivo.[7,8] A variety of strategies to prepare PEGylated Au and Ag NPs have been proposed depending on the structure, the size, and the charge of PEG and also on the intended application.[7] An advantage of PEG is that it is a hydrophilic but at the same time a relatively neutral molecule. Various lengths of the PEG chain, from shorter ones with molecular weight 100−250 g/mol[9−11] to longer ones with molecular weight 2000−5000 g/mol,[8,12,13] have been employed to coat Ag NPs. The NPs coated with longer PEG seem to be better suited for biological applications because of higher stability and biocompatibility as discussed

Received: January 17, 2014
Revised: March 3, 2014
Published: March 17, 2014

   dx.doi.org/10.1021/jp5005709 | J. Phys. Chem. C 2014, 118, 7690−7697

below. The synthesis of PEGylated Ag NPs involves one of two basic strategies. The first one is the attachment/adsorption of PEG molecules to the surface of previously prepared Ag NPs. The second strategy is the formation of NPs by the Ag salt reduction in the presence of PEG which serves as the stabilizing agent and/or as the reducer. It has been demonstrated that PEG of both high[8] and low[10] molecular weight can be applied for heat-mediated Ag reduction and stabilization of the resulting NPs. Nevertheless, from the point of view of SERS, protocols using PEG as the principal reducing agent appear to have several drawbacks: (i) the need of a large excess of PEG; (ii) PEG oxidation to potentially toxic byproducts; (iii) the weak polymer to particle association through physisorption on the metal surface; (iv) the competition between PEG and analytes for adsorption to the metal surface. These drawbacks can be avoided if conventional reducing agents such as citrate or borohydride are used for Ag reduction and PEG serves only as the stabilizing agent.

In this context, we have recently published a protocol of PEGylated Ag NP synthesis in which Ag salt is reduced by sodium borohydride in the presence of thiol-terminated PEG 5000 (SH-PEG, MW 5000 g/mol).[13] In this protocol, the thiol terminal groups of the polymeric chains provide nucleation seeds during the early stages of the particle formation, resulting in a small NP size. Furthermore, the strong affinity of the thiol group for Ag ensures high stability of the resulting Ag-PEG NPs against aggregation. This was seen even in the high ionic strength of biologically relevant media, which was proven by dynamic light scattering (DLS) and UV−vis spectroscopy.[13] The PEG coating can also serve to functionalize the NPs with targeting ligands. Another expected advantage of the long-chain PEG coating for bioanalytical applications is that the steric repulsion of the hydrated chains hinders the adsorption of macromolecules to the NP surface. This can prevent, for instance, the adsorption of proteins from the culture media in vitro or of the immune system proteins involved in the foreign body recognition and elimination from blood (so-called opsonines) in vivo.[14] On the other hand, this also means that only small and mobile analytes would be able to diffuse through the polymer coating to the Ag surface and provide SERS signal. Therefore, the long-chain PEG coating can be considered an advantage as well as a limitation. To develop the polymer-coated SERS substrates for bioanalytical applications, it is important to understand better the accessibility of the Ag surface for the studied analytes and the way of the analyte adsorption.

In this work, free-base porphyrins were employed as analytes. They were previously used as probe molecules in the following studies containing Ag NPs: surface properties of ablated and chemically reduced Ag colloidal solutions,[15] interaction of analytes with large biomolecules such as nucleic acids,[16] and efficiency of different molecular spacers.[17,18] These studies benefitted from the possibility to spectrally monitor the porphyrin metalation, i.e., incorporation of Ag from the Ag NPs into the porphyrin core, when two hydrogen atoms are replaced by a Ag atom, a gradual process that can last from seconds to days. Chemical structures of both free-base and Ag-metalated porphyrin cores are shown in Figure 1. In the case of cationic 5,10,15,20-tetrakis(1-methyl-4-pyridyl)-porphyrin (H_2TMPyP), a quantitative analysis[19] of its two forms, free-base (form I) and Ag^+-metalated (form II), was enabled using the intensity ratio of their characteristic metalation marker Raman bands (free-base/Ag^+-metalated) 330/395 cm^{-1} and

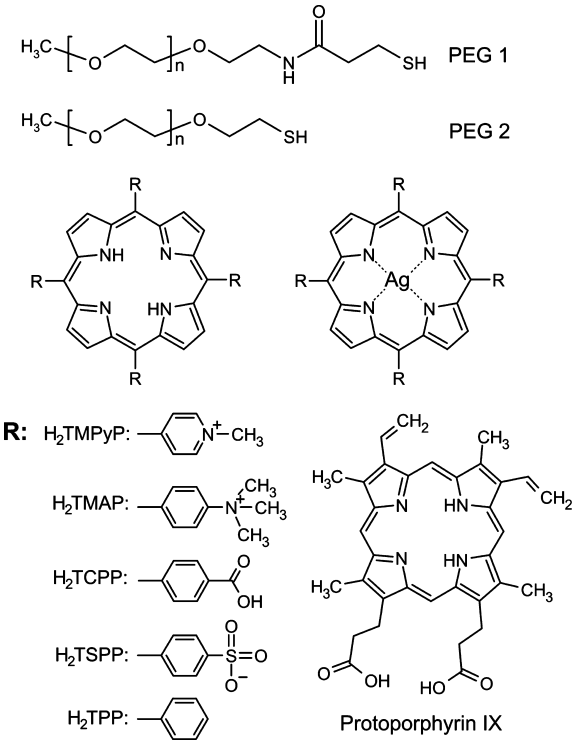

Figure 1. Chemical structures of two types of the polyethylene glycol polymers (top). Free-base and Ag-metalated porphyrin cores (middle, R: various porphyrin side groups). Free-base protoporphyrin IX (bottom).

(1335 + 1360)/1340 cm^{-1}. Apart from those, spectral features at ca. 385 cm^{-1} and 1350 + 1365 cm^{-1} have been observed in some cases, e.g., in the presence of sodium thiosulfate[20,21] or some mercaptans,[17,18] and assigned to Ag(0)-metalated TMPyP (form III).[20,21] Molecules such as H_2TMPyP or 2,2′-bipyridine can be applied to probe the state of the Ag surface. It was found that the Ag(0) sites appear after treatment of the NPs with chlorides (e.g., HCl, NaCl) or in a strongly reducing environment in the presence of an analyte capable of stabilizing these sites.[22]

In the present work, since the used excitation (441.6 nm) is in resonance with both the SPE band of isolated Ag-PEG NPs (ca. 400 nm) and the Soret electronic absorption band of the porphyrins (ca. 420 nm), surface-enhanced resonance Raman scattering (SERRS) spectra of porphyrins were measured. The metalation process of several porphyrins differing in size and charge adsorbed on Ag NPs coated with two types of thiol-terminated PEG 5000 (see Figure 1) was followed to evaluate the influence of chemical structure of the analyte and the PEG coating. The effect of chlorides on accessibility of the Ag surface was also evaluated. Information about the location and interaction of porphyrins in the vicinity of the Ag surface was obtained from the free-base and metalation marker bands.

2. EXPERIMENTAL SECTION

2.1. Materials. All chemicals and reagents were of analytical grade and used as received. Deionized water was used for all preparations.

Silver nitrate ($AgNO_3$) and sodium borohydride ($NaBH_4$) from Sigma-Aldrich (France), ethanol from Carlo Erba (France), and thiolated polyethylene glycols, *O*-[2-(3-mercaptopropionylamino)ethyl]-*O*′-methylpolyethylene glycol

dx.doi.org/10.1021/jp5005709 | J. Phys. Chem. C 2014, 118, 7690−7697

(PEG1, MW 5000 g/mol), from Sigma-Aldrich (France) and α-methoxy-ω-mercaptopolyethylene glycol (PEG2, MW 5000 g/mol) from Rapp Polymere (France) were used for the synthesis of PEGylated Ag NPs. $AgNO_3$ and $NaBH_4$ purchased from Sigma-Aldrich (Germany) were used for the preparation of the conventional Ag NPs.

Sodium chloride (NaCl), dimethyl sulfoxide (DMSO, ≥99.5%), and porphyrins were obtained from Sigma-Aldrich (Germany): 5,10,15,20-tetrakis(1-methyl-4-pyridyl)-21*H*,23*H*-porphine (H_2TMPyP), 5,10,15,20-tetrakis(4-trimethylammoniophenyl)-21*H*,23*H*-porphine (H_2TMAP), both with tetra-*p*-tosylate as the counterion, 5,10,15,20-tetrakis(4-carboxyphenyl)-21*H*,23*H*-porphine (H_2TCPP), 5,10,15,20-tetrakis(4-sulfonatophenyl)-21*H*,23*H*-porphine (H_2TSPP), and 5,10,15,20-tetraphenyl-21*H*,23*H*-porphine (H_2TPP), except the protoporphyrin IX, which was purchased from Fluka (USA).

Dialysis membranes (MWCO 8000 Da) were purchased from Interchim (Montluçon, France).

2.2. Preparation Procedures. The Ag-PEG NPs were prepared according to ref 13, which is a modification of the method described in ref 23. The reaction was carried out under nitrogen atmosphere to prevent oxidation of the reducer and polyethylene glycol during formation of the metal NPs. An amount of 4 mL of 7.5 mM $AgNO_3$ ethanol solution was mixed with 75 mg of PEG-SH powder and sonicated for 5 min. Ag reduction was achieved by a dropwise addition of 1.3 mL of 90 mM $NaBH_4$ ethanol solution to the $AgNO_3$ solution with PEG-SH under vigorous stirring. After 2 h reaction time in the dark, the obtained brown suspension was diluted 4 times with deionized water and dialyzed against deionized water to remove the excess of PEG molecules. Both batches (Ag-PEG1 and Ag-PEG2) were reconcentrated by evaporation to 1 g of Ag per liter, to use them at the same concentration.

The conventional (uncoated) Ag NPs were prepared by reduction of $AgNO_3$ with $NaBH_4$ (borohydride-reduced).[24] To 75 mL of a 1.2×10^{-3} M $NaBH_4$ aqueous solution (cooled to 2 °C in an ice bath) was added dropwise 9.0 mL of a 2.2×10^{-4} M $AgNO_3$ aqueous solution at constant stirring. The stirring was continued for 45 min to adapt the colloid to room temperature.

Ag-PEG NPs/porphyrin and borohydride-reduced Ag NPs/porphyrin systems were prepared by the addition of an appropriate amount of a porphyrin solution to the NP suspension. H_2TCPP, H_2TPP, and protoporphyrin IX had to be dissolved in DMSO first, and then they were diluted with water. The concentration of the water-insoluble porphyrins was achieved only approximately. NaCl was added after porphyrins, its final concentration in the Ag NP/porphyrin system being 0.01 M in all SERS experiments.

2.3. Instrumentation. The hydrodynamic diameter of the Ag-PEG NPs was determined by dynamic light scattering (DLS): samples were measured using an Autosizer 2c (Malvern Instruments, Orsay, France) equipped with a He−Ne laser operating at 632.8 nm (output laser power 4 mW), with a scatter angle of 173°.

A Malvern NanoZ (Malvern Instruments, Orsay, France) with a He−Ne laser operating at 632.8 nm (output laser power 4 mW), with a scatter angle of 17°, was used on the same samples to determine the surface charge (zeta potential) of the NPs. In both cases, the samples were diluted in deionized water or in NaCl solutions (0.1 M). Each measurement was performed at 25 °C at least three times.

Surface plasmon extinction (SPE) spectra were measured in a quartz cuvette (optical length 2 mm) using a UV−vis absorption spectrometer (Analytik Jena Specord 250).

SERRS spectra were acquired at room temperature (20 °C) in a 90° scattering geometry by a Raman spectrometer equipped with a 1800 grooves/mm grating monochromator (Jobin-Yvon-Spex 270 M) and a nitrogen-cooled CCD detector (Princeton Instruments). Laser lines 441.6 nm (He−Cd laser, Liconix, ∼3 mW at the sample) and 532.0 nm (a diode-pumped frequency-doubled Nd:YVO_4 laser, Verdi, Coherent, ∼100 mW at the sample) were used as excitation. The typical accumulation time was 1 s × 60, but 5 s × 60 was used in the case of poor signal-to-noise ratio. Baseline correction of the SERRS spectra was performed in GRAMS/AI (Thermo Fisher Scientific Inc.) software.

3. RESULTS AND DISCUSSION

3.1. Chemical Structure of PEG and Porphyrin Species. Chemical structures of the employed polymers and porphyrins are shown in Figure 1. The PEG with a polar propionylamino moiety next to the thiol terminal group and the second one with a neutral chain are hereafter called PEG1 and PEG2, respectively. The six used porphyrins differ in the charge and the size of their side groups. H_2TMAP and H_2TMPyP both possess four positive charges on nitrogen atoms, but the trimethyl side groups of H_2TMAP are sterically larger than the methyl groups of H_2TMPyP. H_2TCPP carries four carboxyl functional groups and H_2TSPP four sulfonyl groups. Each sulfonyl group contains a negative charge on the oxygen atom, and the carboxyl group can also be negatively charged if dissociated. Protoporphyrin IX, the largest porphyrin of the set, is substituted by six nonpolar and two carboxyl groups which can be negatively charged if dissociated. Protoporphyrin IX is an important biomolecule serving as a marker in clinical diagnostics of cancer.[25] H_2TPP is neutral and the smallest used porphyrin.

3.2. Ag-PEG NP Stability in the Presence of Porphyrins and NaCl. The synthesis of both types of Ag-PEG NPs resulted in brown suspensions. As in our previous paper[13] we first verified the state and stability of the prepared Ag-PEG NPs. Their excellent stability is explained due to the steric repulsion confirmed by zeta pontential measurements (data not shown) where nearly neutral surface charge was detected over a wide range of pH. DLS measurements showed that the stability is preserved even at high ionic strength. Average hydrodynamic diameters were 156 and 144 nm for Ag-PEG1 NPs and Ag-PEG2 NPs, respectively. The addition of NaCl (0.1 M) did not modify their hydrodynamic diameter, and it remained 147 and 148 nm for Ag-PEG1 NPs and Ag-PEG2 NPs, respectively.

UV−vis spectra of Ag-PEG1 NPs (data not shown) and Ag-PEG2 NPs (Figure 2) had a characteristic SPE band with a maximum at ca. 400 nm corresponding to well-dispersed isolated Ag NPs, similarly to ref 13. The addition of H_2TMPyP (1×10^{-7} M final concentration) and NaCl (0.01 M final concentration) led to only a slight decrease of the intensity in the SPE maximum (Figure 2). The spectrum did not change within the time it was monitored (6 days), meaning that the Ag-PEG NPs remained nonaggregated.

3.3. SERRS Study of Ag-PEG NPs Using Porphyrins As a Probe. The particularity of using nonaggregating NPs is that, for efficient SERS, the excitation wavelength has to be in resonance with the surface plasmon band of the isolated Ag

dx.doi.org/10.1021/jp5005709 | J. Phys. Chem. C 2014, 118, 7690−7697

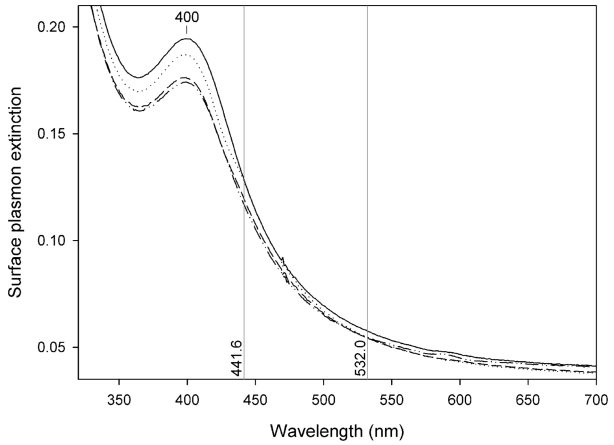

Figure 2. Surface plasmon extinction spectra of Ag-PEG2 NPs: NPs alone (solid line), NPs with 1×10^{-7} M H_2TMPyP (dotted line), NPs with 1×10^{-7} M H_2TMPyP and 0.01 M NaCl (dashed line), and NPs with 1×10^{-7} M H_2TMPyP and 0.01 M NaCl after 6 days (dot-and-dashed line).

NPs (which has the maximum at ca. 400–420 nm).[26] With the excitation wavelength at 488 nm, i.e., at the edge of the plasmon resonance band of nanosized Ag, it was possible to record satisfactory SERS spectra of the anticancer drug mitoxantrone with Ag-PEG 5000 NPs.[13] However, with limited plasmon resonance and in the absence of interparticle plasmon coupling (hot spots), the SERS sensitivity of mitoxantrone detection on the Ag-PEG NPs was about 100 times lower than on aggregated conventional citrate-reduced Ag NPs.[13] More recently Stiufiuc et al. reported SERS spectra of methylene blue, aminothiophenol, and amoxicillin obtained from PEG-200-reduced Ag NPs.[11] Surprisingly, they achieved the SERS detection with 532 and 632.8 nm excitations situated far from the resonance with the plasmon band of isolated Ag NPs. Furthermore, the authors comment on the comparable SERS intensity and spectral shape of PEGylated and aggregated conventional Ag NPs. Since DLS or SPE data excluding possible particle aggregation in the presence of adsorbates are missing in their paper, one might speculate about a substantial SERS enhancement from interparticle junctions.

In the present study, with 532.0 nm excitation that is far from the SPE band of Ag-PEG NPs (Figure 2), porphyrin spectra were significantly weaker, and a good signal-to-noise ratio was reached only for the 10 μM concentration range, i.e., that achievable with resonance Raman scattering. On the other hand, using 441.6 nm excitation which is in resonance with isolated Ag-PEG NPs, good SERRS spectra of porphyrins have been obtained. Therefore, this excitation wavelength was chosen for our study.

3.3.1. Accessibility of the Ag-PEG NP Surface for the Cationic Porphyrins. Cationic H_2TMPyP is known to undergo the metalation process on Ag NPs.[19−21] Figures 3 and 4 show SERRS spectra obtained from 1×10^{-7} M H_2TMPyP adsorbed on Ag-PEG1 NPs and Ag-PEG2 NPs, respectively. Spectra *a* were measured immediately after the addition of H_2TMPyP. Spectra *b* to *e* represent measurements made immediately after the addition of NaCl to porphyrin/Ag-PEG NPs and their evolution within 6 days. The spectra show characteristic SERRS bands of the free-base H_2TMPyP (form I) at ca. 330 cm^{-1} and of two metalated forms:[20,21] AgTMPyP (form II) at ca. 395 cm^{-1} and Ag(0)TMPyP (form III) at ca. 385 and 1350 + 1365 cm^{-1}. Also other changes appeared during the time evolution

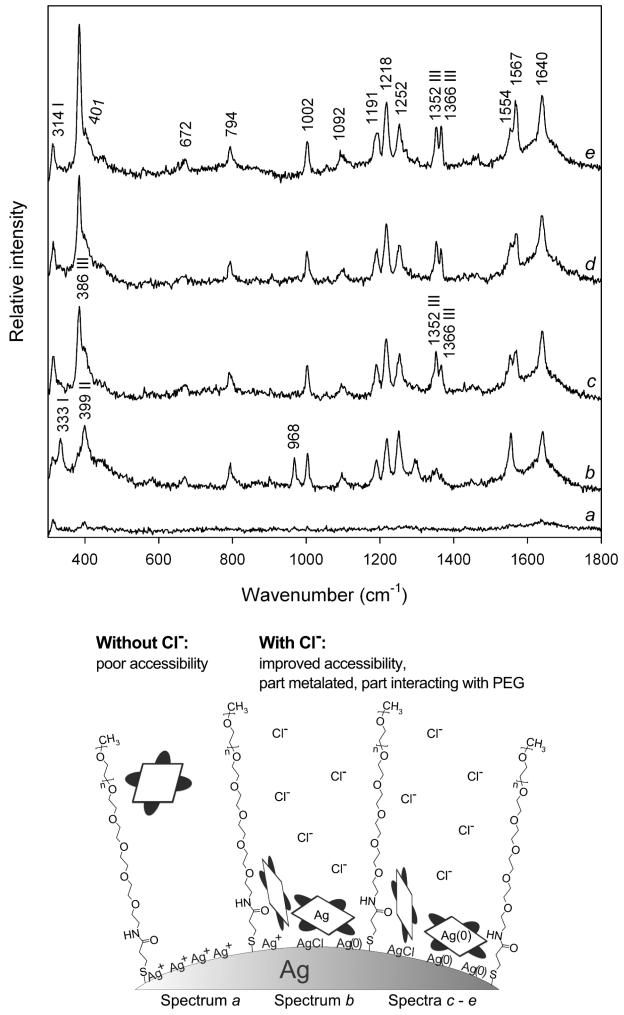

Figure 3. Top: SERRS spectra obtained from 1×10^{-7} M H_2TMPyP adsorbed on Ag-PEG1 NPs before and after addition of NaCl (0.01 M): (a) no NaCl, (b) with NaCl, (c) with NaCl − 2 days, (d) with NaCl − 3 days, and (e) with NaCl − 6 days. Relevant spectral features of different porphyrin metalation forms are marked with I–III. Bottom: Scheme showing possible adsorption of all three porphyrin forms on Ag-PEG1 NPs.

(disappearance of the 965 cm^{-1} band, change in the intensity ratio of the bands at ca. 1191/1218/1252 cm^{-1}, changes in the 1500–1600 cm^{-1} region). These changes cannot be used as metalation markers since they correspond to the deformation of the macrocycle which can be caused not only by the metalation but also by other interactions such as porphyrin stacking[19] or interaction with PEG.

SERRS spectra of H_2TMPyP obtained from Ag-PEG1 NPs and Ag-PEG2 NPs differed both in the intensity and in the position of the Raman bands. The intensity was related to different surface accessibility for the porphyrin and the band positions to metalation behavior. The addition of NaCl was necessary to obtain a recognizable spectrum of porphyrin using Ag-PEG1 NPs (Figure 3, spectra *a* and *b*). An increase of SERS signal in the presence of Cl^- ions was also reported for mitoxantrone on Ag-PEG1 NPs.[13] On the other hand, no influence of chlorides on SERRS intensity was observed using Ag-PEG2 NPs (Figure 4, spectra *a* and *b*). We suggest that chlorides influence the structure of the PEG1 polymer coating and then increase accessibility of porphyrin molecules for the

dx.doi.org/10.1021/jp5005709 | J. Phys. Chem. C 2014, 118, 7690−7697

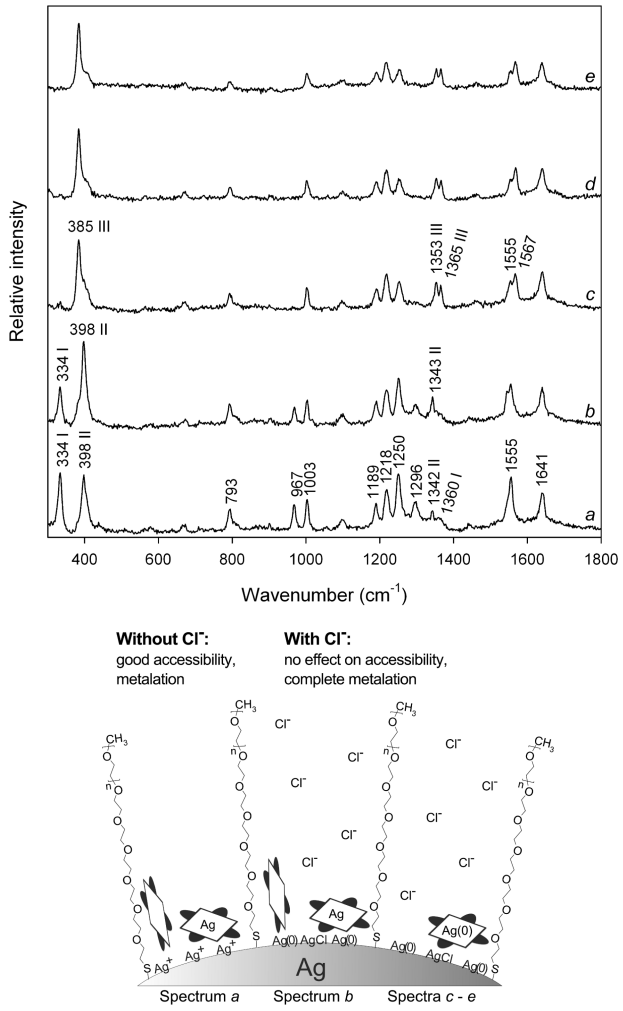

Figure 4. Top: SERRS spectra obtained from 1×10^{-7} M H_2TMPyP adsorbed on Ag-PEG2 NPs before and after addition of NaCl (0.01 M): (a) no NaCl, (b) with NaCl, (c) with NaCl − 1 day, (d) with NaCl − 2 days, and (e) with NaCl − 6 days. Relevant spectral features of different porphyrin metalation forms are marked with I–III. Bottom: Scheme showing possible adsorption of all three porphyrin forms on Ag-PEG2 NPs.

Ag surface which is demonstrated by a significant increase of SERS intensity. Before and just after the addition of chlorides (spectra *a* and *b* in both Figures 3 and 4), the spectra contained both the free-base band at ca. 330 cm^{-1} and the band at ca. 395 cm^{-1} of the metalated form II of AgTMPyP. After the addition of NaCl, the porphyrin spectra showed slow metalation of porphyrin to Ag(0)TMPyP (form III) characterized by an ca. 385 cm^{-1} band on the time scale of 6 days (spectra *c* and *d* in both Figures 3 and 4). The concentration 0.01 M NaCl was sufficient to observe this effect. It was reported previously that the chloride anions adsorbed onto Ag NPs create Ag(0) sites.[22] It is also our case because control measurements on conventional Ag NPs (without PEG coating) carried out under the same experimental conditions clearly showed metalation of H_2TMPyP to the Ag(0)TMPyP as the effect of chloride anions (Figure S1 in the Supporting Information).

It seems that the metalation was faster on Ag-PEG2 NPs than on Ag-PEG1 NPs. In the case of Ag-PEG2 NPs, the free-base band at 334 cm^{-1} disappeared in 2 days (Figure 4, spectrum *d*) because of H_2TMPyP conversion to the metalated form. In the case of Ag-PEG1 NPs, the band at ca. 330 cm^{-1} (Figure 3, spectrum *b*) also disappeared in 2 days (Figure 3, spectrum *c*); however, a band 314 cm^{-1} was present in spectra even after 6 days (Figure 3, spectrum *e*). Since a wavenumber down-shift has been observed in other cases of interactions of H_2TMPyP molecules (e.g., J-aggregates formation),[27] we think that the 314 cm^{-1} band belongs to free-base H_2TMPyP interacting with PEG1 probably with the propionylamino moiety. The absence of this down-shifted band in the spectra from Ag-PEG2 NPs then indicates no porphyrin interaction with the neutral PEG2. These results clearly show that depending on the surface accessibility and molecular interactions with the coating porphyrin may adopt a parallel or perpendicular orientation to the Ag surface, allowing or preventing, respectively, porphyrin metalation (see the schemes in Figures 3 and 4).

Metalation of H_2TMAP on Ag NPs has been previously reported in ref 28, but the free-base and metalation spectral markers of this porphyrin have not yet been clearly described. To determine them, the resonance Raman scattering (RRS) and time development of SERRS spectra after addition of NaCl on conventional borohydride-reduced Ag NPs were measured (see Figure S2 A, B in the Supporting Information). From comparison with the RRS spectrum, one can conclude that the SERRS marker bands of free-base H_2TMAP (form I) lie at ca. 320 cm^{-1} and 1340 + 1365 cm^{-1}. When H_2TMAP is added to the borohydride-reduced Ag NPs, it is metalated to AgTMAP (form II) characterized by an increase of the bands at ca. 380 and 1341 cm^{-1}. In the presence of 0.01 M NaCl, the porphyrin molecules are converted to Ag(0)TMAP (form III), showing bands at ca. 370 cm^{-1} and 1350 + 1365 cm^{-1}. Other band changes observable upon the metalation process are mostly caused by possible deformation of the porphyrin macrocycle interacting with the surface. Figure 5 A, B shows SERRS spectra obtained from 1×10^{-7} M H_2TMAP adsorbed on Ag-PEG1 NPs and Ag-PEG2 NPs, respectively. The spectra *a* were measured immediately after addition of NaCl to the system, and the spectra *b* were recorded after one day of the system evolution. A significant difference in behavior of H_2TMAP can be seen on the two Ag-PEG NP types. On Ag-PEG1 NPs, H_2TMAP remained in its free-base form after the chloride addition (see 320 cm^{-1} and 1340 + 1365 cm^{-1} bands, spectrum *a* in Figure 5A), and one day later only a small fraction of porphyrin has been converted to the metalated Ag(0)TMAP form (see 367 cm^{-1} band, spectrum *b* in Figure 5A). In contrast to that, on the Ag-PEG2 NPs the metalation of H_2TMAP started immediately after the chloride addition (Figure 5B, spectrum *a*) and was almost complete in one day (see Ag(0)TMAP bands at ca. 367, 1353 + 1364 cm^{-1} in spectrum *b*, Figure 5B). It is likely that the majority of H_2TMAP molecules passed through the PEG2 layer and adsorbed on the Ag NPs in an orientation parallel to the Ag surface, allowing the metalation, while the PEG1 layers prevented the H_2TMAP molecules from metalation, possibly by giving them a more perpendicular orientation to the Ag surface as proposed in the schemes in Figures 3 and 4. It is worth noting that we did not see the down-shift of the 320 cm^{-1} free-base band probably indicative of the interaction of H_2TMAP with PEG1 as was the case for H_2TMPyP. This could be caused by a higher sterical protection of the cationic nitrogen in H_2TMAP than in H_2TMPyP.

3.3.2. Concentration Dependence of SERRS Spectra of the Cationic Porphyrins. To study the concentration effect, the

dx.doi.org/10.1021/jp5005709 | J. Phys. Chem. C 2014, 118, 7690−7697

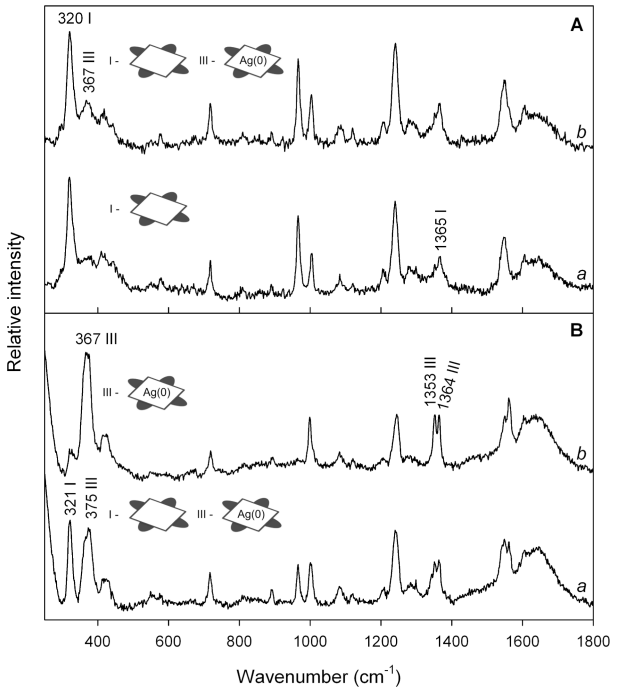

Figure 5. SERRS spectra obtained from 1×10^{-7} M H_2TMAP adsorbed on Ag-PEG1 NPs (A) and Ag-PEG2 NPs (B) after addition of NaCl (0.01 M): (a) with NaCl and (b) with NaCl − 1 day. Different porphyrin chemical structures are depicted, and their spectral features are marked with I–III.

porphyrin SERRS spectra in a concentration range from 10^{-6} to 10^{-9} M recorded one day after the chloride addition were compared. Independently from the PEG or porphyrin used, the spectra at 1×10^{-6} M have less pronounced metalation features than at 1×10^{-7} M concentration. As an example the SERRS spectra obtained from H_2TMPyP adsorbed on the Ag-PEG2 NPs are presented (Figure 6). With concentration decreasing below 1×10^{-7} M, the metalation becomes faster. A higher metalation ratio with decreasing concentration has also been

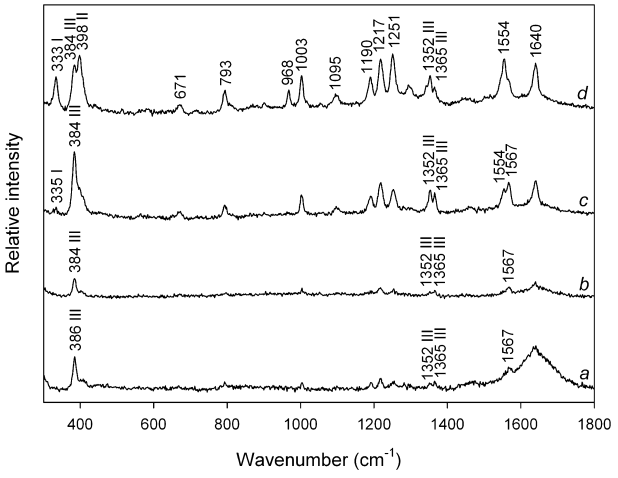

Figure 6. SERRS spectra of different concentrations of H_2TMPyP adsorbed on Ag-PEG2 NPs with 0.01 M NaCl after 1 day: (a) 1×10^{-9} M, (b) 1×10^{-8} M, (c) 1×10^{-7} M, and (d) 1×10^{-6} M. Accumulation time was 1 s × 60 (except the spectrum *a* measured 5 s × 60). Relevant spectral features of different porphyrin metalation forms are marked with I–III.

observed for H_2TMPyP on the ion-free surface of laser-ablated Ag NPs when only the porphyrin molecules limit the metalation by a hindering effect.[15] On the other hand, porphyrin dilution reduced the metalated fraction on the citrate- or borohydride-carrying Ag NPs.[15] This behavior with citrate- and borohydride-reduced colloids was explained by a need of higher porphyrin concentrations to win the competition for adsorption on the Ag surface against the initially adsorbed anions. The similarity to the laser-ablated Ag NPs indicates that the Ag surface of the PEG-SH-coated Ag NPs can be considered as ion-free (one might recall that they were dialyzed against distilled water), meaning that to be adsorbed on the Ag the porphyrin molecules do not have to compete with other species than themselves. Consequently, at lower porphyrin concentrations, the spectral fraction of the metalated porphyrin form is higher. The absence of competition against anions for binding to the Ag surface should be an interesting advantage for some analytes having low affinity to Ag. On the other hand, it is important to underline that both the PEG1 and PEG2 layers remain permeable for diffusion of ions which can influence the porphyrin metalation, as indicated by the spectral changes observed after the addition of chlorides to the porphyrin/Ag-PEG NPs.

From the sensitivity point of view, Ag-PEG2 NPs were more efficient than Ag-PEG1 NPs providing a valid SERRS detection of H_2TMAP and H_2TMPyP in the concentration range 1×10^{-6}–1×10^{-8} M (Figure S3 in the Supporting Information for the SERRS detection limit of H_2TMAP) and 1×10^{-6}–1×10^{-9} M (Figure 6), respectively. The nanomolar concentration can be considered as the SERRS detection limit of H_2TMPyP on the Ag-PEG2 NPs. We note that the detection limit of CuTMPyP using the conventional borohydride-reduced Ag NPs obtained with the same 441.6 nm excitation was also 1×10^{-9} M.[26] Therefore, with resonance excitation, the PEGylated Ag NPs are able to provide an excellent sensitivity, comparable with that of nonaggregated conventional Ag NPs. This quantitative comparison with bare NPs indicates that, for the analytes able to diffuse through it, the PEG coating does not necessarily lead to a dramatic loss of the analyte adsorption sites on the Ag NP surface.

3.3.3. Accessibility of the Ag-PEG NP Surface for the Noncationic Porphyrins. SERRS detection was less sensitive for anionic and neutral porphyrins than for cationic ones. Therefore, it appears that the accessibility of the PEGylated Ag surface is lower for noncationic porphyrins than for cationic ones. Nevertheless, SERRS spectra of anionic and neutral porphyrins with a satisfactory signal-to-noise ratio were obtained for the concentration 1×10^{-6} M after addition of NaCl to the porphyrin/Ag-PEG NPs (Figure 7).

A good SERRS spectrum was obtained only from H_2TPP adsorbed on Ag-PEG1 NPs (Figure 7, spectrum *c*). Free-base and metalation markers of H_2TPP are similar to those of H_2TMPyP.[29] Our spectrum contains a mixture of bands of both the free-base H_2TPP (ca. 330 cm^{-1} band) and the metalated Ag(0)TPP form (379 and 1352 cm^{-1} bands). This observation indicates that at least a part of the porphyrin molecules is able to have a parallel adsorption orientation on the PEGylated Ag surface. Similarly to cationic H_2TMPyP on the Ag-PEG1 NPs, the two bands at 314 and 330 cm^{-1} probably correspond to free-base H_2TPP molecules interacting and noninteracting with PEG1, respectively.

dx.doi.org/10.1021/jp5005709 | J. Phys. Chem. C 2014, 118, 7690–7697

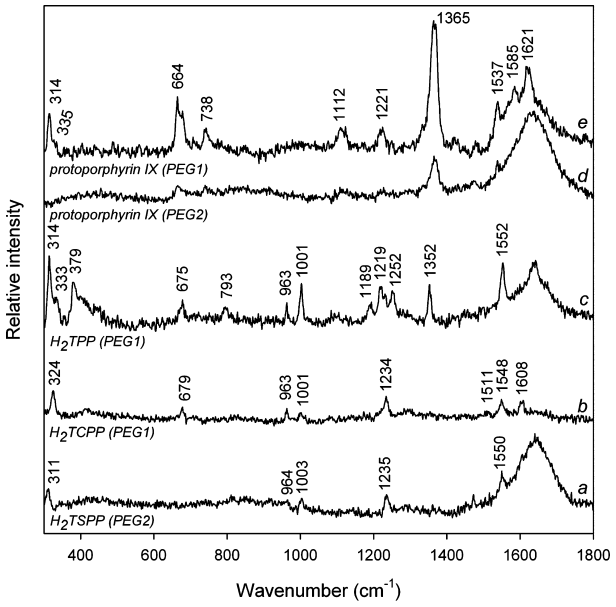

Figure 7. SERRS spectra of noncationic porphyrins obtained from Ag-PEG1 or Ag-PEG2 NPs (approximately 1×10^{-6} M porphyrin and 0.01 M NaCl concentration), accumulation time was 5 s × 60 (except the spectrum *b* measured 1 s × 60).

SERRS detection of negatively charged porphyrins was even less efficient. H_2TCPP provided better SERRS spectra with Ag-PEG1 NPs and H_2TSPP with Ag-PEG2 NPs (Figure 7, spectra *a*, *b*). These porphyrins are also known to be metalated after direct adsorption on the Ag surface: main free-base and Ag^+ metalation markers of H_2TCPP are at ca. 327 and 390 cm^{-1}, respectively,[30] and H_2TSPP in free-base form is characterized by an ca. 315 cm^{-1} band.[31] SERRS spectra of both porphyrins on Ag-PEG NPs showed only free-base marker bands: at ca. 325 and 311 cm^{-1} for H_2TCPP and H_2TSPP, respectively. Therefore, it is probable that in our case the porphyrins are in a perpendicular orientation onto the Ag surface, being thus protected against metalation.

Protoporphyrin IX is also known to undergo metalation when adsorbed on the conventional Ag NPs.[32] We obtained good SERRS spectra of protoporphyrin IX from both types of Ag-PEG NPs (Figure 7, spectra *d* and *e*). Protoporphyrin IX molecules were not metalated, as evident from the free-base marker bands at ca. 330 and 1365 cm^{-1} according to ref 32. Similarly to cationic porphyrins, free-base protoporphyrin IX is probably interacting with polar groups of PEG1 and not with PEG2 which is indicated by the presence of the 314 cm^{-1} band only in the spectra measured from the Ag-PEG1 NPs (Figure 7, spectra *e*, *d*).

4. CONCLUSIONS

Our study sheds light on the action mechanisms of polymer-coated NP surfaces as a new generation of SERS substrates. The metalation process of several porphyrins differing in size and charge was used as a sensitive SERS spectral probe of Ag NPs coated with two types of thiol-terminated PEG 5000. New information about accessibility of the Ag surface for particular porphyrin molecules, their location, orientation, possible interaction with PEG layers, as well as influence of porphyrin concentration and of chloride anions in studied system was obtained.

The results demonstrate that the accessibility of the PEGylated Ag NP surface for adsorption of porphyrins depends on the chemical structure of both the polymer and the analyte. The presence of polar groups of the PEG1 polymer near the Ag surface is responsible for stronger interaction of the polymeric coating with some of the used porphyrins (H_2TMPyP, H_2TMAP, H_2TPP, and protoporphyrin IX). As a result, the PEG1 layer was able to hinder the porphyrin metalation by the Ag, presumably by imposing a more perpendicular porphyrin orientation on the Ag surface. Metalation was less efficient for H_2TMAP than for H_2TMPyP, probably due to the sterical hindrance of cationic charge from three methyl side groups of H_2TMAP. In contrast to PEG1, the PEG2 coating without any polar side groups was not able to decrease the porphyrin metalation but enabled a good, nonselective accessibility of porphyrins to the Ag surface which is necessary for a sensitive SERRS detection. The lowest detection limits of ca. 10^{-9} M were obtained with cationic porphyrin H_2TMPyP on Ag-PEG2 NPs. Metalation was more efficient at lower porphyrin concentrations than at higher concentrations, which is connected with the absence of competition of porphyrins with anions for adsorption on the Ag surface. The chloride anions induced Ag(0) sites on the Ag surface and thus favored the conversion of free-base and/or Ag^+-metalated porphyrin to the Ag(0)-metalated form. Moreover, chlorides influenced the structure of the polymer coating because they significantly increased the SERRS signal on the Ag-PEG1 NPs but not on the Ag-PEG2 NPs. The active role of the PEG coating in the selective adsorption of analytes was also revealed by the fact that the SERRS sensitivity decreased on going from cationic to neutral and anionic porphyrin derivatives.

■ ASSOCIATED CONTENT

Ⓢ Supporting Information

SERRS spectra of H_2TMPyP and H_2TMAP on borohydride-reduced Ag NPs (time evolution) and a resonance Raman spectrum of H_2TMAP solution. This material is available free of charge via the Internet at http://pubs.acs.org.

■ AUTHOR INFORMATION

Corresponding Author

*E-mail: prochaz@karlov.mff.cuni.cz.

Present Address

[§]Université de Rouen, Laboratoire de Pharmacie Galénique, Faculté de Médecine-Pharmacie, 22 Bvd Gambetta, 76183 Rouen Cedex, France (J.G.).

Notes

The authors declare no competing financial interest.

■ ACKNOWLEDGMENTS

Financial support from the Czech Science Foundation (P205/12/G118), from the Charles University in Prague (No. 267304) and Ministry of Education Youth and Sports of the Czech Republic (project Barrande 7AMB12FR023), and French Ministry of Foreign Affairs (project Barrande No. 26593TA Partenariats Hubert Curien 2013, Campus France) is gratefully acknowledged.

■ REFERENCES

(1) Le Ru, E. C.; Etchegoin, P. G. *Principles of Surface-enhanced Raman Spectroscopy and Related Plasmonic Effects*; Elsevier: Amsterdam, The Netherlands, 2009.

(2) Kneipp, K.; Moskovits, M.; Kneipp, H., Eds. *Surface-enhanced Raman scattering: physics and applications, Top. Appl. Phys. 103*, Springer-Verlag: Berlin Heidelberg, 2006.
(3) Schlücker, S., Ed. *Surface Enhanced Raman Spectroscopy, Analytical, Biophysical and Life Science Applications*: Wiley-VCH: Weinheim, Germany, 2011.
(4) Procházka, M.; Štěpánek, J. Surface-enhanced Raman Scattering (SERS) and its Application to Biomolecular and Cellular Investigation In *Applications of Raman Spectroscopy to Biology - From Basic Studies to Disease Diagnosis*; Ghomi, M., Ed., IOS Press: Amsterdam, The Netherlands, 2012; pp 1−30.
(5) Chourpa, I.; Lei, F. H.; Dubois, P.; Manfait, M.; Sockalingum, G. D. Intracellular Applications of Analytical SERS Spectroscopy and Multispectral Imaging. *Chem. Soc. Rev.* **2008**, *37*, 993−1000.
(6) Aroca, R. F.; Alvarez-Puebla, R. A.; Pieczonka, N.; Sanchez-Cortes, S.; Garcia-Ramos, J. V. Surface-Enhanced Raman Scattering on Colloidal Nanostructures. *Adv. Colloid Interface Sci.* **2005**, *116*, 45−61.
(7) Jokerst, J. V.; Lobovkina, T.; Zare, R. N.; Gambhir, S. S. Nanoparticle PEGylation for Imaging and Therapy. *Nanomedicine* **2011**, *6*, 715−728.
(8) Luo, C.; Zhang, Y.; Zeng, X.; Zeng, Y.; Wang, Y. The Role of Poly(ethylene Glycol) in the Formation of Silver Nanoparticles. *J. Colloid Interface Sci.* **2005**, *288*, 444−448.
(9) Nam, S.; Parikh, D. V.; Condon, B. D.; Zhao, Q.; Yoshioka-Tarver, M. Importance of Poly(ethylene Glycol) Conformation for the Synthesis of Silver Nanoparticles in Aqueous Solution. *J. Nanopart. Res.* **2011**, *13*, 3755−3764.
(10) Popa, M.; Pradell, T.; Crespo, D.; Calderon-Moreno, J. M. Stable Silver Colloidal Dispersions Using Short Chain Polyethylene Glycol. *Colloid. Surf. A: Physicochem. Eng. Asp.* **2007**, *303*, 184−190.
(11) Stiufiuc, R.; Iacovita, C.; Lucaciu, C. M.; Stiufiuc, G.; Dutu, A. G.; Braescu, C.; Leopold, N. SERS-Active Silver Colloids Prepared by Reduction of Silver Nitrate with Short-Chain Polyethylene Glycol. *Nanoscale Res. Lett.* **2013**, *8*, 47.
(12) Bo, L.; Yang, W.; Chen, M.; Gao, J.; Xue, Q. Simple and 'Green' Synthesis of Polymer-Based Silver Colloids and Their Antibacterial Properties. *Chem. Biodiversity* **2009**, *6*, 111−116.
(13) Shkilnyy, A.; Soucé, M.; Dubois, P.; Warmont, F.; Saboungi, M.-L.; Chourpa, I. Poly(ethylene Glycol)-Stabilized Silver Nanoparticles for Bioanalytical Applications of SERS Spectroscopy. *Analyst* **2009**, *134*, 1868−1872.
(14) Lankveld, D. P.; Rayavarapu, R. G.; Krystek, P.; Oomen, A. G.; Verharen, H. W.; van Leeuwen, T. G.; De Jong, W. H.; Manohar, S. Blood Clearance and Tissue Distribution of PEGylated and Non-PEGylated Gold Nanorods after Intravenous Administration in Rats. *Nanomedicine* **2011**, *6*, 339−349.
(15) Procházka, M.; Štěpánek, J.; Turpin, P.-Y.; Bok, J. Drastically Different Porphyrin Adsorption and Metalation Processes in Chemically Prepared and Laser-Ablated SERS-Active Silver Colloidal Substrates. *J. Phys. Chem. B* **2002**, *106*, 1543−1549.
(16) Procházka, M.; Turpin, P.-Y.; Štěpánek, J.; Bok, J. Metallation Kinetics of a Free Base Porphyrin in Surface-Enhanced Resonance Raman Scattering Active Ag Colloid System as a Probe of Porphyrin-Nucleic Acids Interaction. *J. Mol. Struct.* **1999**, *482*−*483*, 221−224.
(17) Šmejkal, P.; Vlčková, B.; Procházka, M.; Mojzeš, P.; Pfleger, J. Testing Anionic Spacers by SERRS (Surface-Enhanced Resonance Raman Scattering) of a Cationic Free-Base Porphyrin in Systems with Laser-Ablated Ag Colloids. *Vib. Spectrosc.* **1999**, *19*, 243−247.
(18) Šmejkal, P.; Vlčková, B.; Procházka, M.; Mojzeš, P.; Pfleger, J. SERRS Spectra of Cationic Free-Base Porphyrin Species Adsorbed on Laser Ablated Ag Colloids Modified by Mercaptoacetate Spacers. *J. Mol. Struct.* **1999**, *482*−*483*, 225−229.
(19) Hanzlíková, J.; Procházka, M.; Štěpánek, J.; Bok, J.; Baumruk, V.; Anzenbacher, P., Jr. Metalation of 5,10,15,20-Tetrakis(1-methyl-4-pyridyl)porphyrin in Silver Colloids Studied via Time Dependence of Surface-Enhanced Resonance Raman Spectra. *J. Raman Spectrosc.* **1998**, *29*, 575−584.
(20) Procházka, M.; Turpin, P.-Y.; Štěpánek, J.; Vlčková, B. SERRS of Free Base Porphyrin in Laser-Ablated Colloids: Evidence for Three Different Spectral Porphyrin Forms. *J. Raman Spectrosc.* **2002**, *33*, 758−760.
(21) Procházka, M.; Vlčková, B.; Štěpánek, J.; Turpin, P.-Y. Probing of Porphyrin Surface Chemistry in Systems with Laser-Ablated Ag Nanoparticle Hydrosol: Role of Thiosulfate Anions. *Langmuir* **2005**, *21*, 2956−2962.
(22) Šloufová, I.; Šišková, K.; Vlčková, B.; Štěpánek, J. SERS-Activating Effect of Chlorides on Borate-Stabilized Silver Nanoparticles: Formation of New Reduced Adsorption Sites and Induced Nanoparticle Fusion. *Phys. Chem. Chem. Phys.* **2008**, *10*, 2233−2242.
(23) Ang, T. P.; Chin, W. S. Dodecanethiol-Protected Copper/Silver Bimetallic Nanoclusters and Their Surface Properties. *J. Phys. Chem. B* **2005**, *109*, 22228−22236.
(24) Creighton, J. A.; Blatchford, C. G.; Albrecht, M. G. Plasma Resonance Enhancement of Raman Scattering by Pyridine Adsorbed on Silver or Gold Sol Particles of Size Comparable to the Excitation Wavelength. *J. Chem. Soc., Faraday Trans. 2* **1979**, *75*, 790−798.
(25) Krieg, R. C.; Fickweiler, S.; Wolfbeis, O. S.; Knuechel, R. Cell-Type Specific Protoporphyrin IX Metabolism in Human Bladder Cancer in Vitro. *Photochem. Photobiol.* **2000**, *72*, 226−233.
(26) Procházka, M.; Mojzeš, P.; Vlčková, B.; Turpin, P.-Y. Surface-Enhanced Resonance Raman Scattering from Copper(II) 5,10,15,20-tetrakis(1-methyl-4-pyridyl)porphyrin Adsorbed on Aggregated and Nonaggregated Silver Colloids. *J. Phys. Chem. B* **1997**, *101*, 3161−3167.
(27) Šišková, K.; Vlčková, B.; Mojzeš, P. Spectral Detection of J-Aggregates of Cationic Porphyrin and Investigation of Conditions of Their Formation. *J. Mol. Struct.* **2005**, *744*−*747*, 265−272.
(28) Procházka, M.; Hanzlíková, J.; Štěpánek, J.; Baumruk, V. Metalation of Positively Charged Water Soluble Mesoporphyrins Studied via Time-Resolved SERRS Spectroscopy. *J. Mol. Struct.* **1997**, *410*−*411*, 77−79.
(29) Hajduková, N.; Procházka, M.; Molnár, P.; Štěpánek, J. SERRS of Free-Base Porphyrins on Immobilized Metal Gold and Silver Nanoparticles. *Vib. Spectrosc.* **2008**, *48*, 142−147.
(30) Vlčková, B.; Matějka, P.; Šimonová, J.; Čermáková, K.; Pančoška, P.; Baumruk, V. Surface-Enhanced Resonance Raman Spectra of Free Base 5,10,15,20-tetrakis(4-carboxyphenyl)porphyrin and Its Silver Complex in Systems with Silver Colloid: Direct Adsorption in Comparison to Adsorption via Molecular Spacer. *J. Phys. Chem.* **1993**, *97*, 9719−9729.
(31) Itabashi, M.; Kato, K.; Itoh, K. Electrochemical Processes of Meso-tetrakis(4-sulfonatophenyl)porphine at a Silver Electrode Studied by Surface-Enhanced Resonance Raman-Spectroscopy. *Chem. Phys. Lett.* **1983**, *97*, 528−532.
(32) Sládková, M.; Vlčková, B.; Mojzeš, P.; Šlouf, M.; Naudin, C.; Le Bourdon, G. Probing Strong Optical Fields in Compact Aggregates of Silver Nanoparticles by SERRS of Protoporphyrin IX. *Faraday Discuss.* **2006**, *132*, 121−134.